TRANSPORT AND THERMOMAGNETIC PROPERTIES OF METALLIC GLASSES

BY

RATNAMALA ROY
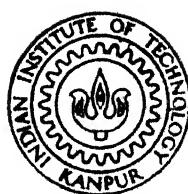
DEPARTMENT OF PHYSICS
INDIAN INSTITUTE OF TECHNOLOGY, KANPUR
MAY, 1984

TRANSPORT AND THERMOMAGNETIC PROPERTIES OF METALLIC GLASSES

A Thesis Submitted

in Partial Fulfilment of the Requirements

for the Degree of

DOCTOR OF PHILOSOPHY

BY

RATNAMALA ROY

to the

DEPARTMENT OF PHYSICS

INDIAN INSTITUTE OF TECHNOLOGY, KANPUR

MAY, 1984

PHY - 1984 - D - ROY - TRA
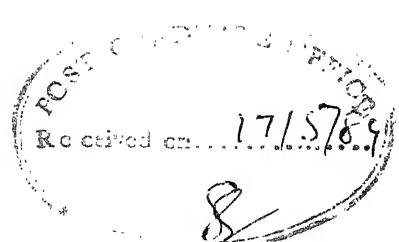
Department of Physics
Indian Institute of Technology
Kanpur-208016, India.

CERTIFICATE

This is to certify that the work reported in this thesis entitled 'Transport and Thermomagnetic Properties of Metallic Glasses' has been carried out by Ratnamala Roy under our supervision. No part of this work has been submitted elsewhere for a degree.

(Alak Kumar Majundar)
Assistant Professor

(R.K. Ray)
Professor

TABLE OF CONTENTS

LIST OF FIGURES

LIST OF TABLES

SYNOPSIS

TRANSPORT AND THERMOMAGNETIC PROPERTIES
OF METALLIC GLASSES

A thesis submitted
In Partial Fulfilment of the Requirements
for the degree of
DOCTOR OF PHILOSOPHY
by
Ratnamala Roy
Department of Physics
Indian Institute of Technology, Kanpur
April, 1984

Since the historical prediction of ferromagnetism in glassy
metals was made by Gubanov, the interest in the study of
metallic glasses has increased rapidly. The survey of the
literature of metallic glasses suggests that the properties
of these glasses may vary considerably from one set of samples
to the other. The scatter and the disagreement in the results
are believed to arise mainly from the uncertainty of the pre-
paration conditions as well as compositions. Hence, any
correlation or comparison would be meaningful only if different
measurements are made on the same set of samples. For this
purpose we have chosen a very simple and fundamental binary
glass series, namely, $Fe_{100-x}B_x$ ($13 \leq x \leq 26$) made by Allied
Chemical Corporation, USA. The characterization of such a
system is important towards the understanding of more compli-
cated systems. Very few systematic studies of the galvano-
magnetic properties on such a simple binary alloy series, with

metalloid variation, are available in the literature. In the present work we have studied electrical resistivity, magneto-resistance and Hall effect of Fe-B series over the available range of composition. Wherever possible, we have compared our results with those of liquid phase or crystalline state.

Chapter I of this thesis starts with an exact definition and a short discussion on the historical development of metallic glasses. Methods of preparation and structure of these glasses are also discussed. A brief review is given for the electrical and magnetic properties studied so far in these glasses. This chapter also establishes the subject and motivation of the present investigation.

There is no general theory available particularly for the disordered or amorphous state. In the absence of anything better, generally the results of the measurements are made to fit into different theories available for crystalline or liquid phase. Chapter II introduces those relevant theories which are needed to discuss the results of our measurements.

Chapter III deals with the experimental procedures. The fabrication and design of a cryostat and the electrical circuit used for all these measurements are described. Particular methodologies used for different measurements are also explained.

In Chapter IV the results of our measurements of :

(i) Variation of electrical resistivity ρ with temperature T in two different series, (a) $Fe_{100-x}B_x$ ($13 \leq x \leq 26$), in the temperature range $77K \leq T \leq 300K$ and (b) $Fe_{80}B_{20-x}Si_x$ ($0 \leq x \leq 12$), in the temperature range $4.2K \leq T \leq 300K$,

(ii) Variation of ρ with concentration x in $Fe_{100-x}B_x$ series at 300K,

(iii) Variation of ferromagnetic anisotropy of resistivity (FAR) with x in $Fe_{100-x}B_x$ series at 77K and 300K, and,

(iv) Concentration (x) dependence of spontaneous Hall constant R_s in $Fe_{100-x}B_x$ series at 77K and 300K, are presented.

The results of all these measurements are discussed in Chapter V and can be summarized as follows,

(i) The temperature coefficient of resistivity, α, was found to be positive for the entire range of compositions in both the series, $Fe_{100-x}B_x$ and $Fe_{80}B_{20-x}Si_x$

(ii) We have been able to find experimentally the concentration dependence of α and $\Delta\rho/\rho$ (the percentage change of resistivity over the entire temperature range) for $Fe_{100-x}B_x$ and $Fe_{80}B_{20-x}Si_x$ metallic glasses in the whole range of composition

(iii) These quantities are also calculated for the first time in this Fe-B series, using the extended Ziman theory and they are in reasonable agreement with our data

(iv) An attempt is made to correlate them in terms of structure factor and stability of this amorphous series

(v) An estimation of the Debye temperature Θ_D for the $Fe_{100-x}B_x$ series is made. Its variation with x shows a minimum around x = 20 and this behaviour is explained in terms of the Invar anomaly.

(vi) The values of Θ_D in Fe-B-Si series are much smaller compared to those of Fe-B. In this series the variation of Θ_D with x might indicate some structural changes, which could not be verified because of the non-availability of the structural data in this series

(vii) It is shown from both theory and experiment that the absolute values of resistivity ρ increase with boron concentration x

(viii) The limitation of the applicability of the extended Ziman theory to these glasses is also pointed out

(ix) Like many other properties of the Fe-B series, FAR versus x plot shows a smeared out peak at 300K and a sharper one at the lower temperature of 77K around x = 16. A physical explanation is provided for this observation.

(x) We have tried to find out ρ and FAR at 300K for amorphous Fe from our resistivity and magnetoresistance data.

(xi)   Forced magnetoresistivity ($\frac{1}{\rho}\frac{\partial\rho}{\partial H}$ at high fields), un-
       expectedly becomes less negative at lower boron concen-
       tration. This is again attributed to the Invar anomaly

(xii) The angle θ between the spontaneous magnetization and
       the ribbon axis is calculated for the whole series and is
       found to lie between $30^{\circ}-40^{\circ}$.

(xiii) The R_s versus x curves ~~also~~ show a prominent peak around
       x=13 at 300 and 77K.This peak is also attributed to the
       Invar anomaly. From R_s vs x and ρ vs x plots it is
       concluded that R_s does not vary as ρ^2

(xiv) The correlation between Hall effect and magnetoresistance
       which was proposed earlier is shown to fail in these
       metallic glasses.

Chapter VI of the thesis deals with systematic thermo-
magnetic and galvanomagnetic studies of two metallic glasses,
namely, 2605SC ($Fe_{81}B_{13.5}Si_{3.5}C_2$) and 2605 ($Fe_{80}B_{20}$). The
final crystalline phases of these two amorphous alloys were
found out by various methods like, M(T), Mossbauer, Differential
thermal analysis and X-ray. It is concluded that 2605SC is
more stable than 2605 as an amorphous ferromagnet. The thermo-
magnetic properties are seriously affected by the replacement
of B by Si and C while the galvanomagnetic properties have
changed only quantitatively.

vi

At the end, it is to be emphasised again that because of the nonavailability of any general theory, most of the results are interpreted in terms of physical arguments and are correlated with other relevant properties. From an experimentalist's point of view, we believe that a systematic set of data of various electrical and magnetic properties taken on the same set of samples would be of considerable use in developing theories of galvanomagnetic properties in amorphous systems.

CHAPTER 1

INTRODUCTION

During the last twenty five years or so, the interest in metallic glasses has increased steadily. If the progress made during this time could be measured in some units, it is probable that the curve would be close to an exponential[1]. . The research in this field helps our understanding of non-crystalline material in general. The interpretation of the properties of metallic glasses promises a particular challenge because, there is no general theory available (as to understand crystallinity, a fascinating theory of translational invariance has been developed) for the disordered or amorphous state. Before dealing with the subject, we should be particularly clear about a few terms like, 'glass', 'amorphous', 'disorder' etc. In fact 'disorder' is at the heart of 'amrophous' ferromagnets, but what we should understand is that 'amorphous' and 'disordered' do not mean the same thing. 'Amorphous' refers to the lack of crystallinity, which indirectly implies that amrophous materials are 'disordered'. But this is not vice-versa true, i.e., all 'disordered' materials are not 'amorphous'. There exist disordered crystalline materials too, where different atoms irregularly occupy sites of a regular crystal lattice. 'Metallic glasses' are 'amorphous' whereas most

practical magnetic alloys like Permalloy are 'disordered', but not 'amorphous'. The distinction between amorphous materials and disordered crystalline alloys leads us to consider two different aspects of 'disorder' _

(i) structural disorder which refers to the lack of crysta-
     llinity, and

(ii) chemical disorder which refers to the local environments;

'Disordered crystalline alloys' have only chemical disorder, but 'amorphous materials' have both structural and chemical disorder.

After recognizing the difference between 'disordered' and 'amorphous materials', let us try to differentiate between the two terms 'amorphous' and 'glassy' metals. Amorphous metals can be prepared by a variety of methods : (i) Evaporation of metals in vacuum and their condensation on a cooled substrate. (ii) Sputtering by which the atoms are removed from the source under bombardment with energetic inert gas atoms. (iii) Chemical deposition, a method in which ions in aqueous solution are deposited onto substrates by chemical reactions. (iv) Electrodeposition, where the chemical reaction requires the presence of an external potential. (v) Rapid quenching from the liquid state. By definition, a glass is a solid which does not crystallize during cooling from the liquid state. Only the amorphous alloys prepared by the last method,

i.e., by liquid quenching, satisfy the definition and hence from now onwards we would use the term 'metallic glasses' or 'glassy metals' for these alloys only.

A BRIEF HISTORICAL SURVEY

Earlier, it was believed that because of the lack of atomic ordering ferromagnetism could not exist in amorphous solids. However, in 1960 Gubanov[2] predicted on the basis of theoretical analysis, that ferromagnetism could occur in amorphous solids, based on the argument that the electronic band structure of crystalline solids did not change in any fundamental way on transition to the liquid state. This implies that the band structure depends more on short-range, rather than long-range order. Hence, ferromagnetism, which depends on short-range order, should not be destroyed in the corresponding amorphous solid. After this important prediction was made, interest in amorphous solids took a rather interesting turn. Since then a large number of different alloys have been produced as metallic glasses and the scientific and technological interest in these materials has been growing rapidly. The history of metallic glasses starts from the report of Cal. Tech. group led by P. Duwez[3] on the preparation and properties of amorphous metallic alloys. The X-ray diffraction pattern of Au-Si alloy prepared by them indicated the absence of crystallinity. However, as stated by Duwez[1] himself , at that time they were not

unquestionably convinced about the amorphosity of the alloys. Cohen and Turnbull[4] pointed out that the favourable condition for glass formation is that, in a metal-metalloid alloy, the eutectic point of the alloy should be at a rather low temperature compared to the melting point of the constituent metals. The next report was on Pd-Si metallic glasses with Si concentration around 20 at.% published by Duwez et al[5]. Shortly after this paper, there appeared two very important papers by Chen and Turnbull[6,7] on the specific heat measurements of Au-Ge-Si and Pd-Si liquid quenched alloys. Their measurements established for the first time the presence of glass transition temperature in these alloys, which in turn proved that the liquid-quenched alloys were indeed glassy and the name 'metallic glasses' was completely justified for these alloys. The first strongly ferromagnetic metallic glass $Fe_{75} P_{15} C_{10}$ was also prepared by Duwez et al[8] in late 1960s. A compact view of the discovery and development of metallic glasses in historical perspective is given in Table 1.1[9].

PREPARATION

Let us discuss the methods of preparation of metallic glass in brief. The basic principle of obtaining these materials is that the liquid must be quenched very rapidly as a droplet or jet thrown on a cooled substrate of highly conductive metal (generally copper). The cooling rate, which is a crucial point in the preparation of metallic glass, should be high enough to

Table 1.1   Headlines in the discovery and development of metallic glasses

---

1960   Gubanov : Ferromagnetism does not require crystallinity

1960   Klement, Willens, Duwez : The first metallic glass $Au_{80}Si_{20}$

1961   Cohen and Turnbull : Composition requirements for metallic glass formation

1965   Duwez, Willens and Crewdson : Pd-Si metallic glasses

1967   Duwez and Lin : Fe rich liquid-quenched alloys, $H_c = 3.0e$

1968-71 USSR, USA, UK : Full perception - 'Amorphous' → no magnetic anisotropy ==> low H_c

1969-70 Pond and Maddin, Chen and Miller : Production techniques, liquid quenched ribbons

1974   Allied Chemical Corpn: METGLAS ®, narrow ribbons commercially available

1975 H_c → 0.01 Oe or lower ($T_{80}M_{20}$)

Today   Intense activity : Development of wider ribbons, tailored properties, Possibility of replacing high permeability Ni-Fe alloys and for power applications of Si-Fe steels

---

bypass the crystallization. Generally, to get samples of

~ 20-40 μm thickness, by this melt spinning process, a cooling

rate of about (10^6-10^7)K/sec is needed[10]. At the eutectic

composition, minimum cooling rate is required. There are two

common techniques for liquid quenching.

(a) Splat Cooling :

In this method a droplet is squeezed between a rapidly moving piston and a fixed anvil (see Fig. 1.1). The obtained splat is between 15 and 30 mm in diameter and 20-80 μm thick. These splat cooling devices give slower cooling rates than the melt spinning devices described next.

(b) Melt Spinning :

In this method a rapidly spinning cold copper or steel wheel is used to conduct the heat away from the molten jet of liquid and thus quenching it at a high cooling rate (see Fig. 1.2). The ribbons produced by this method have typical dimensions of 1-3 mm width and 20-60 μm thickness.

Some new techniques of obtaining metallic glasses are still developing. These are laser glazing[11], electric field emission of ions from the melt[12] and electric arc furnace quenching[13].

COMPOSITION OF METALLIC GLASSES

At present, all the metallic glasses reported in the literature can be classified in a few different families[14,15]. They are tabulated with representative systems and particular composition range in Table 1.2.

LIQUID DROPLET

ANVIL

PISTON
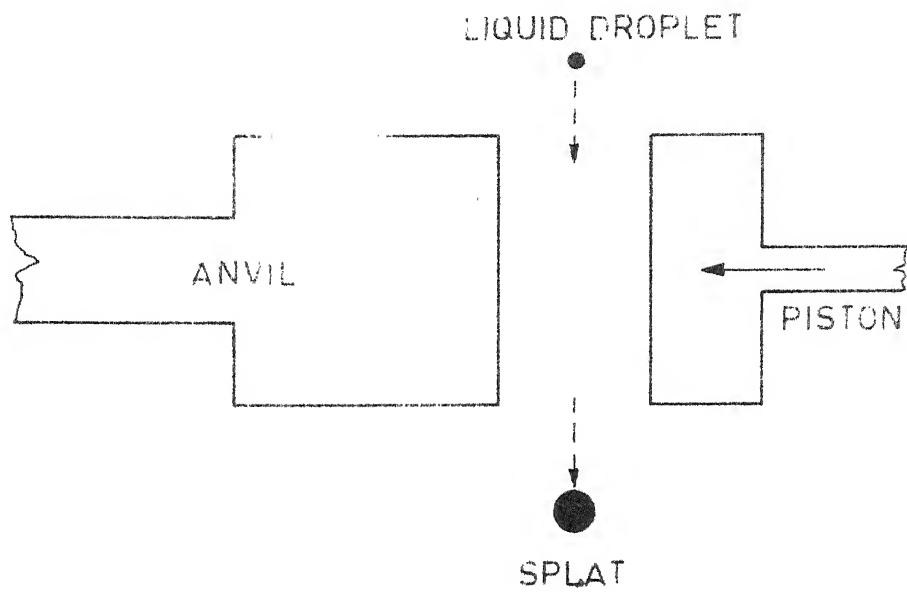
SPLAT

SPLAT-COOLING TECHNIQUE

FIG. 1.1

MOLTEN
JET

RIBBON OF
METALLIC GLASS
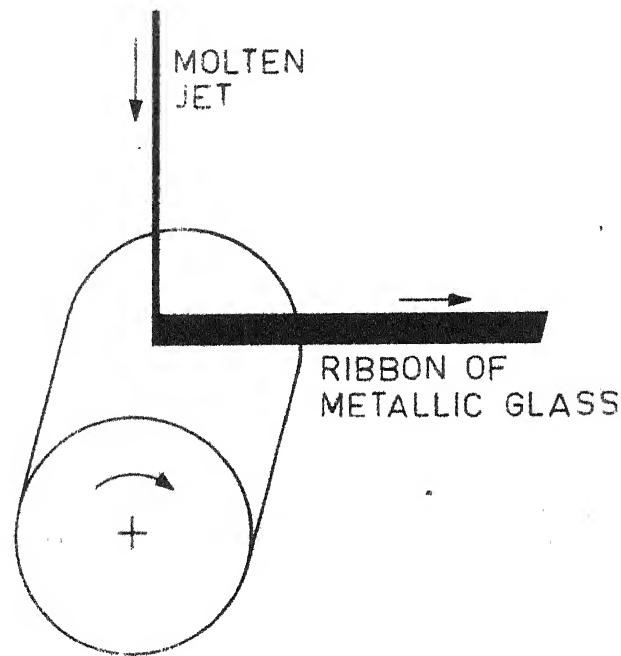
MELT-SPINNING TECHNIQUE

FIG. 1.2

Table 1.2   Classification of glass forming alloy systems

Category	Representative Systems	Typical composition range, at. %
i) T or N-M	Fe-B, Pd-Si, Au-Si	15-25 M
ii) AM-BM	Mg-Zn, Ca-Mg, Mg-Ga	Variable
iii) T_E-T_L (or Cu)	Zr-Fe, Zr-Ni, Zr-Cu, Nb-Ni, Ti-Ni, Y-Cu, Ta-Ir	30-65 Cu or T_L, or smaller range
iv) T_E-AM	(Ti,Zr) Be	20-60 Be
v) U-T	U-Fe, U-Cr, U-V	20-40 T
vi) RE-M	$La_{70} Al_{30}$	
vii) RE-N	$La_{80} Au_{20}$	
viii) RE-T_L	$Gd_{70}Co_{30}, Gd_{70}Ni_{30}$	

Here T is transition metal, M is polyvalent metal, AM is Li, Mg group metals, BM is Cu,Zn,Al group metals, T_E is early transition metals, T_L is late transition metals, N is Noble metals.   RE is rare earth metals and U denotes uranium.   In each category of glasses there is a particular range of composition over which the glasses are formed.   This range might be quite narrow, as in Pd-Si ($\sim$ 5 at.%) or wide as in Cu-Zr ($\sim$ 35 at.%).   As stated earlier, in a few cases where the phase diagram is known, there is a low-melting eutectic at or near

the easy glass formation range. The existence of eutectic
means that the liquid state is stable to relatively low
temperatures, and suggests that the amorphous state and the
crystalline state are not much different in energy. The
reason for the presence of glass forming tendency, only over a
particular range is not clear[10,16], and this has been an
interesting open question in this field. Different groups of
scientists have suggested different reasons to explain 'why
only over a particular range of composition stable glasses are
formed'. One suggestion[17,] based on geometrical argument,
is that these glasses exist essentially in a Bernal structure
of densely-packed hard sphere metal atoms (a) and the smaller and
 softer metalloid atoms   (b) (20 at.% in T-M type) can just
get in and occupy the open spaces in the otherwise densely
packed array and thus stabilize the random configuration.
But the short coming of this model is that in some cases the
glass forming composition predicted by the model falls well
outside the observed range, and in many cases the softer 'b'
atoms are even larger than the 'a' atoms - e.g. Pt-Sb and
$(Au,Ag)_{25}Pb_{75}$[18]. The second model suggested by Chen[19] is that
the destabilization of the crystalline mixture, rather than
the stabilization of the glassy phase near the eutectic compo-
sition, determines the stability and the ease of glass forma-
tion. Chemical affinity due either to electron transfer or to
ionization among constituent atoms, stabilizes the stochiometric

a_3b, a_2b or ab crystalline phases and leads naturally to
eutectic compositions near 20,25 or 35 at.% of 'b' atom.
Duwez has proposed what he calls a 'confusion principle' to
the effect that complex mixtures of constituents have greater
glass forming tendency than binary mixtures and whatever the
underlying rationale of this empirical observation may be,
designers of commercial glasses have evidently accepted this
principle as valid. Another important model suggested by
Nagel and Tauc[20] is an electronic band-structure argument
based on the reduction in the d-electron band energy by amorphous
short-range order. This   model will be discussed in some
detail in Chapter II of this thesis. Also, the validity of
this criterion for our amorphous alloys is discussed in
Chapter V.

STRUCTURES

In 1975 Cargill[21] concluded that no microcrystalline model
was able to match the experimental radial distribution fun-
ctions (RDF) of the majority of glasses and there remains no
doubt that the kinds of samples we are discussing are truly
amorphous. Conventional X-ray diffraction techniques, which
give information about the metal atoms almost exclusively, are
in fairly good agreement with results predicted for an assembly
of dense-random packed spheres (DRPS). Many models were
suggested based on   DRPS. Finney, in 1970[22] developed the
mechanical model of dense random packing of hard spheres

(DRPHS) suggested by Bernal. Computer modelling was first used by Bennett[23]. Starting from seed cluster, atoms are added one at a time, each atom is brought into hard sphere contact with one of the atoms already in the cluster. Both these models could not reproduce the second peak in the RDF. The most successful structural model of amorphous metals is the relaxed DRPS model of Cargill and Kirkpatrick[24]. The algorithm used to generate this model is similar to the one of Bennett except that the atom being added to the cluster is allowed to move to the nearest position where it can make contact with three atoms in contact with each other to form a nearly perfect tetrahedron. This model is extremely successful in that it exhibits the second peak in the RDF. In the study of metallic glasses many new techniques other than X-ray diffraction are introduced. These are pulsed neutron scattering methods, small angle neutron scattering, Mössbauer effect, EXAFS (extended X-ray absorption fine structure) and EDXD (energy dispersive X-ray diffraction). Pulsed neutron scattering methods can provide a high resolution RDF in the high wave vector region, which show structural details of short-range order (SRO) not detected in previous diffraction studies. EXAFS has the unique capability of probing the near neighbour environment in multicomponent systems where EXAFS from each element can be studied. Study of Mössbauer effect provides another tool to probe the local environment. The main

application of EDXD technique lies in real time study of the kinetics of structural relaxation by annealing and in the study of compositional SRO of metallic glasses. Based on these models, the present understanding of the structure of amorphous metals is : the major features are nearly 12-fold coordinated dense random packing (DRP) structure (like fcc or hcp close-packed crystals) but beyond first nearest neighbours correlations are very weak. The metalloid atoms have a lower coordination number than the metals. In DRP structures there are a number of types of interstitial spaces that are not possible in close-packed crystals. These spaces, known as Bernal holes may play a role in amorphous structures in accommodating the metalloid atoms in T-M alloys. Surroundings of metalloid atoms are probably similar to those in crystalline compounds of the same composition.

A BRIEF REVIEW OF THE ELECTRICAL AND MAGNETIC PROPERTIES OF METALLIC GLASSES

Until recently the major efforts in solid state physics have been confined to the understanding of crystalline materials. Amorphous solids now represent a new state of matter. Some of their properties are entirely as predicted and some of them show anomalous behaviour. The most significant experimental results reported in the recent literature are the large absolute values of electrical resistivity, very small temperature coefficient of resistivity, very small values

of ferromagnetic anisotropy of resistivity and a nearly
temperature independent anomalous Hall coefficient. Interest
in metallic glasses was accelerated due to the ferromagnetism
in them, hence the study of magnetic properties in these
materials bears a special significance. The amorphous state
influences mainly the electronic transport properties. Hence,
the electrical resistivity, Hall resistivity, magnetoresis-
tance are other important properties to be studied to under-
stand the non-crystallinestructure. The subject of magnetic
behaviour of metallic glasses is so extensive that it is very
difficult to touch upon all the topics. We would discuss
here only a few important ones.

(i) Saturation Magnetization :

This is a widely studied property of ferromagnetic
amorphous alloys. The considerable scatter and disagreement
in the results (e.g., the variation of saturation magnetic
moment with boron concentration in $Fe_{100-x}B_x$ alloys studied
by Hiroyoshi et al[25] show a broad maximumaround x = 14,
whereas the same study in the similar series, done by Hasegawa
and Ray[26] show a continuous decrease with increasing x) can be
attributed to various causes - (a) the inherent difficulty
to measure magnetization on small samples, (b) the other major
experimental uncertainty is because of the uncertain composi-
tion of the samples and (c) a further difficulty for some

alloys like Ni-Co series and the compositions near pure Ni, have fairly high susceptibilities at high fields, making the definition of saturation magnetization uncertain. However, one point is certain that magnetic moments of the amorphous glasses are smaller than those of pure crystalline forms of the transition metals which they contain. The direct influence of the structural disorder on the moments is very small. It is shown by Kazama et al[27] that the moments are lower because of the change in local environment provided by the presence of metalloids. To explain the magnetic moment in amorphous alloys we then assume that metalloid with more sp electrons will contribute more electrons to the d-band of transition metals and thus shifting the peak of Slater-Pauling curve towards a lower transition metal electron concentration[28]. Hence, the magnetization would decrease with increasing metalloid concentration (this is true for both amorphous and crystalline alloys). According to Luborsky[29], the magnetic moment of the transition metal, T atoms in amorphous alloy $T_{1-z-y}F_zG_y$ can be expressed as,

$$\mu = [m(1-z-y) - fz - gy]/(1-z-y) \qquad (1.1)$$

or for moment per atom of alloy as,

$$\mu = m(1-z-y) - fz - gy \qquad (1.2)$$

where F and G represent the metalloid or glass forming atomic

species, m is the original number of unpaired spins in the transition metal alloy, and f and g are number of electrons transferred from F and G atoms respectively. Since the number of nearest neighbours in an amorphous alloy is essentially the same as in the fcc crystalline phase, one can assume m to be the same. Thus m = 0.6, 1.6 and 2.6 for Ni, Co, Fe respectively. Using these values in eqn. (1.1) or (1.2) the theoretically calculated μ tallies well with the experimentally observed values.

Alben et al[30] have discussed the saturation magnetization in the light of chemical bonding. The first extensive measurements of saturation moment for a wide range of alloys, were given by Mizoguchi et al[31]. Durand and Yung[32] too have performed a detailed investigation of the moment and Curie temperature of amorphous alloys, Fe-P-B over the entire range of amorphosity.

The study of the variation of magnetization with temperature M(T), in amorphous alloy systems is also quite important. This leads one to the understanding of amorphous to crystalline transition and helps to study the equilibrium phases present in any particular amorphous alloy by identifying T_c of different crystalline phases present in it. From magnetization measurements directly, or from Mössbauer measurements, assuming that the hyperfine field H_{eff} is proportional to M, the change in magnetization with temperature is given by (as in crystals),

$$(M_O - M_T)/M_O = \Delta M/M_O = BT^{3/2} + CT^{5/2} + .. \qquad (1.3)$$

where M_O, M_T are magnetization at O and T and B and C are con-
stants characteristic of the low temperature, long wavelength
spin waves. From neutron scattering, assuming a dispersion
relation of the form $E(k) = Dk^2$, the spin-wave dispersion
coefficient D may be determined. The values of D and B are
related by

$$B = \zeta \ (3/2) \ (g\mu/M)(K/4\pi D)^{3/2} \qquad (1.4)$$

where g is the g-factor ($\sim$ 2.1), μ is the Bohr magneton in
emu (9.27×10^{-21} emu), M is the magnetization in emu/$\text{\AA}^3$, K is
the Boltzmann constant (8.61×10^{-5} ev/K) with D in eV $\text{\AA}^2$, to
obtain B in $K^{-3/2}$. ζ is the zeta function = 2.612. Like
crystalline ferromagnets, in these amorphous alloys too $T^{3/2}$
term is dominant. Recent experiments[27] show that the increase
in B is largely due to chemical effects rather than to stru-
ctural disorder.

(ii) Curie temperature :

Inspite of their chemical and structural disorder amor-
phous ferromagnets have well defined magnetic ordering or
Curie temperature T_c. For most glasses of practical interest
T_c lies in the range 600-700K[15]. Most of the glasses show a
sharp transition near T_c[33-35] but some alloys with two or more
transition metals show a spread out Curie transition[36]. Chemical

inhomogenety appears to be the reason behind such spreading of Curie transition. The T_c's of amorphous transition metal-metalloid alloys are found to be significantly lower than those of the pure crystalline samples. Chemical composition and chemical disorder is thought to be the reason for this reduction in T_c[37]. The degree of dependence of T_c on metalloid content varies greatly between the alloys based on Co and on Fe. T_c apparently decreases nearly linearly with increasing metalloid content in former, whereas the latter have a much weaker dependence of T_c on metalloid content[37,38]. In some of the Fe based alloys (e.g. in $Fe_x(PB)_y$ alloys) T_c increases as x decreases, i.e., alloys of higher Fe content have lower T_c, but this is not true for all the alloys with Fe as the only transition metal. In fact, T_c is generally sensitive to Fe-Fe interatomic spacing, which in turn depends on both the metalloid species and their concentration. Hence, clearly the increase or decrease of T_c with metalloid content depends upon the particular metalloid the alloy contains and also on the percentage weight of metalloid present in the alloy. Chen et al[39] have shown that in binary (Fe) amorphous alloys T_c decreases in the order Fe-Si, Fe-B, Fe-C, Fe-P, where the values for $Fe_{80}Si_{20}$ and $Fe_{80}C_{20}$ are found by the extrapolation of their data on $Fe_{80}(BSi)_{20}$, $Fe_{80}(PSi)_{20}$ and $Fe_{80}(BC)_{20}$, $Fe_{80}(PC)_{20}$ respectively.

Many workers[31,40] have shown that the substitution of other transition metals, like, Cr, Mn, V, Mo etc. for Fe sharply brings down the Curie temperature.

However, generally in amorphous systems Curie temperature T_c is a smooth function of alloy composition over the eutectic range. As pointed out by Luborsky[29], though the theoretical treatment of spin ordering, and hence Curie temperature, in amorphous solids is a very difficult problem, in the molecular field approximation T_c could be given by,

$$T_c = [2S(S+1)/3K] \sum_{ij} J_{ij} \qquad (1.5)$$

where S is the spin number, K is Boltzmann's constant and J_{ij} is the exchange interaction between atoms at the position r_i and r_j and can be expressed in terms of radial distribution function.

(iii) Magnetic Anisotropy :

The absence of crystallinity in metallic glasses should give a corresponding absence of magnetocrystalline anisotropy. But, in actual practical cases, this is not found to be true. In fact, while quenching the metals, inhomogeneous stresses result from differential thermal contraction. This stress then interacts with the magnetostriction to cause local magnetic anisotropy K_λ. This type of anisotropy is called strain-magnetostriction anisotropy. An important case where this

particular anisotropy is present is in $T_{80}(P,B,Al \ldots)_{20}$ type
of metallic glasses. The non-uniform strain developed during
the preparation of the ribbon results in a periodic fluctuation
in the perpendicular component of anisotropy along the length
of the ribbon. Thermal annealing removes the internal stresses
and then the anisotropy disappears. Luborsky[29] has discussed
many other types of anisotropies which can be present in the
metallic glasses. These are structural and compositional
anisotropy, directional order anisotropy or induced anisotropy
and exchange anisotropy. On an atomic scale, magnetic anisotropy
exists even in an ideally homogeneous amorphous alloy. Each
magnetic ion experiences an anisotropic electric field or ex-
change field due to its neighbouring ion. These local anisotro-
pies vary from place to place within the amorphous structures.
Rhyne et al[41] have shown that in metallic glasses containing
rare-earth elements such local anisotropy is often very strong
whereas in transition metal containing metallic glasses exchange
interaction overrides local anisotropy and thus within a domain
all the spins are essentially parallel. Berry and Pritchet[42]
first observed that by annealing amorphous alloys in magnetic
field one can get a non-random distribution of local environments
and this in turn gives rise to the induced anisotropy (or magne-
tic annealing anisotropy) in these alloys. The anisotropy in
amorphous alloys is largest when two transition metals are
present in equal concentration. For metallic glasses all these
anisotropies are uniaxial.

(iv) Magnetostriction :

When an amorphous alloy is subjected to an elastic stress, the neighbouring ion positions are slightly changed and results in a microscopic anisotropy. This in turn results in a macroscopic anisotropy with uniaxial symmetry. Also, within each uniformly magnetized domain, there will be a spontaneous strain to minimise the elastic strain energy and anisotropy energy. This spontaneous strain resulting from the strain dependence of the anisotropy energy is called Magnetostriction. Since the amorphous alloy is macroscopically isotropic, the magnetostriction is explained by a single constant, the saturation magnetostriction, λ_s. The magnetostrictive strain can then be expressed as $\lambda = \lambda_s \cos^2 \emptyset$, where $\emptyset$ is the angle between the direction of measured strain and the direction of magnetization. Magnetostriction of glasses is an interesting property because it was assumed that a glass with $\lambda = 0$ would have virtually infinite permeability. Ohnuma and Masumoto[43] have examined in detail how the permeability of a range of glasses is affected by λ and heat-treatment. Values of λ_s reported by Brooks[44] for the series $(Fe_{1-x}Co_x)_{75}P_{16}B_6Al_3$, and Sherwood et al[45] for $(Fe-Ni-Co)_{75}P_{16}B_6Al_3$ showed that a zero magnetostrictive composition occurred at $(Fe_{0.04}Co_{0.96})_{75}P_{16}B_6Al_3$. Another Co-based metallic glass Vitrovac E6010, $Co_{58}Ni_{10}Fe_5 Si_{11}B_{16}$ has $\lambda \leq 5 \times 10^{-7}$[15]. Tsuya et al[46] studied λ of $Fe_{80}P_{13}C_7$ from $-76^{\circ}C$ to room temperature and got a universal result that the

material did not appear to be isotropic. Narita et al[47] have shown that in Fe-B and Co-B glasses a nearly quadratic relation exists between magnetostriction and saturation magnetization. O'Handley[48] has reported a systematic study of λ_s on $(Fe Ni)_{80}B_{20}$ and $(Fe-Co)_{80}B_{20}$ series. In this report he has also discussed the possible origin of magneto-striction in amorphous alloys. A few measurements of the temperature dependence of λ_s have been reported with conflicting results[46,49,50,51]. Jagielinski et al[51] measured the temperature dependence of λ_s for a large number of alloys between 77 and 300K and found λ_s increasing in some cases and decreasing in others. There can also be a volume magne-tostriction, ω, that appears as an anomaly in volume thermal expansion at Curie temperature and as a field dependent volume change at any temperature where the saturation magnetization is field dependent. Jagielinski et al[51] have reported the volume magnetostriction for several alloys.

(v) Low Temperature Specific Heat :

Since the electronic, lattice and ferro-magnetic contri-butions to the specific heat defined as $C_p = \gamma T + \alpha T^3 + \sigma T^{3/2}$, can be well separated, specific heat measurement is an important tool for investigating the interdependence between the electronic and magnetic properties. Krause et al[52] have measured the low temperature specific heat in Fe-B-P, Fe-B-Si and Fe-Ni-B alloys and discussed the effect of B and P

on the lattice and magnetic specific heat. Golding et al[53]
have measured C_p for $Pd_{80}Si_{20}$ metallic glass. Recently
Matsuura et al[54] have measured the low temperature specific
heat of $Fe_{100-x}B_x$ glasses. They found that both electronic
specific heat coefficient γ and the Debye temperature Θ_D
decrease rapidly with increasing B content. For amorphous
materials Θ_D is generally $\sim$ 10-20% lower than Θ_D in crysta-
lline transition metals whereas γ value is twice as large as
that for pure bcc Fe. The value of Θ_D in this Fe-B series
is very high even compared to the other metal-metalloid
amorphous alloys. Also, the spin-wave stiffness constant D
of these alloys were found to be small. All these findings
led them to the conclusion that the Fe-B amorphous alloys
showed the characteristic features of Invar alloys.

Specific heat measurement is also an important tool to
find out the glass transition temperature T_g of these glassy
metals. The sudden increase in the specific heat of glass
upon heating, is the thermal manifestation of the glass transi-
tion and the point of inflection of rising C_p is defined as
T_g. Chen and Turnbull[55] observed this behaviour in AuGeSi
alloys.

(vi) Electrical Resistivity :

Non-crystallinity of the materials directly affects the
electronic transport properties. Hence, the study of

electrical resistivity in metallic glasses is very important.
The variation of resistivity ρ with temperature T can be
divided into three main categories :

(i)   Low temperature region, $\lesssim$ 20K a logarithmic term of
        disputed origin is observed

(ii)   Intermediate temperature region, 20K $\lesssim$ T $\lesssim$ 100K, where,
        generally a T^2 dependence is reported

(iii) High temperature range, above 150K, a linear dependence
      is found.

The model which is generally used to interpret the inter-
mediate and high temperature range is the extended Ziman's
theory of resistivity. Since we are interested in the ρ values
between 20K $\leq$ T $\lesssim$ 300K, Ziman's theory is discussed in detail
in Chapter II of this thesis. But recently the applicability
of this theory to metallic glasses is criticised by many
workers. Theoreticians[56,57,58] have questioned the validity
of this theory for systems with strong scattering potentials.
In fact, the Boltzmann equation is the basis of this theory
and is frequently questioned for strong scattering systems such
as amorphous transition metal based alloys[59]. But one has to
use this theory for metallic glasses (assuming these glasses to
be similar to liquid metals) in the absence of anything better.
The Ziman's theory could. however, yield good agreement with expe-
rimental results[60,61] when the Fermi energy E_F, effective valence z

and a suitable muffin-tin potential for a liquid are reasonably adjusted. As argued by Yonezawa[56] for liquid metals (we can use the same argument for metallic glasses too), inspite of its quantitative successes, the extended Ziman formula is neither based upon theoretical first principles since little is known of the physical circumstances under which it might be valid, nor of the corrections that should be applied when these conditions are not well satisfied. It has been noted[58] that the theoretical calculation of ρ on the basis of this theory is very sensitive to the three parameters E_F, Z and the choice of a suitable muffin-tin potential as described above. This fact reflects the vulnerability of the extended Ziman theory. The multiple scattering effect which is important for strong scattering systems, is absent in the original Ziman's formula. Attempts have been made to remove this difficulty by including some of the multiple scattering terms and thus modifying the extended Ziman theory[62], but the extended Ziman's formula still remains parameter sensitive. More sophisticated approaches based on the Kubo formula[63] have been successfully applied to the transport in completely random liquids and crystalline alloys. Beginning with Kubo formula, Chen, Weisz and Sher (CWS)[64] made a number of simplifying assumptions, computed the Green's functions and then the conductivity. The important results of this approach is that it

explains the negative temperature coefficient of resistivity α somewhat successfully.

CWS showed that as the strength of the effective scattering potential in a completely random alloy increases, an energy gap in the electron density of states begins to form and that, if the Fermi energy falls near this gap, one can get negative temperature coefficients of resistivity, α. Other workers[65,66,67] have also applied this CWS approach to their own models and have successfully explained the negative temperature coefficient of these high resistivity ($\geq$ 100 $\mu\Omega$cm) metallic glasses. However, to get negative α

i) the effective scattering must be strong enough to initiate the energy gap formation in the density of states curve and

ii) E_F has to be near the energy gap.

These theoretical studies which completely ignore the structure of the disordered materials have their own shortcomings e.g., they cannot explain $\rho = a + bT^2$ behaviour in the intermediate temperature region. Despite these shortcomings attempts to explain the transport behaviour directly from Kubo formula, does not fail in strong scattering systems and seem promising. Yonezawa[56] has tried to establish a systematic scheme of studying transport properties of materials with strong scattering potentials using the effective medium approximation (EMA) for conductivity. We also face another

controversial point in ρ-T plots of metallic glasses -
the dependence on T in the intermediate temperature range.
Ziman's theory considers the electron-ion potential scattering
and at low temperatures it evolves into a T^2 dependence.
Bergmann et al[68] and Richter et al[69] have worked out the
effect of the electron-magnon scattering and get a $T^{3/2}$
dependence. Experimental evidence of this $T^{3/2}$ dependence
of ρ has been claimed by many workers[70,71]. Mogro-
Campero et al[72] have argued in their report that though the
best fit to the equation $\rho = a+bT^n$ is obtained with n = 1.5 in
the intermediate temperature range, it cannot be claimed
definitely that it is the electron-magnon scattering which
governs the ρ-T dependence in the intermediate temperature
range. They have suggested that it is possible that electron-
ion potential scattering alone can explain the observations.
It may be that the intermediate temperature regime is the
transition region between the asymptotic T and T^2 behaviours
and in the temperature interval $20K \leq T \leq 100K$ this transition
can be well described by power law with exponent n $\sim$ 1.5.

(vii) Magnetoresistance :

The anisotropic magnetoresistance ($\rho_{11} - \rho_{1}$), being an
inherent material property, does not depend on the initial
magnetic domain structure and remains unchanged by heat
treatment etc. Hence one can compare other magnetic properties
in terms of this quantity[73,74,75]. The practical quantity

which is generally measured is the ratio of $(\rho_{||} - \rho_{\perp})$ and the specific resistivity ρ of the material. This quantity $(\rho_{||} - \rho_{\perp})/\rho$ or $\Delta\rho/\rho$ is known as the ferromagnetic anisotropy of resistivity (FAR). As stated earlier, in amorphous glasses, magnetostriction contributes greatly to the appearance of finite values of magnetic anisotropy. With regard to this significant behaviours of λ, another problem of interest is the magnetoresistance of these amorphous alloys[76]. It appears that the anomalous magnetoresistance depends upon the magnetic domain structure associated with stress magneto-striction. The magnitude of the anisotropic magnetore-sistance may depend upon the electronic mechanism asso-ciated with amorphous structure which is related to the chara-cteristics of magnetostriction. However, the available data on the magnetoresistance of the amorphous alloys are not sufficient to discuss the above problem. Recently, the investigation of magnetoresistance in amorphous alloys has become a subject of several studies[77,78,79]. Bhönke and Rosenberg[80] have studied the magnetoresistance of Fe-Ni-P-B metallic glasses at different temperatures. From the dependence of FAR on temperature they predicted that $\Delta\rho/\rho$ at 0K increases with the amount of Fe, and that above T_c the magneto-resistivity becomes isotropic. Fukamichi et al[75] have studied FAR in Fe-B glasses and pointed out that the concentration and temperature dependences of the FAR for Fe-B alloys are very

similar to those of the saturation magnetization and the linear magnetostriction. In another report[81], where they have studied FAR of Fe-P alloys, they have shown that $\lambda_s \propto M_s^2$ is not valid in this system but FAR and λ_s vary similarly at room temperature. Naka, Kern and Gonser[73] have studied FAR in Fe-B-P system. They have verified the correlation between FAR and saturation magnetic moment in this series ($\Delta \rho / \rho = A \mu^m$). An important result of FAR is that the FAR of amorphous alloys are an order of magnitude smaller than those of their crystalline counterparts. Nigam and Majumdar[82] have shown that the field dependence of resistivity, and other corresponding features like ~~magneto~~*ferromagnetic*anisotropy of resistivity (FAR) etc. of amorphous ferromagnets behave in a manner which is similar to that of crystalline ferromagnets.

(viii) Hall Effect :

Hall effect is an important galvanomagnetic property which is widely studied[83,84,85]. One of the most important questions regarding amorphous materials concerns their stability against thermal cycling. For instance, some of the amorphous alloys are metastable at 300K, show irreversible effects on heating and eventually crystallize upon heating to temperatures 600-800K. They crystallize into different structures depending upon the temperature and the composition of the material. Hall resistivity is strongly influenced by thermal cycling[86,87] and hence it could be an important tool

to understand the occurrence of new phases during any trans-
formation process. A good review on Hall effect studies of
amorphous glasses from an experimental point of view is
presented by T.R. McGuire et al[88]. An open question in this
area is the understanding of the sign and magnitude (always
larger than those of their crystalline counterparts) of the
Hall coefficients of these amorphous alloys[14,56]. The Hall
coefficient in these glasses does not obey the free electron
formula and is often positive.

(ix) Invar Property :

Another property which would frequently enter our
discussion in Chapter V is the Invar property. As reported
by Wohlfarth[89] the Invar behaviour is almost always observed
for weak itinerant ferromagnets and should thus arise for
some of the amorphous alloys. $(Fe_x Ni_{100-x})_{80} P_{10} B_{10}$,
Fe-Mn-P-C, Ni-P, Fe-Ge are the examples of weak itinerant
ferromagnets. Invar problems are closely related to the
origin of ferromagnetism in transition metals and alloys[90]
and hence is an important research field in ferromagnetic
materials. To find out whether a particular material has
Invar characteristics or not one should check as follows.
The expected observations are[89] - (1) low saturation magneti-
zation (2) low T_c (3) large high field susceptibility (4) large
volume magnetostriction (5) large negative linear thermal

expansion at low temperatures, (6) low thermal expansion at 300K[91], (7) large negative pressure derivative of saturation magnetization, leading to a critical pressure for the disappearance of ferromagnetism, (8) large negative pressure derivative of T_c, (9) small spin-wave stiffness constant D, and (10) anomalies at the Curie temperature. According to Masumoto[92] high magnetic moment and a low Curie temperature are empirical principle of finding Invar alloys.

After this brief review of magnetic and electric properties we conclude that most of the properties of metallic glass are qualitatively similar to those of their nearest available crystalline counterparts. Whatever quantitative differences are there between amorphous and crystalline alloys arise from the chemical disorder, not from structural disorder. Some of the results concerning the thermal and transport properties are very specific for glasses. These are :

i) Specific heat shows a term almost linear in T at very low temperatures

ii) The T^2 dependence of resistivity ρ at low temperatures

iii) Negative temperature coefficient of resistivity α, at high temperatures.

The appeal of these amorphous magnetic ribbons lies in the following factors : (1) the lack of magnetocrystalline anisotropy, with low domain wall energy, nearly reversible wall

motion and easy magnetization direction along the ribbon axis
(2) moderately high resistivity (higher compared to the
conventional metallic materials used for devices) which
results in smaller eddy current contributions to the permea-
bility and losses, which is specially important at higher
frequencies, (3) the combination of high resistivity and thin
gauge of the ribbons (0.003 to 0.005 cm), reduces the
magnetic loss by a factor of 10 compared to polycrystalline 3%
Si-Fe sheets in conventional thickness (Note: the achievement
of very thin gauge in Si-Fe is very expensive) and (4) presu-
mably, inexpensive to manufacture.

SUBJECT OF PRESENT STUDY

In the present investigation we have chosen a very simple
transition metal-metalloid (T-M) metallic glass series, namely,
$Fe_{100-x}B_x$ ($13 \leq x \leq 26$). Characterization of such simple
binary metallic glasses is important towards understanding the
properties of more complicated amorphous systems. We have
studied the absolute values of electrical resistivity as a
function of composition, the temperature dependence of electri-
cal resistivity in the temperature range $77K \leq T \leq 300K$, the
ferromagnetic anisotropy of resistivity (FAR) and the Hall
effect in the Fe-B series. All these experiments were done
on the same set of $Fe_{100-x}B_x$ ($13 \leq x \leq 26$) samples manufactured
by Allied Chemical Corporation, USA. Since the composition
range is rather wide it is ideal for studying the composition

dependence of the above galvanomagnetic properties. Here, any correlation and comparison of physical properties are meaningful since various measurements are made on the same set of samples. This is especially desirable for metallic glasses.

An order of magnitude calculation for α and $\Delta\rho/\rho$ was reported by us[93] for the first time. Also, the variations of the absolute values of resistivity ρ, the spontaneous Hall constant R_s and the spontaneous Hall conductivity γH_s with the boron concentration in Fe-B alloys are also presented for the first time in our work. The results of magnetoresistance measurements are included. The angle Θ between the spontaneous magnetization M_s and the ribbon axis for the whole series is reported. We have tried to estimate the absolute resistivity and FAR for amorphous Fe from our magnetoresistance and resistivity data. An attempt is made to consistently explain our observations in terms of the structure, known physical properties and Invar anomaly of Fe-B series.

The variation of ρ with temperature, in the temperature range $4.2K \leq T \leq 300K$, for another series of metallic glass, $Fe_{80}B_{20-x}Si_x$ ($0 \leq x \leq 12$) is also presented. These samples are manufactured by General Electric Co., USA.

CHAPTER II

THEORY

2.1 ELECTRICAL RESISTIVITY

There is a striking similarity in the structure, magnitude of electrical resistivity ρ and the temperature coefficient α of resistivity of liquid metals and glassy metals. Keeping this in view, we believe that a model which explains the high temperature electrical transport behaviour of liquid metals can be used to explain glassy metals too. Hence, we may try to use Ziman's theory of liquid metals[94] to explain the behaviour of metallic glasses. The most common metallic glasses are the alloys of T-M type where T is a transition metal (Fe,Co,Ni,Pd, etc) and M is a polyvalent metal (B,Si,P,C etc.). Obviously, the electronic properties of such alloy are affected most by the d-states. These glasses consist of randomly distributed ions and the conduction electrons. The ions are positioned in a random close-packed distribution. The arrangement of the ions in the glassy (i.e., frozen liquid) state can be described in terms of a pair correlation functioning $g(r)$. The function $g(r)$ determines the probability of finding two ions separated by the distance r. This function has a typical shape: zero for small distances (where the atomic cores cannot overlap) and unity for large distances, with a

number of oscillatory peaks between these two limits. The
Fourier transform of the pair correlation function is the
structure factor S(k) i.e., the interference function. The
intensity of beam scattered from the alloy depends on this
function S(k). A typical example of the S(k) vs k graph is
shown in Fig. 2.1. The main peak represents the nearest
neighbour distance of the alloy in k space, denoted by k_p.
The distribution functions S(k) and g(r) are deduced from
X-ray and neutron scattering experiments, statistical
mechanics calculations and computer experiments. The
conduction electrons are supposed to form a degenerate free-
electron gas with a spherical Fermi surface. The electrical
resistivity can be explained only by interaction of the
conduction electrons with the ions. The electrons represented
as plane waves are scattered by the irregular arrangement of
the metal ions.

According to Ziman the electrical resistivity of liquid
metal can be given as,

$$\rho = \frac{3 \pi \Omega}{4 e^2 \hbar v_F^2 k_F^4} \int_0^{2k_F} S(k) |V(k)|^2 k^3 \, dk \qquad (2.1)$$

where Ω is the atomic volume, v_F the Fermi velocity, k_F the
radius of the Fermi-sphere, S(k) the structure factor and V(k)
is a suitably chosen electron-ion potential. For liquid transi-
tion metals, Evans et al[95] have extended the Ziman's formula,

SCHEMATIC STRUCTURE FACTOR S(k)
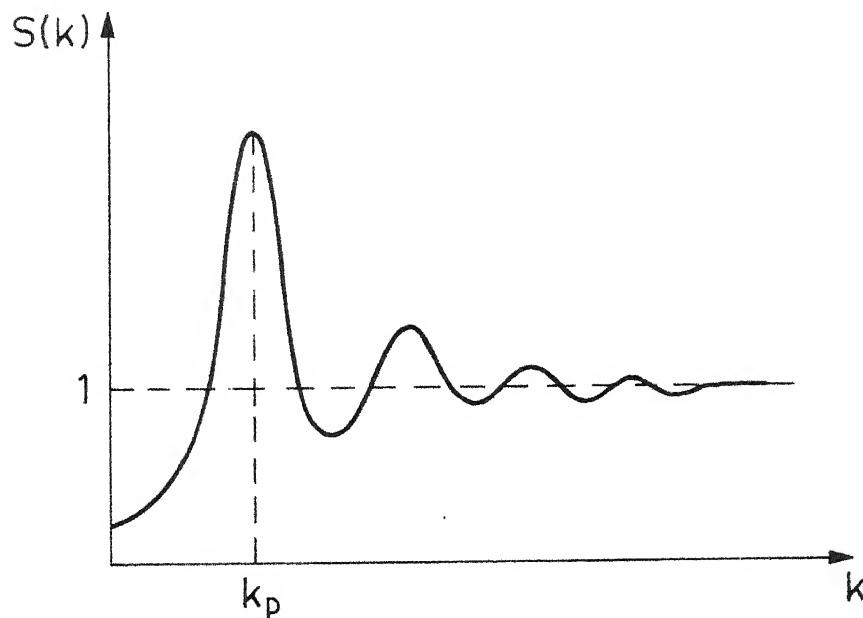
FIG. 2.1

TOTAL POTENTIAL OF ONE TRANSITION METAL ION. V_{CB} IS CENTRIFUGAL BARRIER, V_{MT} IS MUFFIN-TIN POTENTIAL.
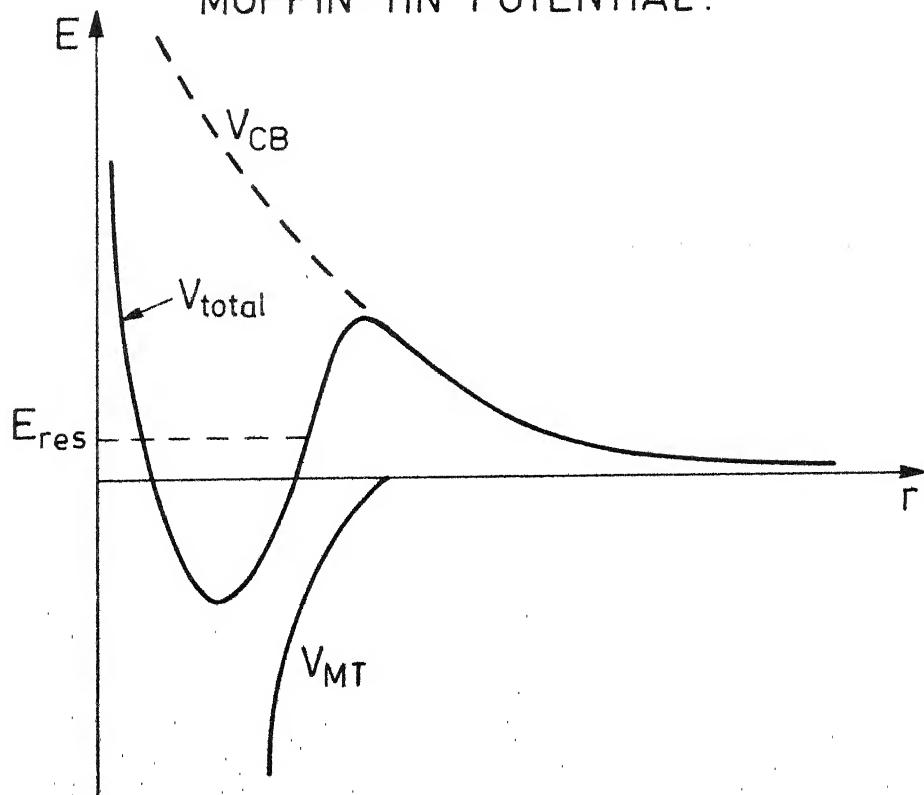
FIG. 2.2

using mainly physical arguments, by bringing in the t-matrix
of the muffin-tin potential for one ion. The total potential
is a superposition of muffin-tin potential and the centrifugal
barrier arising for d-electrons (Fig. 2.2). The d states act
as resonance state. The conduction electrons scattered by
this potential experiences a delay or resonance scattering.
The strength of the scattering depends on the difference
$(E_{res}-E_F)$. Gyorffy, Szabo and Evans[96] have derived an exact
expression of resistivity in terms of phase shifts and the
ion positions. The extended Ziman's formula for resistivity
is (following Busch and Güntherodt)[97]

$$\rho = \frac{3\pi\Omega}{4e^2\hbar v_F^2 k_F^4} \int_0^{2k_F} S(k)\ |t(k)|^2\ k^3\ dk$$

where t(k) is the single-site t matrix which is defined in the
partial wave representation as

$$t(k) = \frac{-2\pi\hbar^3}{m(2mE)^{1/2}}\ \frac{1}{\Omega}\ \sum_l\ (2l+1)\ \sin\eta_l(E)\ \exp i\eta_l(E)\ P_l(\cos\theta)$$

where m is the electron mass, E_f is the Fermi energy (measured
relative to the muffin-tin zero) and the sum is over various
partial waves contributing to the scattering. $P_l(\cos\theta)$ is
the Legendre polynomial of order l and the η_l are the partial
wave phase shifts describing the scattering of the conduction
electrons by the ion cores. If the d-phase shift η_2 is domi-
nant at the Fermi energy in transition metals, we can write

$$\rho = \frac{30\pi^3 \hbar^3}{m e^2 k_F^2 E_F \Omega} \sin^2 \eta_2(E_F) \ S(2k_F)$$

or

$$\rho = \frac{30\pi^3 \hbar^3}{m e^2 k_F^2 E_F \Omega} \ S(2k_F) \ \frac{\Gamma^2}{\Gamma^2 + 4(E_{res} - E_F)^2} \qquad (2.2)$$

where Γ is the width and E_{res} is the energy of the scattering resonance lying approximately at the centre of the 3d band (Fig. 2.3).

Thus the electrical resistivity ρ is governed by two major factors,

(i)   the structure factor or 'interference function' $S(k)$, and

(ii)   the resonant scattering of conduction electrons from the
       3d — states lying in the conduction band, by the ion cores.

As can be seen from Fig. 2.3, with the increase of the number of 3d electrons the Fermi energy E_F increases, the difference $E_{res} - E_F$ increases and hence from eqn. (2.2) the resistivity value ρ should decrease.   From Fig. 2.3, it can be predicted that amorphous Fe will have a larger resistivity value than the amorphous Ni.   The large resistivity values of metallic glasses are due to this resonance scattering.

2.1.1   Temperature Dependence of Electrical Resistivity

In Ziman's theory of liquid metals the temperature dependence of electrical resistivity is included by taking into account the change in the structure factor $S(k)$ as the

CONTRIBUTION OF RESONANCE SCATTERING
IN TERMS OF PHASE SHIFT η_2 AND $(E_{res} - E_F)$.
ARROWS INDICATE THE FERMI ENERGIES OF
TRANSITION METALS RELATIVE TO E_{res}. THE
LARGEST CONTRIBUTION ARISES IF $\eta_2(E_F)$ IS
CLOSE TO THE VALUE OF $\pi/2$ OR IF THE
DIFFERENCE $(E_{res} - E_F)$ IS SMALL.
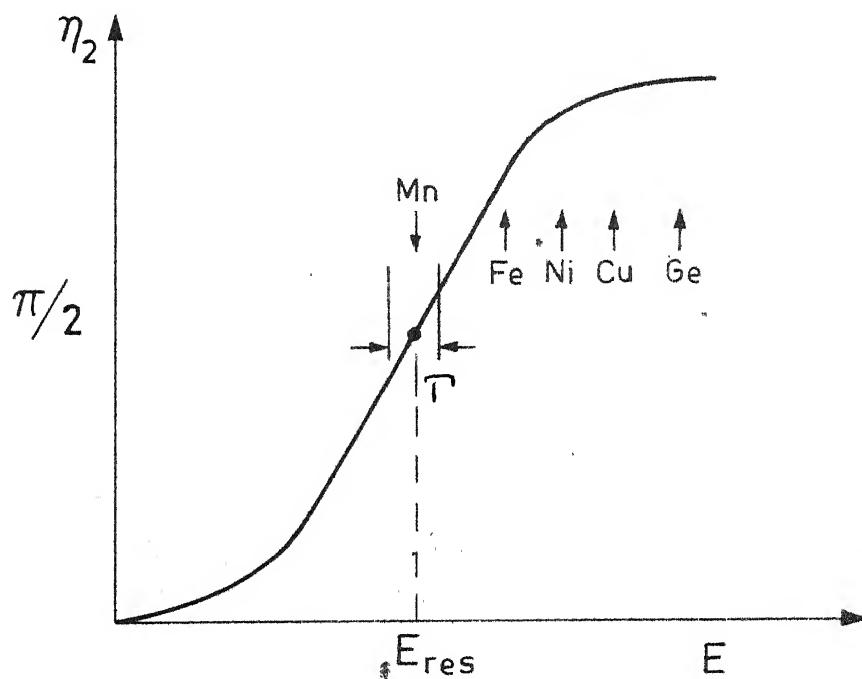
FIG. 2.3

temperature T is varied. However, in the solid the change
in S(k) should be calculated as due to the vibration of ions
around their equilibrium positions. An expression for this
change is derived by including the Debye-Waller factor. The
first peak height of S(k) versus k graph decreases with
increasing temperature, giving rise to a negative α, whereas
the number of phonons increase with increasing temperature
resulting in a positive α. In case of metallic glasses
these two mechanisms are competitive. The final sign of α
is determined by the dominant one.

Following Nagel[98] the electrical resistivity ρ of
metallic glass is given by,

$$\rho = \frac{30\pi^3\hbar^3}{m e^2 k_F^2 E_F \Omega} \sin^2\eta_2(E_F) \ S(2k_F) \tag{2.3}$$

where $\eta_2(E_F)$ is the l = 2 partial wave phase shift at the Fermi-
energy E_F.

In this equation, the temperature-dependence of ρ will be
determined by the temperature dependence of $S(2k_F)$. In calcu-
lating the temperature dependence of $S(2k_F)$, i.e., $S_T(2k_F)$,
care must be taken to include not only the decrease in the
intensity of the structure factor but to include phonon terms
as well. The resulting expression for $S_T(k)$ is given by

$$S_T(k) \simeq 1+[S(2k_F)-1]e^{-2W(T)} \tag{2.4}$$

Now the resistivity as a function of temperature can be expressed as

$$\rho(T) = \frac{30\pi^3 \hbar^3}{m\,e^2 k_F^2 E_F \Omega} \sin^2[\eta_2(E_F)] \times \{1+[S_o(2k_F)-1]e^{-2[W(T)-W(o)]}\}$$

$$(2.5)$$

where k_F is the Fermi wave vector, Ω is the atomic volume, $W(T)$ is the Debye-Waller factor at a temperature T, $S_T(2k_F)$ is the structure factor corresponding to $k = 2k_F$, and $\hbar$, m and e have their usual meaning.

Also,

$$\alpha = \frac{1}{\rho_{RT}}\frac{\partial \rho_T}{\partial T} \simeq 2[\frac{1-S_T(2k_F)}{S_T(2k_F)}]\frac{\partial W(T)}{\partial T} \qquad (2.6)$$

Since $\partial W(T)/\partial T > 0$, α is negative only if $S_T(2k_F) > 1$, i.e., if $2k_F$ is near k_p, the position of the first peak in the S(k) versus k graph. Coming back to eqn. (2.6), the asymptotic temperature dependence of $W(T)$ in the Debye approximation is given by,

$$W(T) = \begin{cases} W(o)+4W(o)\,\frac{1}{6}\,\pi^2(T/\theta_D)^2 & \text{for} \quad T \ll \theta_D \ , \ (2.7) \\[2ex] W(o)+4W(o)(T/\theta_D) & \text{for} \quad T \geq \theta_D \ , \ (2.8) \end{cases}$$

where

$$W(o) = \frac{3\hbar^2 k^2}{8M K \theta_D} \qquad ; \qquad (2.9)$$

here M is the atomic weight and K is Boltzmann constant.

Thus an estimate of α could be made for individual alloys, from eqns. (2.6) and (2.8), if the structure factor $S(k)$ at the corresponding $2k_F$ value (which depends on the number of conduction electrons per unit volume) and Θ_D are known. The percentage change of resistivity $\Delta\rho/\rho$ from 300 to 80K is given by,

$$\frac{\Delta\rho}{\rho} = \frac{\rho(300K) - \rho(80K)}{\rho(80K)}$$

$$= -C \frac{[S_T(2k_F) - 1]}{S_T(2k_F)} \qquad (2.10)$$

This expression along with the constant C would be derived from eqns. (2.5), (2.7) and (2.8). Using the same equations, Θ_D is found to be,

$$\Theta_D = \frac{\pi^2}{6} \frac{\alpha}{S} \qquad (2.11)$$

where $\quad S = \dfrac{\partial \rho_T}{\rho_{RT} \partial(T^2)} \quad$ for $T \ll \Theta_D$ $\qquad (2.12)$

It is clear from eqns. (2.5), (2.7) and (2.8) that the resistivity ρ is expected to vary as T^2 at low temperatures (low with respect to the Debye temperature) and vary as T at high temperatures. The functional relationship predicted for electron-ion potential scattering is given by,

$$\rho = a + bT^n \qquad (2.13)$$

where asymptotically n=1 or 2.

The non-magnetic term changes from T to T^2 as one moves to lower temperature, and the transition depends on the value of Debye temperature.

At very low temperatures, a minimum of the electrical resistivity is observed. There are two main mechanisms which are suggested for explaining this resistivity minimum (i) the Kondo effect[99] which is magnetic in origin and (ii) tunneling-state scattering,[100] which is completely nonmagnetic in origin and is believed to be a manifestation of the amorphous structure. We generally restrict our interest in the range above this minimum, i.e., in the temperature range 20K $\leq$ T $\leq$ 300K.

2.1.2 Composition Dependence of Electrical Resistivity

As stated earlier, the main contribution to the large values of electrical resistivity of liquid transition metals comes from the resonant scattering of conduction electrons from the d-states. As discussed by Nagel and Tauc[20] when these transition metals are alloyed with polyvalent metals and quenched to solid state, the result is a frozen liquid structure, with the effective number of conduction electrons Z_{eff} which increases in accordance with the relation

$$Z_{eff} = Z_1(1-x) + Z_2 x \qquad (2.14)$$

where Z_1 and Z_2 are the number of conduction electrons of corresponding metals.

This, in turn, increases the value of $2k_F$ giving rise to a larger contribution to the resistivity via the structure factor. The assumption made in formulating this model is that the Group VIII transition metals (Fe,Co,Ni) as well as the noble metals can be treated as if they had one free-electron per atom in the liquid state. Faber and Ziman[101] predict that on such alloying the resistivity will reach a maximum when $2k_F$ passes through k_p. Also, when $2k_F \sim k_p$, negative temperature coefficients (NTC) occur.

In calculating the resistivity of metallic glasses as a function of composition, we assume that in eqn. (2.5), $\sin^2[\eta_2(E_F)]$ and Ω are approximately the same for the whole series. Using the relation $E_F \alpha k_F^2$ we can write eqn. (2.5) as,

$$\rho = \frac{C'}{k_F^4} \; \{ 1 + [S_o(2k_F) - 1] \; e^{-2[W(T) - W(o)]} \},$$

where C' takes care of the constants.

Since we are calculating the room temperature resistivity in eqn. (2.14) we use $W(T) - W(o)$ from eqn. (2.8).

Then eqn. (2.14) can be written as ,

$$\rho = \frac{C'}{k_F^4} \; \{ S_o(2k_F) + 8W(o) \frac{T}{\theta_D} [1 - S_o(2k_F)] \} \qquad (2.15)$$

The values of k_F, $S_o(2k_F)$, $W(o)$ and θ_D change with

changing metalloid concentration x and thus we can roughly estimate the nature of variation of resistivity ρ with composition x.

2.1.3 Electronic Stability Criterion

Nagel and Tauc[20] have suggested a model to understand the stability of the metallic glasses, i.e., to understand 'why the metallic glasses are structurally stable only over a limited range of composition '. The metallic glasses which are basically metals are treated as a nearly free-electron gas. In a crystal the structure factor $S(k)$ depends on both magnitude and direction of k, but in amorphous materials $S(k)$ is spherically symmetric. Hence, in the case of metallic glasses the relationship between $2k_F$ and k_p is of crucial importance. For atoms with Z=1, $2k_F$ lies slightly below k_p and for Z=2, $2k_F$ lies slightly above k_p. The effect of alloying a monovalent metal with an element with higher valence is to shift the effective valence, $Z_{eff} = Z_1(1-x) + Z_2 x$ [eqn-(thus shifting $2k_F$ towards k_p. A system with $2k_F = k_p$ is believed to be more stable against crystallization than a system for which $2k_F \neq k_p$. They have suggested an arbitrary choice of $Z_{eff} = 1.7$, to give a reasonable estimate of the concentration (x), which is needed for the situation $2k_F = k_p$. Depending on the details of $S(k)$ vs k graph, k_p will coincide with $2k_F$ at different values of Z_{eff}.

2.2   MAGNETORESISTANCE

The electrical resistivity of a polycrystalline ferromagnet depends on the angle between the current density $\vec{J}$ and the magnetization vector $\vec{M}$.   The longitudinal magnetoresistance $(\vec{J} \parallel \vec{M})$ is positive while the transverse one $(\vec{J} \perp \vec{M})$ is negative at low fields.   At higher fields there is a slow decrease in resistivity, i.e., a negative magnetoresistance is observed in both orientations.   Assuming a cubic structure for a ferromagnetic domain, the resistivity of a cubic single crystal can be written as[102]

$$\rho(\alpha_i,\beta_i) = a_0 + a_1(\alpha_1\beta_1 + \alpha_2\beta_2 + \alpha_3\beta_3)^2 + 2(a_2-a_1)(\alpha_1\alpha_2\beta_1\beta_2$$

$$+ \alpha_2\alpha_3\beta_2\beta_3 + \alpha_3\alpha_1\beta_3\beta_1), \tag{2.16}$$

where $\alpha_1, \alpha_2, \alpha_3$ are the direction cosines of spontaneous magnetization with respect to the crystal axes and the resistivity is measured in a direction characterized by the direction cosines $\beta_1, \beta_2, \beta_3$.   Under the conditions $\vec{J} \parallel \vec{M}$ and $\vec{J} \perp \vec{M}$, the saturation values of resistivity, expressed respectively as $\rho_{\parallel S}$ and $\rho_{\perp S}$ can be found out by taking the averages of eqn. (2.16).   One can write then,

$$\rho_{\parallel S} = a_0 + \frac{3}{5} a_1 + \frac{2}{5} a_2 , \tag{2.17}$$

$$\rho_{\perp S} = a_0 + \frac{1}{5} a_1 - \frac{1}{5} a_2 . \tag{2.18}$$

In ideal condition, when all the orientations with respect to the crystal axes are equally probable, and the crystallites are oriented at random, the resistivity ρ_0 in the demagnetized state, can be written as,

$$\rho_0 = a_0 + \frac{1}{3} a_1 = \frac{1}{3} \rho_{\parallel S} + \frac{2}{3} \rho_{\perp S} \qquad (2.19)$$

But, as stated in Chapter I, even in glassy ferromagnetic alloys, where the absence of magnetic anisotropy was expected, it was found out that these alloys had preferred magnetic directions which were induced during the cooling process etc. Thus, the ratio of $\Delta \rho_{\parallel S}/\Delta \rho_{\perp S}$ depends completely on the orientation of this preferred axis. Here $\Delta \rho_{\parallel S} = \rho_{\parallel S} - \rho_0$ and $\Delta \rho_{\perp S} = \rho_{\perp S} - \rho_0$.

2.2.1 Ferromagnetic Anisotropy of Resistivity (FAR)

Though the ratio $\Delta \rho_{\parallel S}/\Delta \rho_{\perp S}$ depends on the initial processing and subsequent heat treatments etc, the quantity $(\Delta \rho_{\parallel S} - \Delta \rho_{\perp S})$ does not depend on the initial magnetic domain structure and hence is a very important inherent property of the ferromagnet. This difference, which is practically always positive is called the anisotropic magnetoresistance. The experimentally measured quantity, the relative change in resistivity $\Delta \rho/\rho_0$ is called the ferromagnetic anisotropy of resistivity, FAR. Hence,

$$FAR = \frac{\Delta \rho}{\rho_0} = \frac{\rho_{\|S} - \rho_{\perp S}}{\rho_0} \quad , \tag{2.20}$$

and the anisotropic magnetoresistance is given as,

$$\Delta \rho_{\|S} - \Delta \rho_{\perp S} = \rho_{\|S} - \rho_{\perp S} , \tag{2.21}$$

where ρ_0, the resistivity in the demagnetized state can be written from eqn. (2.19) as,

$$\rho_0 = \rho + \frac{1}{3} \Delta \rho_{\|S} + \frac{2}{3} \Delta \rho_{\perp S} , \tag{2.22}$$

ρ being the resistivity for $H_{ext} = o$.

In a ferromagnet, because of the presence of spontaneous magnetization within each **Weiss** domain, the effective magnetic field is given by ,

$$H_{eff} = H_{int} = H_{ext} - H_{demag}$$

$$= H_{ext} - \alpha M_S \quad \text{(in MKS units)} \tag{2.23}$$

where α is the domagnetizing factor which depends on the dimensions of the sample and its orientation with respect to the magnetic field and M_S is the saturation magnetization at a particular temperature.

As stated earlier, to get ρ_o, one has to do some kind of averaging over the all possible orientations of the spontaneous domain magnetization. In metallic glasses, since we have a uniaxial anisotropy and the domains are not at random, it is very difficult to do such averaging. However, fortunately enough, these materials have very small magnetoresistance and thus instead of calculating ρ_o we can use

$$\rho_o = \rho \tag{2.24}$$

Thus eqn. (2.20) can be written as,

$$FAR = \frac{\Delta\rho}{\rho} = \frac{\rho_{||S} - \rho_{\perp S}}{\rho} \tag{2.25}$$

To get the anisotropic magnetoresistance $(\rho_{||S} - \rho_{\perp S})$ in terms of the measured quantities one writes,

$$\rho_{||S} = \rho + \Delta\rho_{||S} = \rho(1 + \Delta\rho_{||S}/\rho) \tag{2.26}$$

$$\rho_{\perp S} = \rho + \Delta\rho_{\perp S} = \rho(1 + \Delta\rho_{\perp S}/\rho) \tag{2.27}$$

and thus,

$$\rho_{||S} - \rho_{\perp S} = (\Delta\rho_{||S}/\rho - \Delta\rho_{\perp S}/\rho)\rho \tag{2.28}$$

where $\Delta\rho_{||S}/\rho$ and $\Delta\rho_{\perp S}/\rho$ are obtained by extrapolating the $\Delta\rho/\rho$ versus H_{ext} plots to $H_{ext} = H_{demag}$, such that $H_{int} = 0$.

Hence, in terms of experimentally measured quantities, FAR [Eqn. (2.25)] can be written as,

$$FAR = \frac{\Delta\rho_{\parallel S}}{\rho} - \frac{\Delta\rho_{\perp S}}{\rho} \qquad (2.29)$$

2.2.2 Dependence of ρ on H

This is an effect of purely ferromagnetic origin. As stated by Smit[103], if we compare the change in resistance with the magnetostriction, then the linear saturation magnetostriction corresponds to the Ferromagnetic anisotropy of resistivity both being tensor dependent on the orientation of the magnetization. However, the volume magnetorestriction corresponds to the small negative value of $\partial\rho/\partial H$ at strong fields, independent of the orientation. Clearly, volume effects are due to the effect of increasing intrinsic magnetization with increasing field. The direct influence of volume magneto-striction on resistance is very small[103] ($\frac{1}{\rho}\frac{\partial\rho}{\partial H}$ values are very small) and hence the effects observed are due to a change of the specific resistance. Assuming that the resistivity depends only on magnetization M_S, one can write,

$$\frac{\partial\rho}{\partial H} = \frac{\partial\rho}{\partial M_S}\frac{\partial M_S}{\partial H} \qquad (2.30)$$

Now again assuming that ρ does not vary appreciably with magnetization M_S for normal fields, the dependence of $\partial\rho/\partial H$ on H is determined by that of $\partial M_S/\partial H$, the high field susceptibility.

2.2.3 Formulation of Θ, the Angle between $\vec{J}$ and $\vec{M}$

Since in metallic glasses, we have uniaxial anisotropy, i.e., the domains are preferentially oriented at some angle Θ with the ribbon axis, the resistivity in the demagnetized state can be expressed as,

$$\rho_o = \rho_\perp \sin^2\Theta + \rho_{||} \cos^2\Theta \tag{2.31}$$

where Θ is the angle between the current and the magnetization vectors. Hence, the longitudinal magnetoresistance is

$$\Delta\rho_{11}/\rho_o = \frac{\rho_{||} - \rho_o}{\rho_o} = \frac{\rho_{||} - \rho_\perp \sin^2\Theta - \rho_{||} \cos^2\Theta}{\rho_o}$$

$$= \frac{\left(\rho_{||} - \rho_\perp\right)\sin^2\Theta}{\rho_o}$$

or

$$\frac{\Delta\rho_{||}}{\rho_o} = \text{FAR } \sin^2\Theta \tag{2.32}$$

Similarly, the transverse magnetoresistance is

$$\frac{\Delta\rho_\perp}{\rho_o} = -\text{FAR } \cos^2\Theta \tag{2.33}$$

From eqns. (2.32) and (2.33) we get,

$$\text{FAR} = \Delta\rho_{||}/\rho_o - \Delta\rho_\perp/\rho_o$$

and $\cot^2\theta = -\dfrac{\Delta\rho_\perp/\rho_o}{\Delta\rho_{||}/\rho_o}$ (2.34)

Using eqn. (2.24), we can write this equation as,

$$\cot^2\theta = -\dfrac{\Delta\rho_\perp/\rho}{\Delta\rho_{||}/\rho}$$ (2.35)

2.2.4 Relation Between FAR and Saturation Magnetization

Bhönke et al[79] have shown that $\Delta\rho/\rho$ varies as $T^{3/2}$. The saturation magnetic moment $\mu(\mu_B/\text{Fe atom})$ also varies as $T^3/2$ [104]. Considering these two observations Bhönke et al have suggested an empirical relationship between them as,

$$\dfrac{\Delta\rho}{\rho} = A\mu^m$$ (2.36)

where μ is the saturation magnetic moment/Fe atom and A,m are constants.

2.3 HALL EFFECT

The Hall resistivity ρ_H in a polycrystalline ferromagnet can be written as[102],

$$\rho_H = \dfrac{E_y}{J_x} = R_o B_z + R_S M_z$$

where $\vec{J} \,||\, \hat{x}$ is the electric current density, $\vec{E}$ the electric field and $\vec{B} \,||\, \hat{z}$ is the magnetic induction. The first term has its origin in Lorentz force acting on the conduction electrons and is present in nonmagnetic materials too. R_o is the coefficient of this ordinary Hall effect. The second term

depends on the magnetization and is a characteristic property of ferromagnets. The coefficient R_s is called the extra-ordinary or spontaneous Hall constant. Here we will concentrate only on the spontaneous Hall effect.

An excellent physical picture of the scattering mechanism for R_s is given by Berger[105]. The spontaneous Hall effect depends on the magnetization. When a magnetic moment moving in an electric field sees a magnetic field, its gradient gives rise to a force on the moment. Thus the interaction of the electronic spin (magnetic moment) with the electric field of the screened nucleus defines its spin-orbit interaction. The spin-orbit interaction gives rise to a left-right asymmetry in the scattering of the spin-polarized carriers. This asymmetry is observed as the spontaneous Hall effect. In ferromagnets at ordinary temperatures ($T > 100K$), $R_s \gg R_o$ and can be written as[102],

$$R_s = A \, \rho^n, \qquad (2.37)$$

where A is a constant depending on the metal, but not on temperature and R_s is the spontaneous Hall coefficient, related to the spin-orbit interaction.

Consider an electron wave-packet approaching a scattering potential (Fig. 2.4). Before scattering the centre of mass of the packet moves in a straight line through the periodic crystal.

ASYMMETRIC
SCATTRING
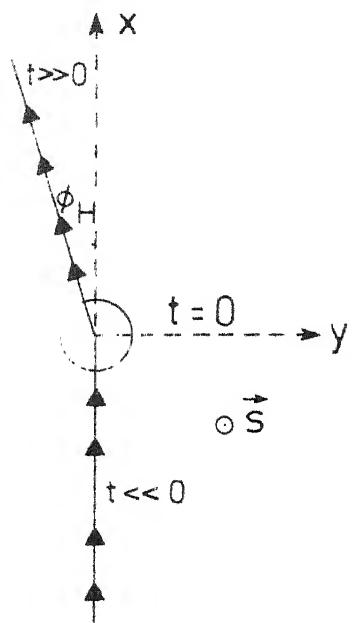
SIDE –JUMP
MECHANISM
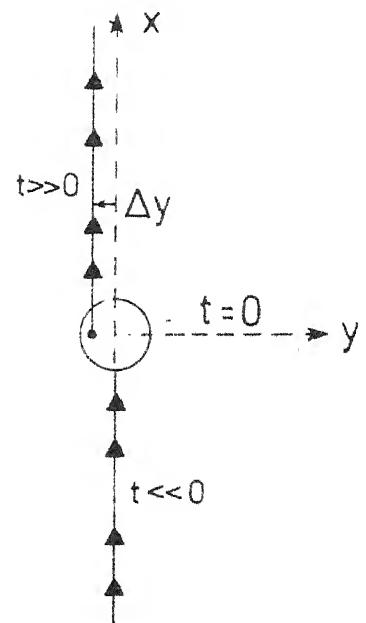
FIG. 2.4

After scattering, the wave-packet is broken into a set of out-going spherical waves. A part of the wave is back-scattered, so the motion of the wave-packet after scattering is rather slow. Still, according to quantum mechanics this motion again follows a straight line, at a constant speed.

If the electron spin $\vec{S}$ is normal to the plane of the picture, the spin-orbit interaction removes any symmetry between right and left. So, the trajectory after scattering differs from the trajectory before scattering. Let us say that the new trajectory is at an angle $\emptyset_H$ [see Fig. 2.4.a) to the old one before scattering. This implies that the electron acquires transverse momentum on scattering. This effect is called skew-scattering and can be derived from classical Boltzmann equation if the differential cross-section has a left-right asymmetry. This effect is characterized by the tangent of the Hall angle $\emptyset_H$, i.e., β

$$\tan \emptyset_H = \beta = \rho_H/\rho \qquad (2.38)$$

Clearly, for skew-scattering $\rho_H \alpha \rho$ and hence in eqn. (2.37) it gives n = 1. This scattering effect vanishes for weak scatterers. The only materials where this mechanism is observed are low-resistivity dilute alloys at 4K.

Instead of deflection of wave-packet at any angle after scattering, the scattering potential can displace the new trajectory by a distance Δy. This transverse displacement is

called the 'side-jump' by Berger[105]. It is a quantum mechanical mechanism. The side-jump $\Delta \dot{y}$ of the carrier wave-packet is approximately related to the Hall angle by the mean free path λ

$$\tan \varnothing_H = \beta = \Delta y / \lambda \; \alpha \cdot \rho \Delta y \qquad (2.39)$$

From eqn. (2.39) it is clear that the side-jump mechanism predicts n = 2 in eqn. (2.37). Thus for a given band structure variation of R_s with ρ is given as,

$$R_s = a \rho + b \rho^2 \qquad (2.40)$$

For a single band[106],

$$\Delta y = 4\pi M_s b(\hbar k_F / n \; e^2) = 4\pi(R_s M_s / \rho^2) (\hbar k_F / n \; e^2) \qquad (2.41)$$

Thus, one can say, that eqn. (2.37), if valid, clearly shows that the spontaneous Hall effect is connected with the electron scattering. In metallic glasses, the validity of this relation $(R_s \alpha \; \rho^2)$ is difficult to confirm experimentally because of the weak temperature dependence of R_s and ρ and also because small variations in metalloid content have comparatively little effect on the resistivity, which is dominated more by disorder. Nevertheless in Chapter V we would try to find out the validity of this relation by comparing the concentration (x) dependence of R_s and ρ. The Hall conductivity γ_{H_s}, given by,

$$\gamma_{H_S} = \dot{\rho}_H / \rho^2 = R_S M_S / \rho^2 \, , \qquad (2.42)$$

becomes almost independent of temperature or concentration if eqn. (2.37) with n = 2 is valid for R_s.

2.4 CORRELATION BETWEEN MAGNETORESISTANCE AND HALL EFFECT

When a d.c. current is passed perpendicular to the domain walls, the current lines get sharply bent at the walls by twice the Hall angle of the material. As a result the current follows a zig-zag path and the ohmic resistance of the sample is expected to increase. In an uniaxial ferromagnet, where the resistivity tensor has an off-diagonal Hall component, Berger[107] has calculated from Maxwell's equations in the neighbourhood of 180° domain walls that there is an increase in ohmic resistivity. When a magnetic field parallel to the easy axis removes the domain walls, a negative magneto-resistance results, which is given (assuming wall spacing << sample width) by,

$$\Delta \rho / \rho' = -\beta^2 \qquad (2.43)$$

Here ρ' is the resistivity in the absence of walls, β is the tangent of the Hall angle and is given by,

$$\beta = \tan \emptyset_H = \rho_H / \rho_\perp \qquad (2.44)$$

On the basis of this theory, a correlation between magnetoresistance and Hall effect can be predicted[108]. Considering the

above mechanism as well as the usual ferromagnetic anisotropy
of resistivity, the resistivity in the demagnetized state
ρ_o can be written as,

$$\rho_o = (\rho_\perp \sin^2\theta + \rho_{||} \cos^2\theta)(1 + \beta^2 \sin^2\theta) \qquad (2.45)$$

or

$$\rho_o - (\rho_\perp \sin^2\theta + \rho_{||} \cos^2\theta) = \rho_o \beta^2 \sin^2\theta$$

or

$$\beta^2 = \frac{\rho_o}{\rho_o \sin^2\theta} - \frac{(\rho_\perp \sin^2\theta + \rho_{||} \cos^2\theta)}{\rho_o \sin^2\theta}$$

This can be simplified to give

$$\beta^2 = -[\frac{\Delta\rho_\perp}{\rho} + \frac{\Delta\rho_{||}}{\rho} \cot^2\theta] \qquad (2.46)$$

where $\Delta\rho_{||}/\rho$ and $\Delta\rho_\perp/\rho$ are the longitudinal and transverse
magnetoresistances respectively and θ is the angle between the
current and magnetization direction as defined in Sec. 2.2.3.

CHAPTER III

EXPERIMENTAL PROCEDURE

The measurements made in the present investigation are electrical resistivity at room temperature (300K), variation of electrical resistivity with temperature between 4.2 and 300K, magnetoresistance at 300K and liquid nitrogen temperature (77K) and Hall resistivity at 300' and 77K. The samples are in the form of thin ribbons, typically 1 mm wide and 30 μm thick and were manufactured by Allied Chemical Corporation, U.S.A.

3.1 CRYOSTAT DESIGN AND FABRICATION

The measurements of electrical and magnetic properties are relatively easy to make in comparison to thermal properties. Most of our measurements were between 77K and room temperature, so the problem of exchange of thermal energy with surroundings was less important.

A common cryostat was fabricated for the measurements of electrical resistivity, longitudinal and transverse magneto-resistances and Hall effect between 77K and room temperature. The sample holders for the electrical resistivity and transverse magnetoresistance, for longitudinal magnetoresistance and for Hall resistivity measurements were separately made and attached to the main tubing assembly [see Figs. 3.1 and 3.2] described later depending on the experiment.
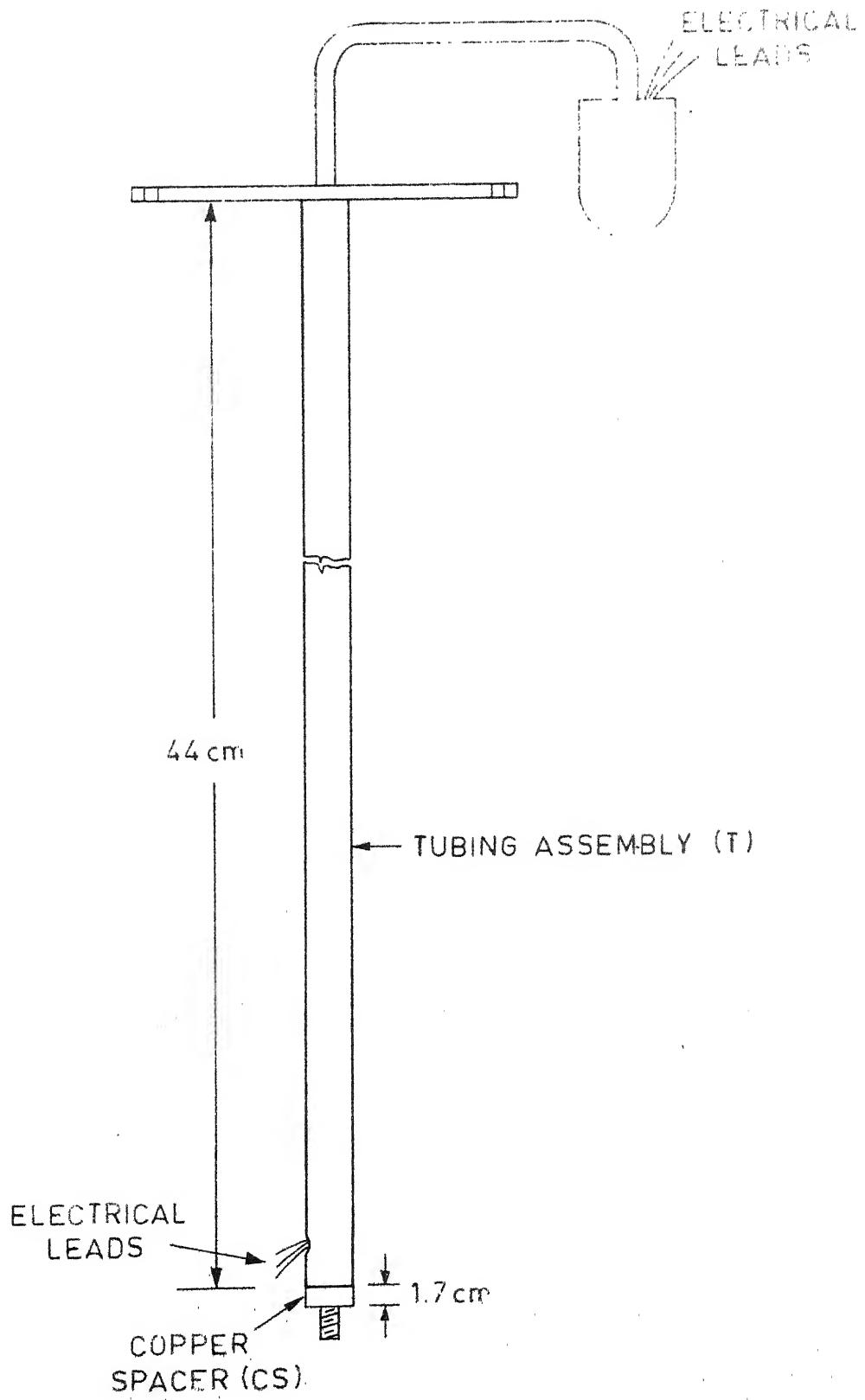
FIG. 3.1

For electrical resistivity and transverse magneto-resistance measurements, the sample holder (SH1) was made of a (~ 5 cms) long cylindrical copper block. Around 0.5 cms width of this copper block was machined to provide a plane rectangular surface which provides a good thermal contact to the specimen. A thin layer of araldite was coated on this surface to insulate the specimen electrically from the copper block. Arrangement was made to attach a copper-constantan thermocouple (CCT) to this copper block for temperature measurements between 77 and 300K. A hole along the axis of the cylinder was machined for its attachment to the main tubing system [see Fig. 3.2.a].

For longitudinal magnetoresistance measurements a similar cylindrical copper block (SH2) of ~ 3.5 cm length was used. All other arrangements were same except the fact that the hole for attaching sample holder to the main tubing system was made perpendicular to axis of the cylindrical block (Fig. 3.2.b).

A fibre glass reinforced plastic sample holder (SH3) was specially designed for the Hall effect measurements. As shown in Fig. 3.2.c the upper portion of this ~ 2 inch piece was filed to get a plain base for mounting the sample. Two copper strips were attached to this sample holder to provide pressure contacts for the current probes. Two other similar plastic

SH 1

Hole for
Thermocouple
(CCT)

(a)

SH 2

(b)

SH 3

(c)
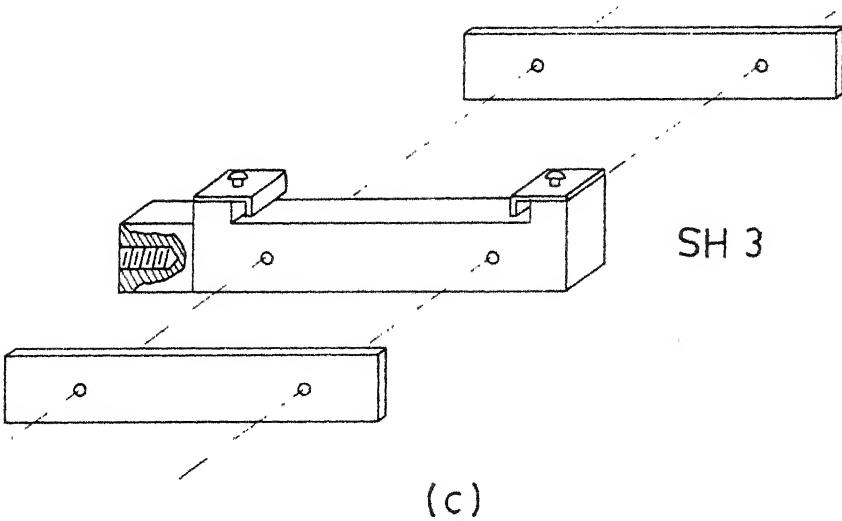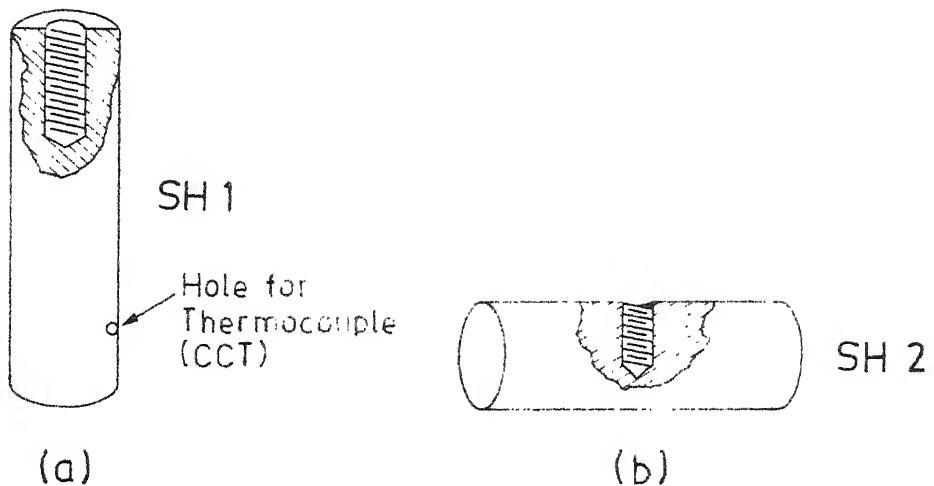
FIG. 3.2

pieces were used to hold the voltage probes against the sample by pressure. Arrangements were made to screw this sample holder to the main tubing system.

Depending on the experiment, the particular type of sample holder was attached to a thin walled non-magnetic stainless steel tube T (Fig. 3.1) of 3/8" diameter through a copper spacer (CS). The tail of this copper spacer has screw threads on it. This tube extends slightly beyond the top plate of the cryostat. The three current leads (2 for connecting to the specimen and 1 extra) with the thermocouple wires (CCT) and the four voltage leads (2 for connecting to the specimen and 2 extra) were put in two different plastic sleeves. These sleeves were taken out for the connection of the leads to the specimen through a hole made on one end of this tube T. The other end of this tube was vacuum sealed with black wax (manufactured by CENCO, USA). This assembly (the tubing system and the sample holder SH attached to it) is surrounded by a copper cryostat C of 4 cms diameter connecting the sample chamber to the vacuum line.

The electrical leads used in the sample holder assembly are of copper. The sample current leads are of 26 gauge which can carry a current upto 1 ampere. The voltage leads are multistrand 40 gauge copper wires. The electrical leads to the sample were soldered to the sample (wherever needed) with a low melting point Cerroseal-35 solder.

The top of the cryostat C is made of brass. A schematic diagram of the cryostat assembly, which fits into a liquid nitrogen dewar, is shown in Fig. 3.3.

3.2 MEASURING CIRCUIT

The detailed block diagram of the measuring circuit is shown in Fig. 3.4. This circuit can measure as small a voltage difference as 0.01 μV and voltage changes of 5 ppm could be detected in these samples. Care was taken to minimise electrical noise and thermal fluctuations in the system. In order to minimise the thermoelectric voltages, thin, long single wires, without any soldered joint, were used as voltage leads. These voltage leads were again directly connected to the voltage circuit, avoiding any soldering. The measuring circuit could be divided into two parts.

(a) Constant Current Circuit :

A constant current of 50 to 100 mA was drawn from a 500 mA/50 volts Model 6177C Hewlett Packard precision constant current source. The current stability was found to be better than 0.001%. In this circuit a Leeds and Northrup (L and N) standard resistance R (1 Ω) and a L and N commutator was used, as shown in the circuit diagram. A digital multimeter was connected to read the voltage drop across the 1Ω resistance and hence the current flowing through the sample. The current could also be measured by finding out the voltage
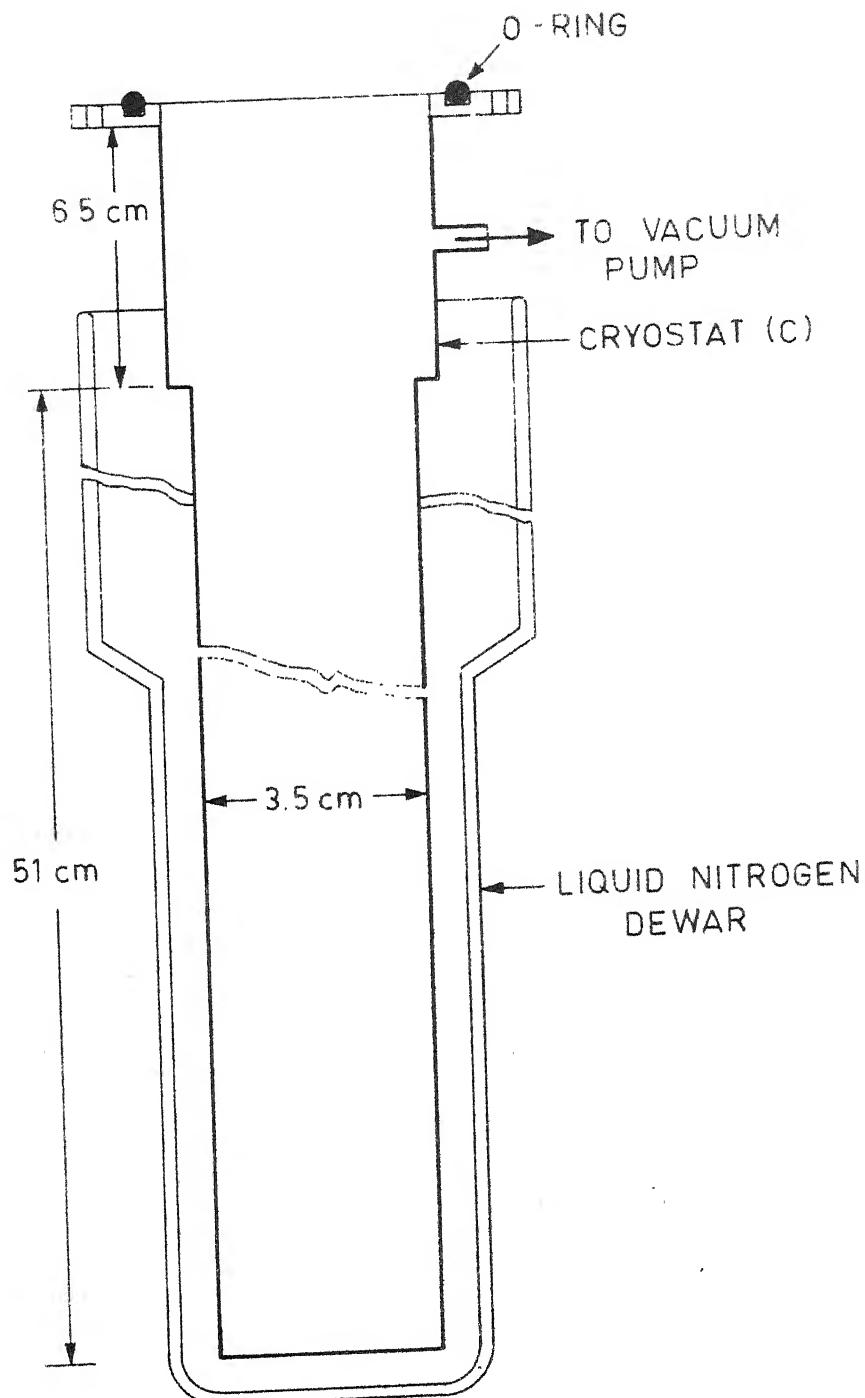
THE CRYOSTAT AND THE LIQUID NITROGEN
DEWAR ASSEMBLY.

FIG. 3.3

drop across R with the help of an L and N K-3 potentiometer and a model 148 Keithley nanovoltmeter (details given in the next paragraph). Using the reversing switch, we could reverse the current direction with the help of the commutator as shown in Fig. 3.4.

(b) Voltage Circuit :

The zero field voltage across the sample was measured by using a voltage compensation technique in the following manner. An L and N K-3 potentiometer which has a sensitivity of 0.5 microvolt was used as a standard voltage source. The voltage, V, due to the sample current, I, was compensated by adjusting the K-3 potentiometer, connected in series opposition. This resulting voltage was read on a model 148 Keithley Nanovoltmeter, which was used as a null detector. In this situation, the voltage read on the K-3 potentiometer was precisely the voltage drop, V, across the sample. To find out the current flowing through the sample the voltage drop across R = 1 Ohm was similarly found out. To minimise the fluctuations due to various pick-up voltages, proper care was taken to shield the wires in this circuit.

3.3 MEASUREMENT OF TEMPERATURE

The cryostat was evacuated with the help of a rotary pump. We could get a vacuum of $\sim$ 100 micron, which was sufficient for our measurements between $77K \leq T \leq 300K$. The

P   : K-3 Potentiometer (L & N)
RS   : Reversing Switch (L & N)
C   : Commutator (L & N)
PS   : DC Power Supply (Hewlett Packard)
DVM   : Digital Volt Meter (Keithley)
N/M VM : Nano/Micro Volt Meter (Keithley)
CL   : Current Lead
VL   : Voltage Lead
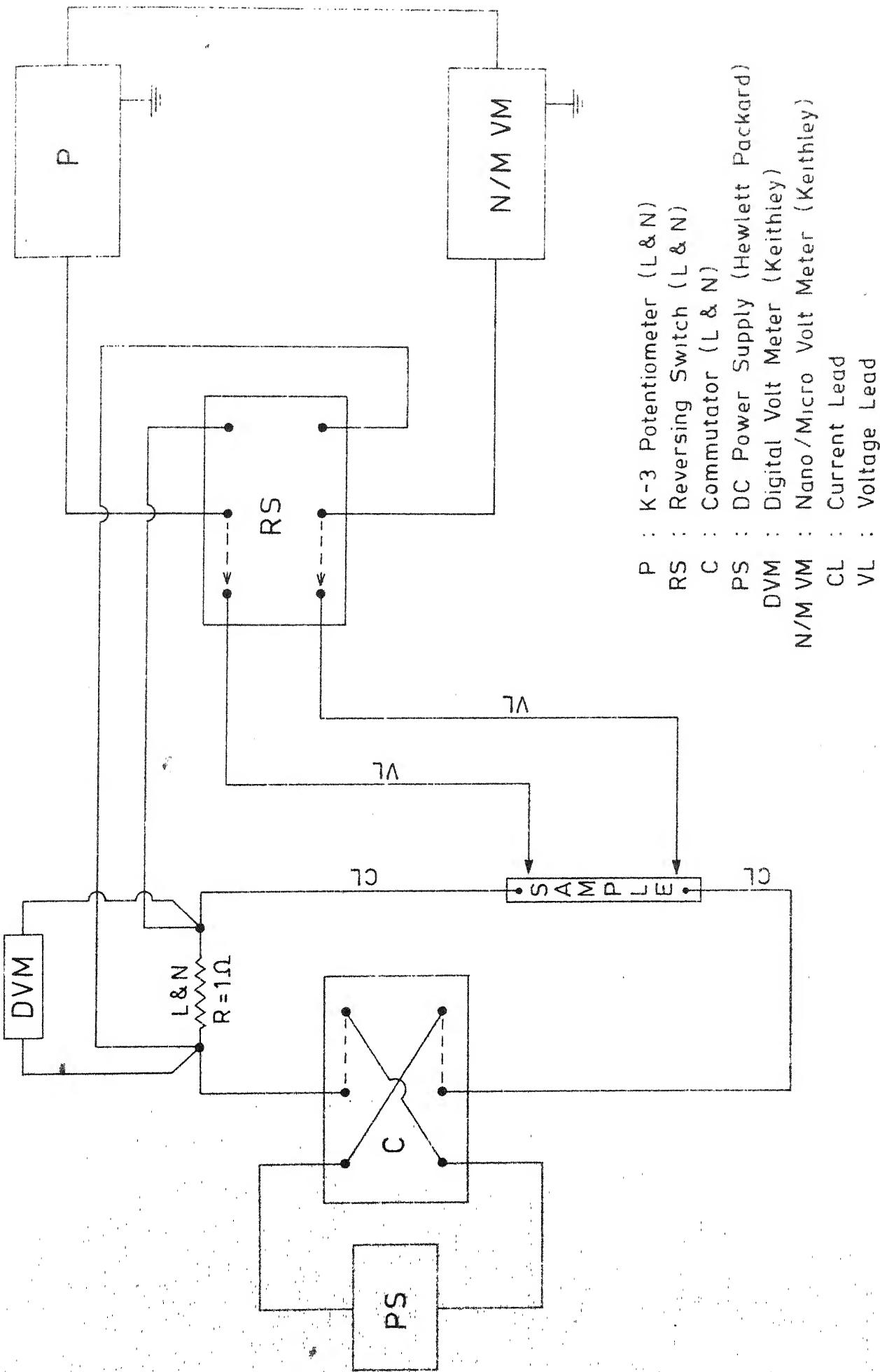
BLOCK DIAGRAM OF THE MEASURING CIRCUIT

FIG. 3.4

copper-constantan thermocouple was used for the measurement
of temperature in this range. The thermocouple voltage was
read on an L and N millivolt potentiometer.

3.4 MEASUREMENT OF ABSOLUTE VALUES OF RESISTIVITY ρ AT 300K

The absolute value of resistivity, ρ , at room temperature
(300K) was measured with the help of a Type 1608 A Impedance
Bridge (General Radio, U.S.A.). The accuracy of this bridge
is 0.1% when a resistance of 1Ω to 1 MΩ was measured. Around 2
to 4 cm in length of sample pieces were taken. These pieces
were then weighed on a Model 2006MP6E Saratorius electronic
balance which could weigh accurately upto 0.1 mg. Now the
resistance of these very sample pieces were directly read on
the impedance bridge. The density of these samples were taken
from the data of Hasegawa and Ray[109]. Thus, with the help
of the knowledge of resistance of a sample of known length,
weight and density, the resistivity could be calculated.

3.5 MEASUREMENT OF TEMPERATURE DEPENDENCE OF RESISTIVITY $\rho(T)$ (77K $\leq$ T $\leq$ 300K)

The samples were cut to ~15 mm length for the measurement
of temperature dependence of resistivity $\rho(T)$ between 77 and
300K. As described in Section 3.1, the sample was mounted on
the sample holder (SH1). The sample was free to expand on the
sample holder. The current and voltage leads were soldered
neatly on the sample with the special low-melting point soft
solder (Cerroseal-35) to prevent excessive heating of the

sample. The flux used was zinc chloride. The large copper chunk which was used as the sample holder, also served the purpose of a heat-sink for the sample. The copper-constantan thermocouple adhered to this heat-sink could measure the temperature of the sample quite accurately. The thermocouple wires were directly connected to a Leeds and Northrup (L and N) millivolt potentiometer, which could read the temperature correct upto 0.25K. The current and voltage lead connections were now made as shown in Fig. 3.4. The cryostat was evacuated (~ 100 micron) and then the system was ready for measurement. A sample current of ~100 mA was passed through the sample. At room temperature (300K) the sample voltage (~ 100 mV) was compensated by adjusting a L and N K-3 potentiometer (see Sec. 3.2), put in series opposition and using a digital voltmeter (Keithley Model 174, sensitivity 0.1 µV) as a null detector. Now the liquid nitrogen was transferred to the dewar, surrounding the cryostat. As the sample was cooled the change in resistivity was directly read on the digital voltmeter and the corresponding thermocouple voltage was simultaneously recorded from the millivolt potentiometer. The heating data were also taken in a similar manner. In the present set up a resistance change of a few parts in 10^6 could be detected. The dimension measurements were unnecessary because finally the ratio of resistivity ρ_T at a particular temperature T and the resistivity at room temperature ρ_{RT} , i.e., ρ_T / ρ_{RT} was plotted against temperature.

3.6 MAGNETORESISTANCE MEASUREMENT

The ferromagnetic anisotropy of resistivity (FAR) at 300 and 77K were measured by the usual four probe d.c. method. For transverse magnetoresistance measurements the sample was mounted on the sample solder SH1 and for the longitudinal measurement it was mounted on SH2. The 2 current and 2 voltage probes were soft soldered to the sample. The usual current and voltage lead connections were made as given in Sec. 3.2. The whole system was now kept in a magnetic field. The magnet used in the present study was a Varian 15" electromagnet, fed by a VFR-2703 highly stable power supply. This gives a magnetic field upto 18 ~ 20 kG. For both the transverse and longitudinal measurements the orientation was such that the field applied (H_{ext}) was parallel to the ribbon plane. The reason for keeping such an orientation is to minimise the effect of the demagnetizing field (see Appendix 2). Another point which was taken care of was the alignment of the sample with respect to the magnetic field. This plays an important role at low fields. If the sample is misaligned, the transverse magnetoresistance at low fields showed a positive value, as observed by many other workers[75,77,110] (see discussion in Chap. V). Keeping all these points in mind, the sample was mounted in such a way that it was lying exactly parallel to the cylindrical axis of the sample holder (SH1). In this way, when the system was mounted inside the magnet pole-pieces in the proper orientation

(H_{ext} parallel to ribbon plane) and a current was passed along its length, the right alignment condition (current I perpendicular to H_{ext} and H_{ext} lying in the ribbon plane)was automatically satisfied.

A current of ~ 50 mA was then passed through the sample (except for $Fe_{87}B_{13}$, which was very thin, lower current ~10 mA was used to avoid the fluctuations due to excessive heating of the sample). The zero field voltage was compensated by the K-3 potentiometer and then the small change in voltage due to magnetic field was directly read on a nanovoltmeter, as stated earlier.

For measurements at 77K, as described in Sec. 3.2 and Sec. 3.3, the system was evacuated and kept in a dewar containing liquid nitrogen. When the system reached this liquid nitrogen temperature (77 K), similar measurements, as stated above, were repeated.

In this measurement, the system could detect changes of resistivity of about a few parts per million.

3.7 HALL EFFECT MEASUREMENTS

The sample was mounted on the sample holder (SH3). The current leads were soldered to the copper strips used as the pressure contact probes for this sample holder. Because of the irregularity of the width of these samples, it was very

difficult to use pressure contact for both the Hall voltage probes. Also, the samples being very thin were forming a ridge if the pressure was applied from both sides, across the width of the sample. So, one of the voltage probes was soft-soldered and a pressure contact was used for the other to minimise the misalignment voltage. Now, this sample holder, enclosed in a cryostat was placed in the electromagnet, in such a way that the applied field, H_{ext}, was perpendicular to the sample plane. This orientation of the sample was necessary to get the Hall voltage along the width of the sample. Also, in this orientation, the magnetic induction inside the sample, B_{in} becomes equal to the applied field H_{ext}.

$$B_{in} = H_{in} + M_s \, ,$$

where M_s is the saturation magnetization and H_{in} is the internal field. Or,

$$B_{in} = (H_{ext} - \alpha \, M_s) + M_s,$$

where α is the demagnetizing factor. Or,

$$B_{in} = H_{ext} + M_s(1-\alpha) \, .$$

In this particular orientation used for this measurement $\alpha \simeq 1$. Hence,

$$B_{in} = H_{ext}.$$

Now, for Hall measurements, we did not use the K-3 potentiometer shown in Fig. 3.4. Instead, the Nanovoltmeter was directly connected to the reversing switch. The K-3 potentiometer was not needed, because the Hall voltages for these samples were quite large, as compared to the changes due to magnetoresistance at higher fields. In zero field if the Hall contacts are not aligned perfectly so as to coincide with the opposite ends of the same equipotential line, an ohmic voltage drop proportional to the sample current will be measured. So, the misalignment voltage was first minimised by sliding one of the voltage probes slightly along the length, by trial and error. Then, the effect of the remaining spurious ohmic drop was eliminated by making the Hall voltage measurements under the reversal of magnetic field. Also, the sample current was reversed to eliminate spurious thermal voltages. The actual Hall voltage obtained then is,

$$V_H = 1/4[V(H_+,I_+)+V(H_-,I_-)-V(H_+,I_-)-V(H_-,I_+)]$$

It is evident that the ohmic drop will be eliminated by this procedure, since the Hall voltage changes sign if either current or field is reversed, while the ohmic drop changes sign only when current is reversed.

The Hall measurements were repeated on the same sample several times and the sample to sample variation was also checked. Within experimental error, these data were found to be

quite reproducible.   Finally, for Hall resistivity ρ_H $(= \dfrac{V_H t}{I}$, where t is the thickness of the samples and I is the current flowing through the sample), the thickness of the samples were measured with the help of a micrometer (least-count = 0.0001 inch).

For the measurements at low temperatures (77 K) the cryostat was evacuated and surrounded by a liquid nitrogen dewar. Similar measurements were repeated when the desired temperature was attained and the system was stable.

3. 8 MEASUREMENT OF RESISTIVITY BETWEEN 4.2 K and 77 K

We measured the variation of resistivity with temperature between 4.2 and 77 K at the Tata Institute of Fundamental Research, Bombay, using their experimental facility. The experimental procedure could be summarised as follows :

(a) The cryostat used in the present measurement was inserted to a liquid helium dewar and this in turn to a liquid nitrogen dewar. The latter provides a thermal shielding to the liquid helium. On the top of the cryostat provision was made for (i) transferring liquid helium (ii) inserting the sample chamber and (iii) recovery of the gas and pumping of the vapour to go below 4.2 K.

(b)   The sample chamber was a double-walled system. Arrange-
      ments were made to flow exchange gas in the space between
      the outer tube and the outer wall of the inner tube and
      also to pump this gas out. The sample chamber could be
      evacuated down to 1 micron with the help of a suitable
      mechanical pump.

(c)   The sample holder was made of a rectangular copper strip
      (~ 5 cms in length). A manganin heater wire was wound
      at the lower part of this sample holder. A precalibrated
      silicon diode sensor (Lake Shore Cryotronics, USA) was
      encapsulated in the sample holder. The merit of this
      sensor is that it can scan a very wide range of temperature,
      from 1.5 to 300K.

(d)   The samples, in the form of thin long ribbons, were mounted
      on the sample holder. The current and voltage leads were
      soldered first by using Cd-Sn (Cd-70%, Sn30%) solder. This
      solder has a melting point ~150°C and is nonsuperconduct-
      ing down to 3.5K (flux used was $ZnCl_2$). A scattering of
      data points near the liquid helium temperature was observed
      when the sample was soldered with the help of this solder.
      To avoid this problem around 4.2K (probably due to the
      superconductivity of the solder material) another soldering
      material Bi-Cd (60% Bi,40% Cd) was used (flux used for
      this was also $ZnCl_2$) in the next set of measurements. This
      solder has a lower melting point ~ 140°C and is
      nonsuperconducting down to 0.8K.

(e) The measuring circuit was principally similar to the one
described in Sec. 3.3.2. A Hewlett-Packard 250 mA power
supply was used as a constant current source and the vol-
tages at particular temperatures were read directly on a
Keithley digital Nanovoltmeter. To control the tempera-
ture of the sample, a Lake Shore Cryotronics temperature
controller was used and the voltage corresponding to the
temperature was read directly on a 5.5 digit voltmeter
of Datron Instruments, U.K.

CHAPTER   IV

EXPERIMENTAL   RESULTS

The present study comprises of the measurements of :

i)   Variation of electrical resistivity ρ with temperature T
      in two metallic glass series - (a) $Fe_{100-x}B_x$ ($13 \leq x \leq 26$),
      and (b) $Fe_{80}B_{20-x}Si_x$ ($o \leq x \leq 12$),

ii)   Variation of electrical resistivity ρ with concentration
      x in $Fe_{100-x}B_x$ series,

iii) Variation of ferromagnetic anisotropy of resistivity (FAR)
      with concentration x in $Fe_{100-x}B_x$ series, and,

iv)   Concentration (x) dependence of spontaneous Hall constant
      R_s in $Fe_{100-x}B_x$ series.

All these measurements, except the resistivity variation with T
in Fe-B-Si series, were made in the temperature range of 77 to
300K.   The ternary series was studied in the temperature range
of 4.2 to 300K.

4.1 VARIATION OF RESISTIVITY WITH TEMPERATURE

The general behaviour of electrical resistivity as a
function of temperature is the same in all the samples.   In
Fig. 4.1 we have plotted the ratio of resistivity at any
temperature T and that at room temperature, ρ_T/ρ_{RT}, against T
in the temperature range $80K \leq T \leq 300K$ for the samples in

RESISTIVITY OF METALLIC GLASSES vs TEMPERATURE

Legend:
- △ $Fe_{84}B_{16}$
- ○ $Fe_{80}B_{20}$
- □ $Fe_{87}B_{13}$
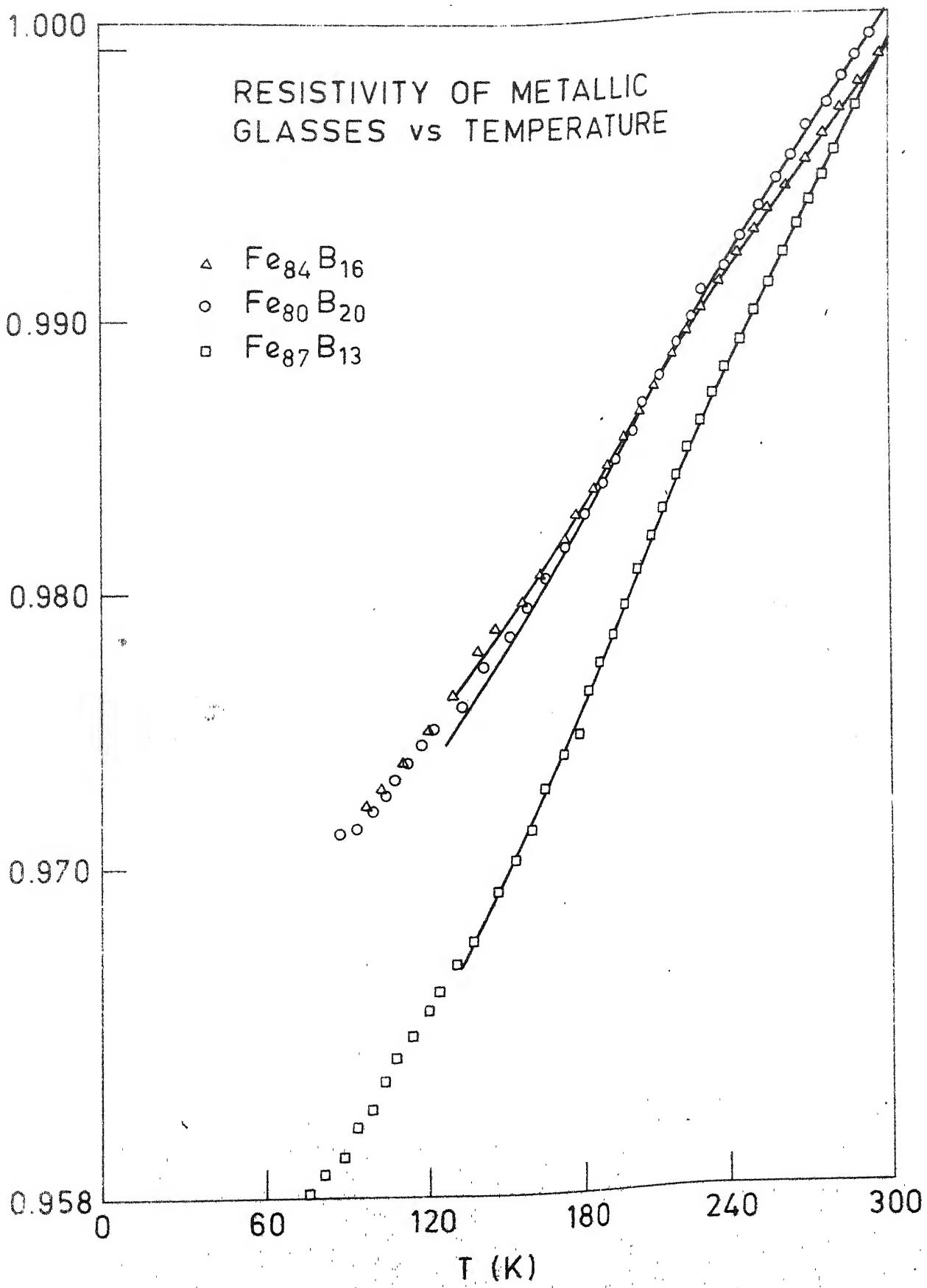
FIG. 4.1

$Fe_{100-x}B_x$ series. The plots of ρ_T/ρ_{RT} against T in the temperature range $4.2K \leq T \leq 300K$ for some of the $Fe_{80}B_{20-x}Si_x$ samples are shown in Fig. 4.2. It is clear from these figures that the resistivity varies linearly in the temperature range $150K \leq T \leq 300K$, below about 150K there is a departure from linearity. In both the heating and the cooling cycles measurements were repeated at least 2-3 times for each sample. Different pieces of the same composition were also measured in a few cases to check for the inaccuracy arising from sample to sample variation. The temperature coefficient of resistivity α (the high temperature slope of the ρ_T/ρ_{RT} vs T graph) is positive over the entire range of x and is reproducible within the error limits. The percentage change of resistivity $\Delta\rho/\rho$ can be found out directly from the ρ_T/ρ_{RT} versus T plots. Fig. 4.3 shows the quadratic behaviour of resistivity at low temperatures ($80K \leq T \leq 150K$) for all the $Fe_{100-x}B_x$ samples. Similarly, Fig. 4.4 shows the ρ_T/ρ_{RT} versus T^2 plot for all the seven samples in $Fe_{80}B_{20-x}Si_x$ samples in the temperature range $80K \leq T \leq 105K$.

In Table 4.1, we have listed the composition, crystallization temperature T_{cr}, the percentage change of resistivity $\Delta\rho/\rho$ in the temperature range $80K \leq T \leq 300K$, α and Debye temperature Θ_D for all the $Fe_{100-x}B_x$ ($13 \leq x \leq 26$) alloys. The large error in Θ_D is introduced because of the uncertainty in the determination of the slope S of ρ_T/ρ_{RT} vs T^2 plots in this

RESISTIVITY OF METALLIC GLASSES
vs TEMPERATURE

- ● $Fe_{80}B_{19}Si_1$
- ○ $Fe_{80}B_{16}Si_4$
- △ $Fe_{80}B_8Si_{12}$

FIG. 4.2

QUADRATIC BEHAVIOUR OF RESISTIVITY OF METALLIC GLASSES.

FIG. 4.3

QUADRATIC BEHAVIOUR OF RESISTIVITY OF METALLIC GLASSES.
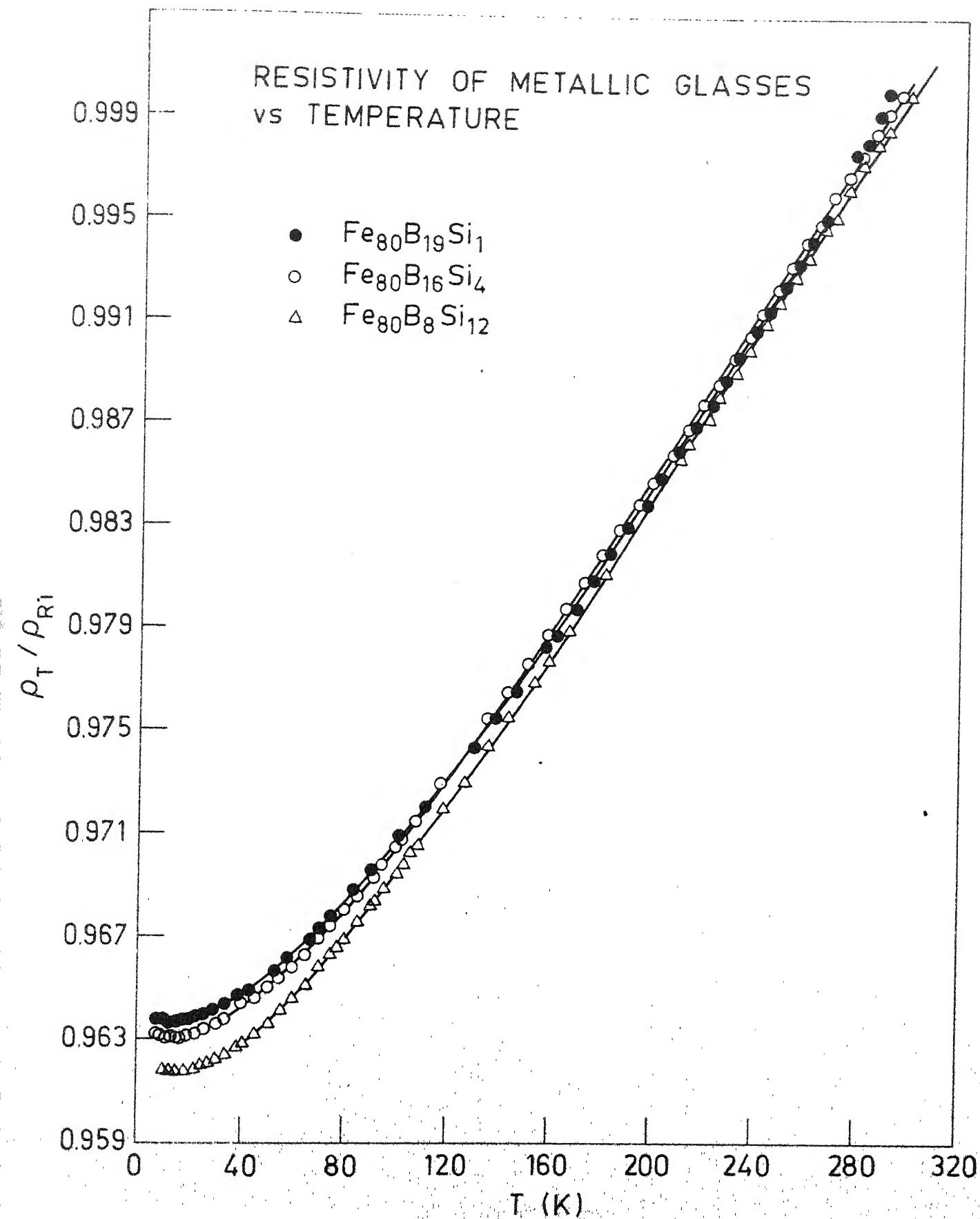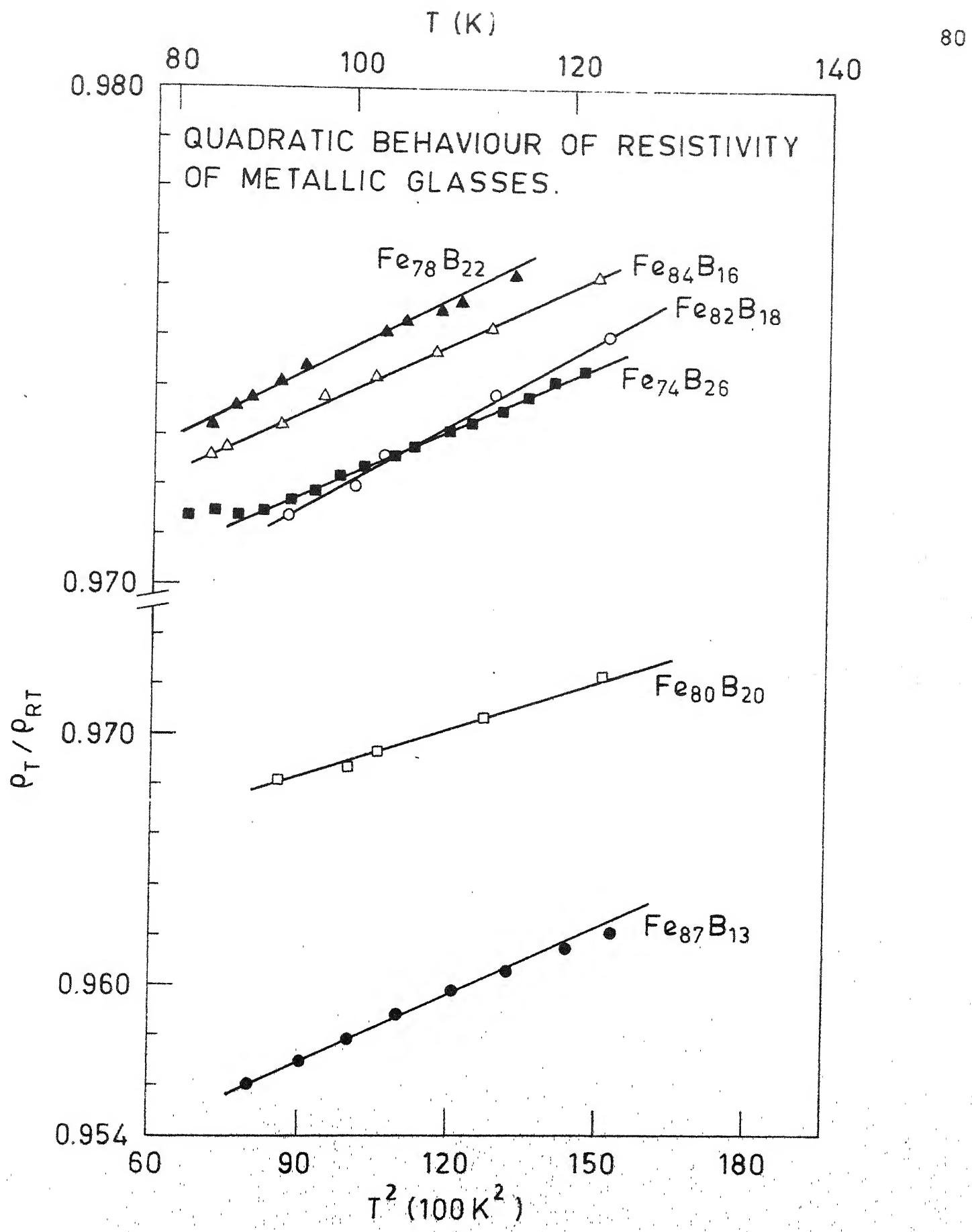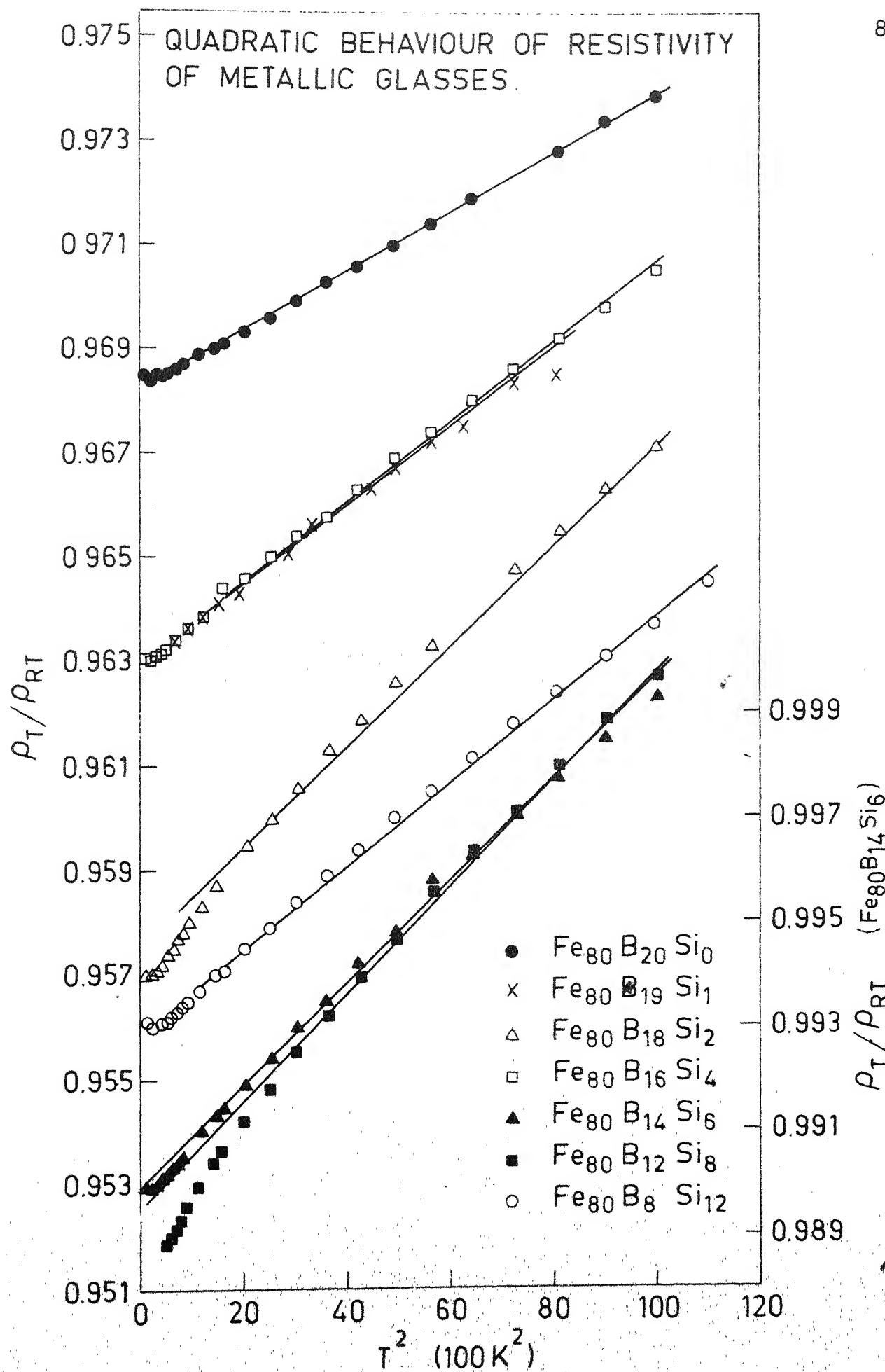
FIG. 4.4

temperature range, as discussed in the next chapter. Table 4.2 gives the composition, $\Delta\rho/\rho$ in the temperature range $4.2K \leq T \leq 300K$, α and Θ_D for all the $Fe_{80}B_{20-x}Si_x$ ($0 \leq x \leq 12$) samples. As can be noticed from these tables, the error in the Θ_D values in $Fe_{80}B_{20-x}Si_x$ series is much less than that in the $Fe_{100-x}B_x$ series.

In Fig. 4.5, we have shown the boron concentration (x) dependence of α, $\Delta\rho/\rho$ in the Fe-B series. Fig. 4.6 similarly shows the dependence of α and $\Delta\rho/\rho$ on the silicon concentration x in $Fe_{80}B_{20-x}Si_x$ series. In $Fe_{100-x}B_x$ both α and $\Delta\rho/\rho$ versus x plots show an abrupt fall in going from x = 13 to x = 16 and then they are more or less independent of x for $16 \leq x \leq 26$. About $Fe_{80}B_{20-x}Si_x$ series one can say that the α value does not change appreciably by replacing one metalloid by another and $\Delta\rho/\rho$ increases first from x = 0 to x = 1 and then remains constant in the range ($1 \leq x \leq 12$).

Figs. 4.7 and 4.8 show the variation of Θ_D with concentration x in $Fe_{100-x}B_x$ ($13 \leq x \leq 26$) and $Fe_{80}B_{20-x}Si_x$ ($0 \leq x \leq 12$) series respectively.

4.2 VARIATION OF RESISTIVITY WITH CONCENTRATION x in $Fe_{100-x}B_x$

In Fig. 4.9 we have plotted the absolute value of resistivity ρ at 300K against x, the boron concentration, for $Fe_{100-x}B_x$ ($13 \leq x \leq 26$) series. It is clear from this figure

VARIATION OF α AND $\Delta \rho / \rho$ WITH BORON CONCENTRATION IN $Fe_{100-x}B_x$

FIG. 4.5

BORON CONCENTRATION x (at. %)

$\Delta \rho / \rho$ (%)
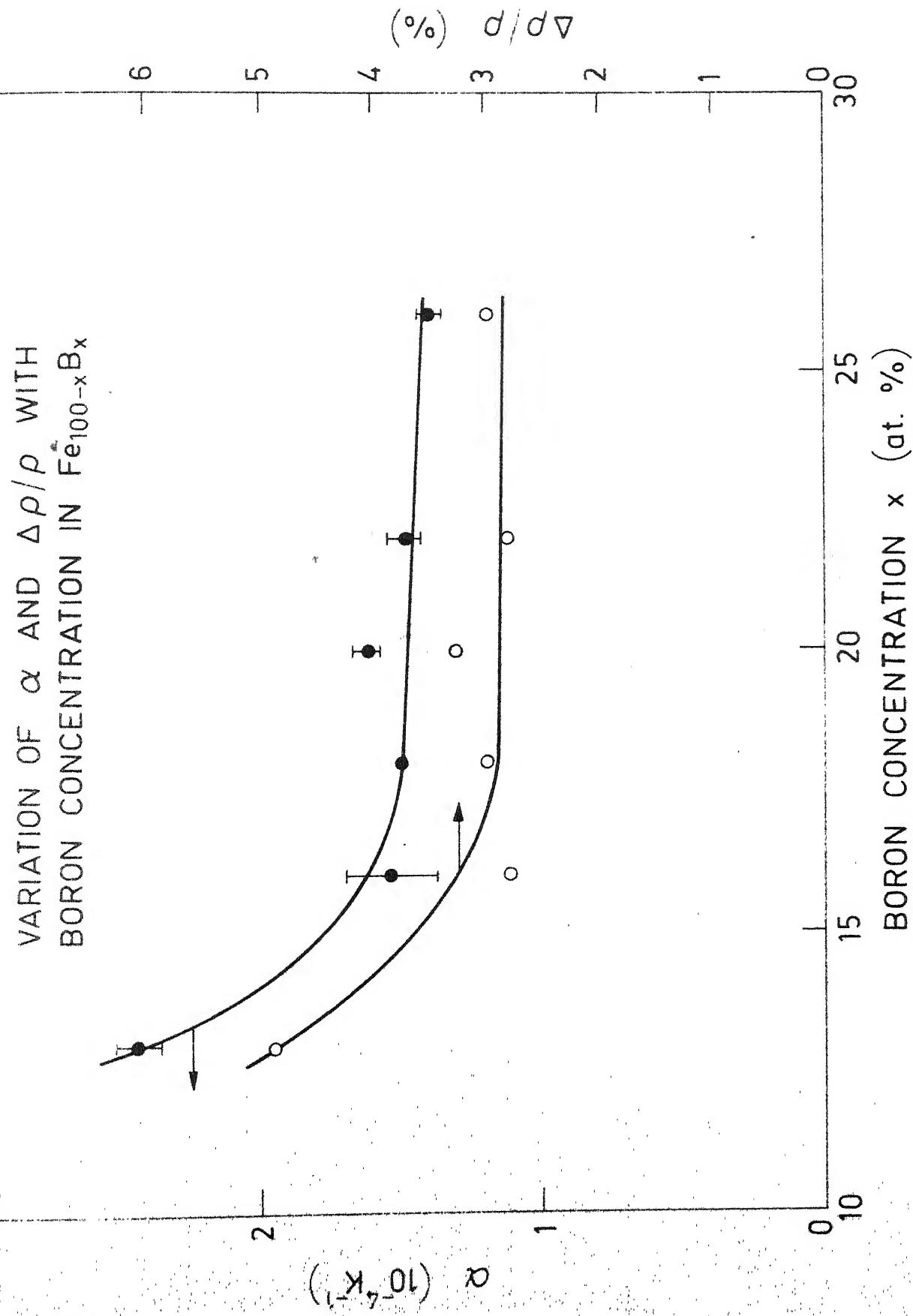
α ($10^{-4} K^{-1}$)

VARIATION OF α AND $\Delta\rho/\rho$ WITH SILICON CONCENTRATION IN $Fe_{80}B_{20-x}Si_x$
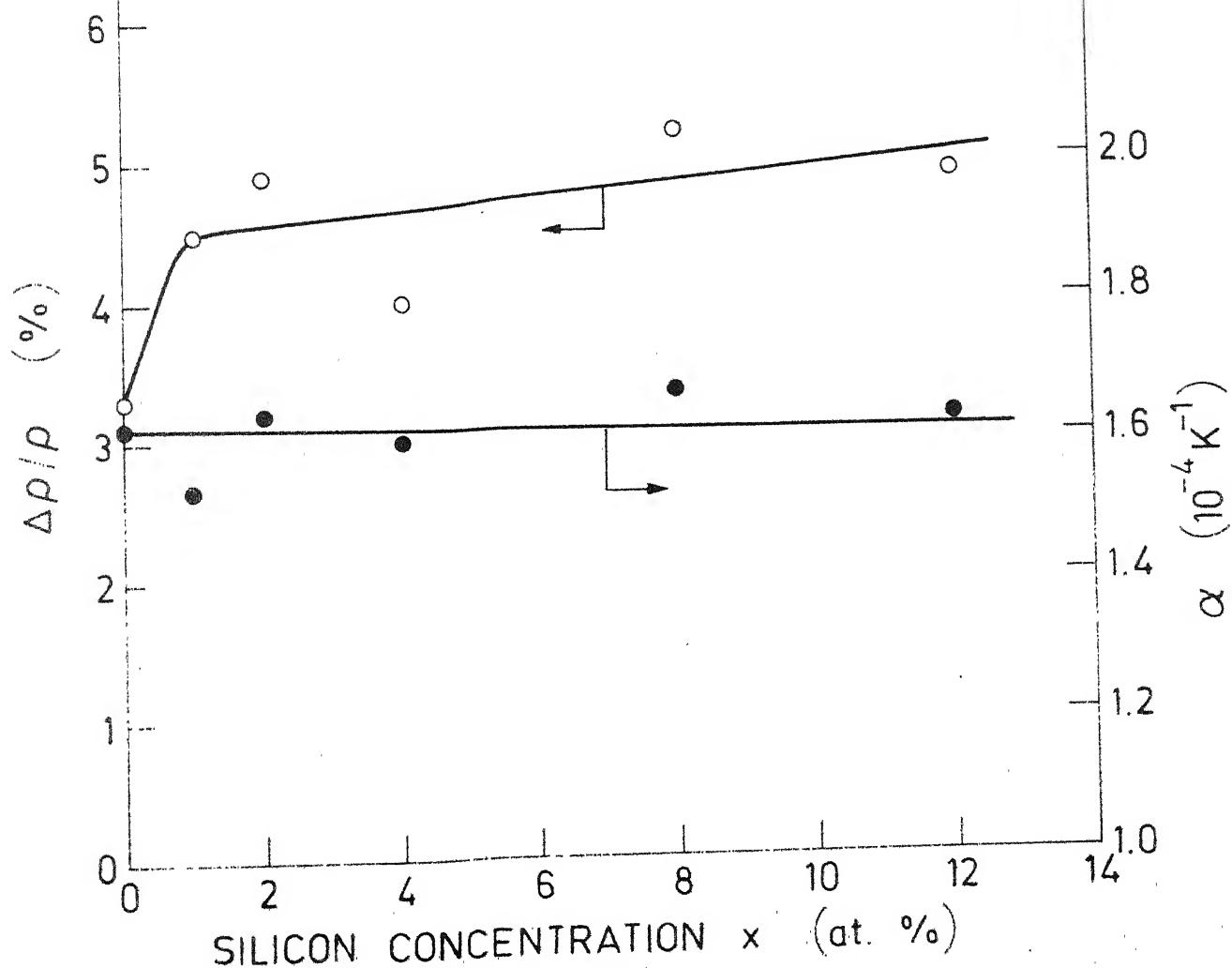
FIG. 4.6

θ_D vs BORON CONCENTRATION IN $Fe_{100-x}B_x$
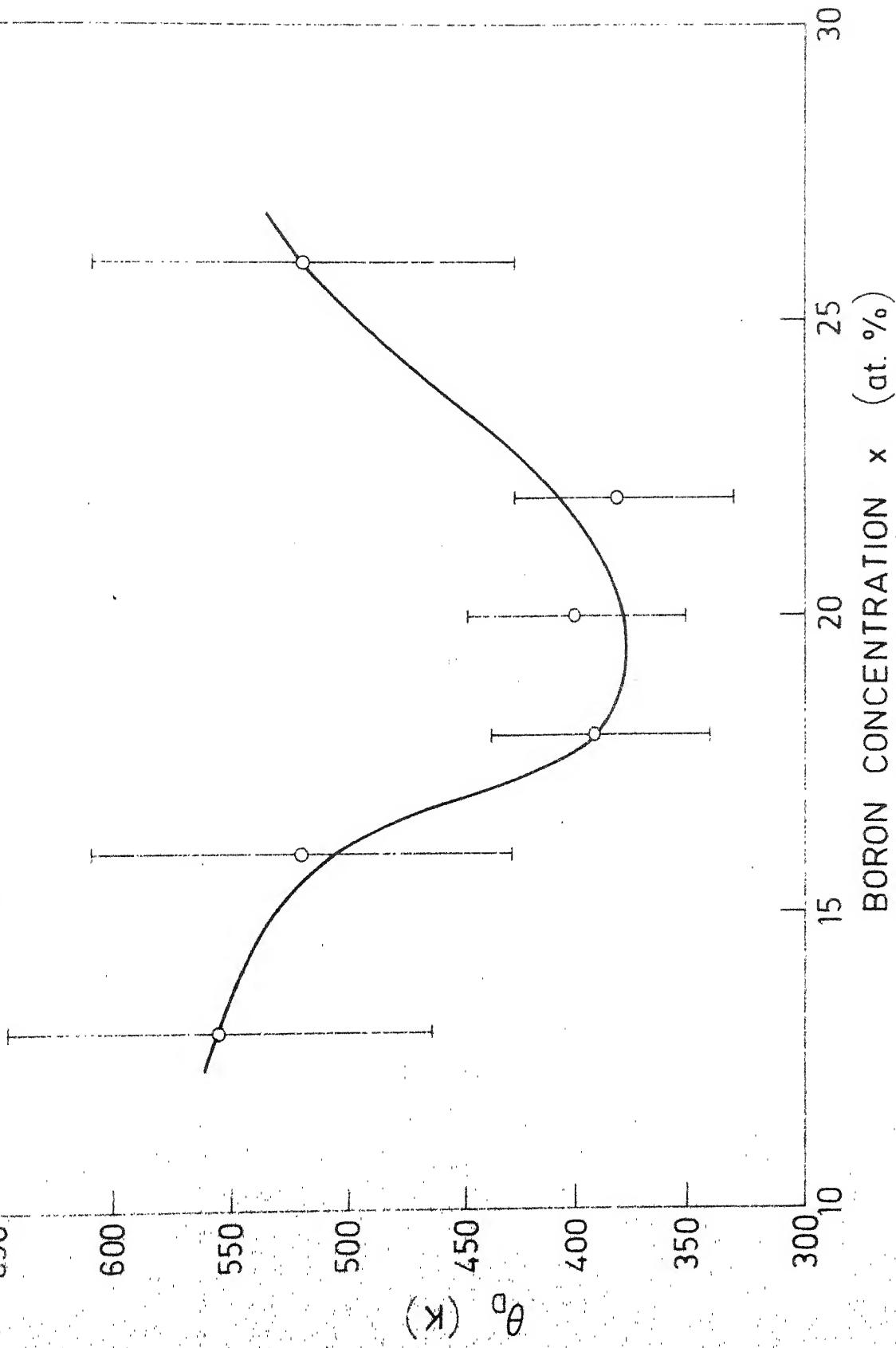
FIG. 4.7
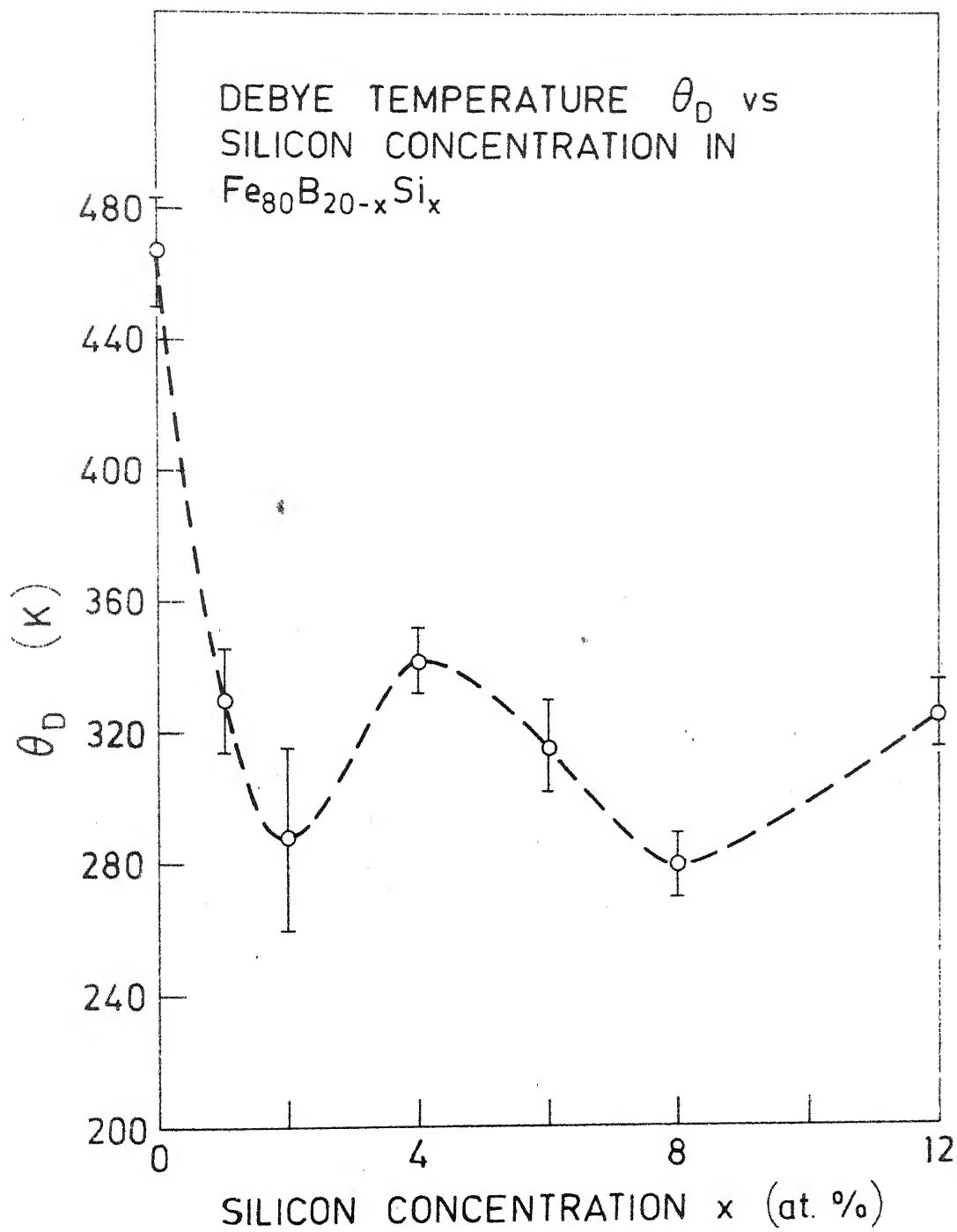
FIG. 4.8

Table 4.1

Values of T_{cr}, $\Delta\rho/\rho$, α and Θ_D in $Fe_{100-x}B_x$ $(13 \leq x \leq 26)$
series in the temperature range $80K \leq T \leq 300K$

Composition	$T_{cr}(K)$	$\Delta\rho/\rho$ (%)	$\alpha(10^{-4}K^{-1})$	$\Theta_D(K)$
$Fe_{87}B_{13}$	586	4.9	2.43 ± 0.07	555 ± 90
$Fe_{84}B_{16}$	643	2.8	1.53 ± 0.15	520 ± 90
$Fe_{82}B_{18}$	660	3.0	1.49 ± 0.01	390 ± 50
$Fe_{80}B_{20}$	660	3.3	1.62 ± 0.04	400 ± 50
$Fe_{78}B_{22}$	666	2.8	1.49 ± 0.06	380 ± 50
$Fe_{74}B_{26}$	688	3.0	1.40 ± 0.04	520 ± 90

Table 4.2

Values of $\Delta\rho/\rho$, α and θ_D in $Fe_{80}B_{20-x}Si_x$ ($0 \leq x \leq 12$)
series in the temperature range $4.2K \leq T \leq 300K$

Composition	$\Delta\rho/\rho$ (%)	$\alpha(10^{-4}K^{-1})$	$\theta_D(K)$
$Fe_{80}B_{20}$	3.3	1.62 ± 0.04	467 ± 17
$Fe_{80}B_{19}Si_1$	4.5	1.53 ± 0.02	330.8 ± 16
$Fe_{80}B_{18}Si_2$	4.9	1.64 ± 0.04	284 ± 28
$Fe_{80}B_{16}Si_4$	4.0	1.60 ± 0.02	341.5 ± 10
$Fe_{80}B_{14}Si_6$		1.84 ± 0.02	315 ± 14
$Fe_{80}B_{12}Si_8$	5.2	1.665 ± 0.02	280 ± 10
$Fe_{80}B_8Si_{12}$	4.9	1.625 ± 0.02	326 ± 10

that the experimental data show an increase of ρ with increasing boron content. As mentioned in Sec. 3.4, the accuracy with which the absolute value of resistance was measured is quite high. In fact, repeated measurements on the same piece and also on different pieces of the same sample, showed similar values within the experimental error limits. The main error of 3% ~ 15% in the determination of absolute value of resistivity was introduced from the inaccuracy involved in the measurements of the length and weight of the samples. The details of these measurements (including the percentage error introduced by each measurement) with the error limits are tabulated in Table 4.3. We have also estimated the values of resistivity of each sample theoretically with the help of eqn. (2.15) and this will be discussed later in Chapter V.

Fig. 4.9 shows the plot of the theoretical values of ρ as a function of boron concentration x. The monotonic increase in the absolute value of the **resistivity** with increasing metalloid concentration is clearly reflected in the theoretical curve.

4.3 MAGNETORESISTANCE MEASUREMENTS IN $Fe_{100-x}B_x$

In Fig. 4.10 we have shown some typical results of our magnetoresistance measurements. In ferromagnetic pure metals and dilute alloys around 4K the ferromagnetic anisotropy of resistivity is generally masked by the so-called normal positive

Table 4.3

Values of resistivity ρ of $Fe_{100-x}B_x$ $(13 \le x \le 26)$ series
with detailed information of experimental errors

Sample	Resistance, $R(\Omega)$	Weight, $M(10^{-3}g)$	Density, $D(g/cm^3)$	Length, $L(cms)$	$\rho(10^{-6}\Omega m)$
$Fe_{87}B_{13}$	4.278	4.15±0.04	7.44	4.285±0.1	1.3±0.04
$Fe_{84}B_{16}$	3.727	4.45±0.22	7.43	3.924±0.1	1.45±0.12
$Fe_{82}B_{18}$	1.663	15.68±0.31	7.42	4.468±0.09	1.74±0.07
$Fe_{80}B_{20}$	2.032	7.57±0.05	7.40	3.790±0.10	1.45±0.04
$Fe_{78}B_{22}$	3.700	4.7 ±0.20	7.30	3.43 ±0.10	2.03±0.14
$Fe_{74}B_{26}$	3.089	2.95±0.30	7.16	2.42 ±0.10	2.07±0.31
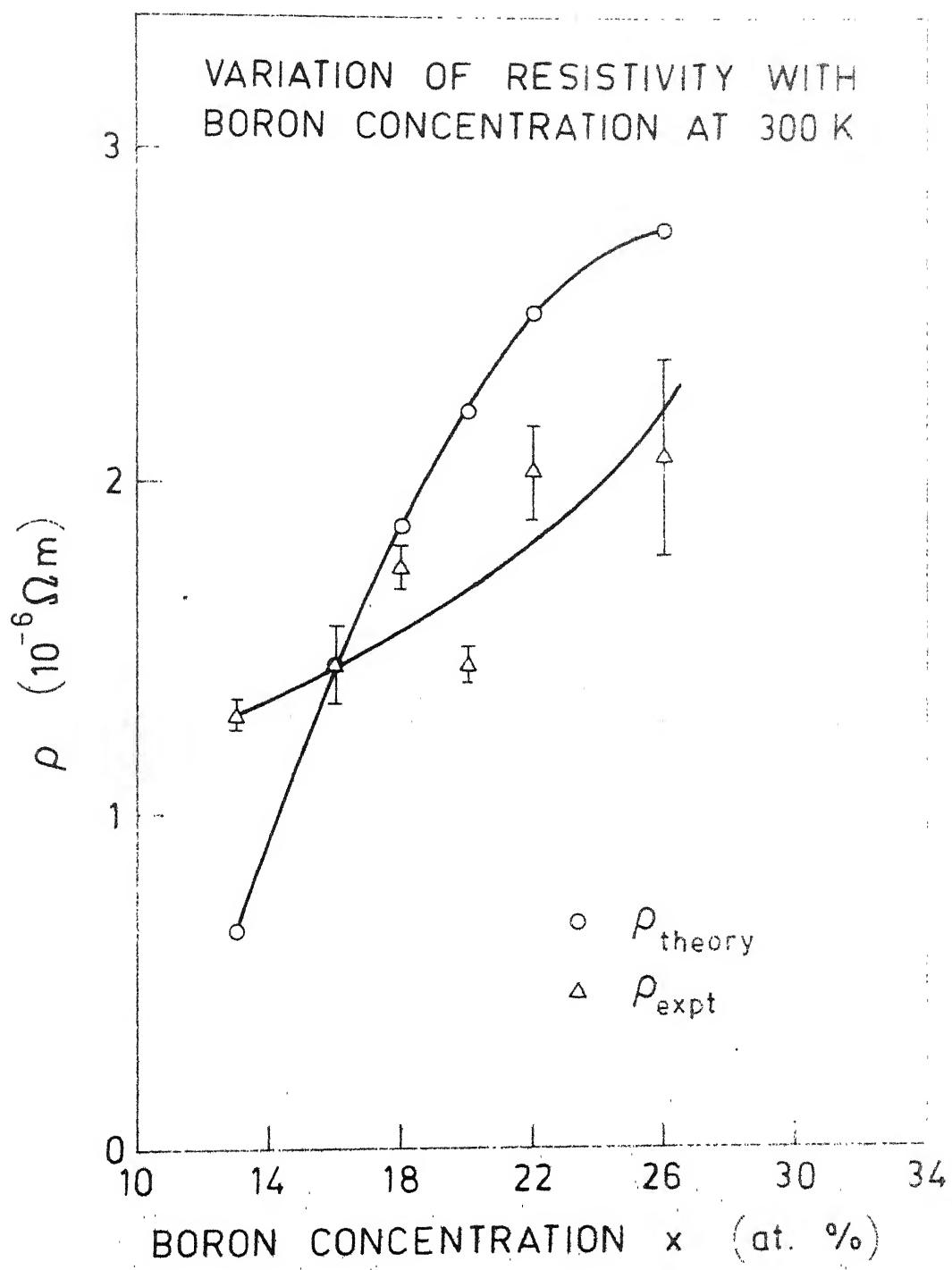
FIG. 4.9
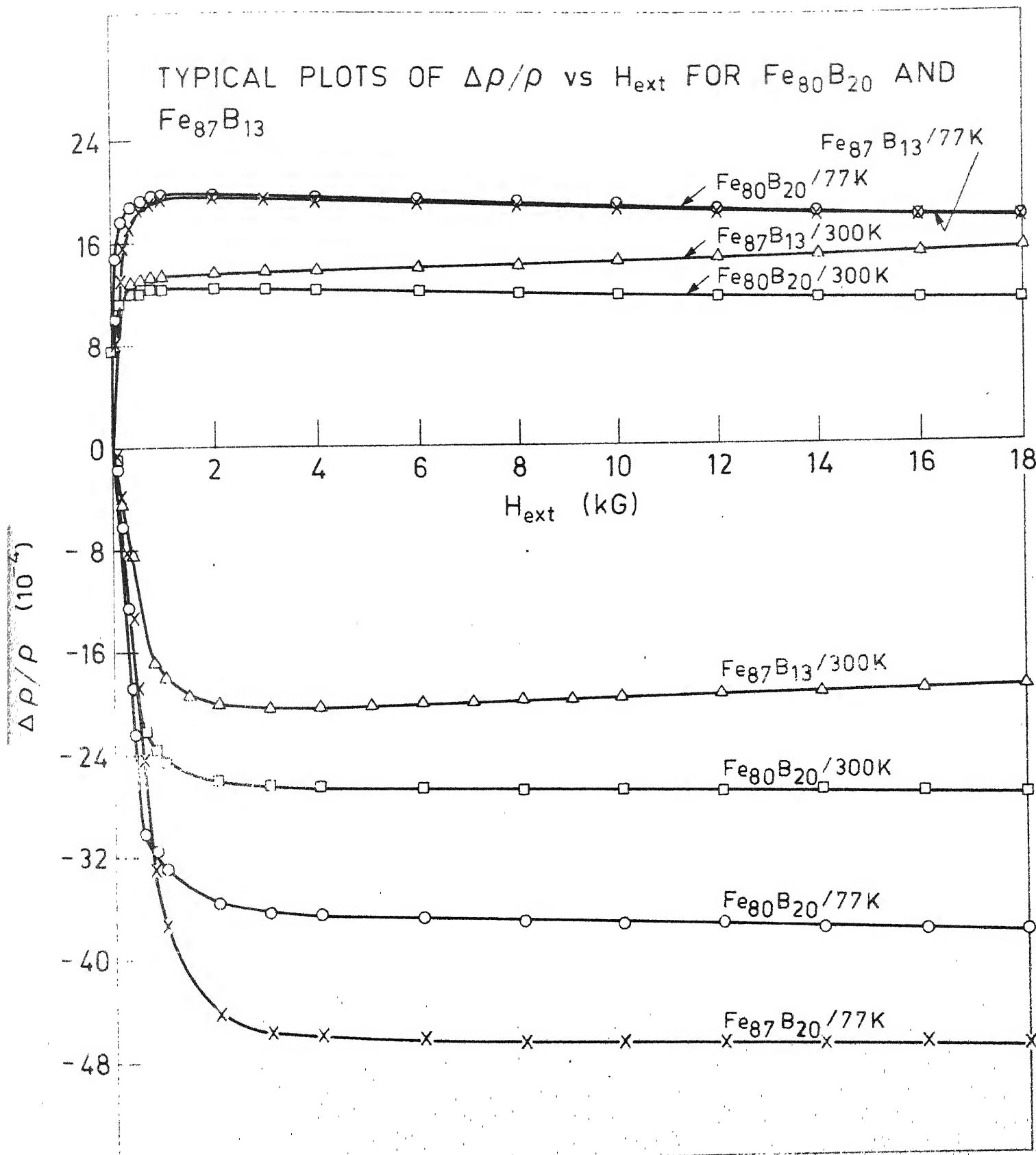
FIG. 4.10

magnetoresistance (due to the Lorentz force acting on the
conduction electrons)[102]. Thus, for concentrated alloys the
most convenient temperature range for studying ferromagnetic
anisotropy is above 77K where it can be assumed that the normal
magnetoresistance will not play a dominant role. Here, in this
study we have measured the longitudinal and transverse magne-
toresistance of $Fe_{100-x}B_x$ series ($13 \leq x \leq 26$) at room tempera-
ture (300K) and at liquid nitrogen temperature (77K). At low
fields, the longitudinal magnetoresistances, $\Delta\rho_{||}/\rho$, are all
positive and rise rather fast with increasing field, whereas
the transverse ones, $\Delta\rho_{\perp}/\rho$ (in magnitude always larger than
$\Delta\rho_{||}/\rho$) are all negative and drop much more slowly with
increasing field. This behaviour of $\Delta\rho/\rho$ versus H_{ext} plots at
low fields is very similar to that of crystalline ferromagnets
with usual domain structures.

The errors in the measurements of the magnetoresistance
are generally introduced through instability of the current,
thermal noise, unregulated magnetic field, geometrical non-
uniformity of the samples, etc. Fortunately, the factor which
finally matters is a ratio, $\Delta\rho/\rho$ (= $\Delta V/V$) (defined in
Chapter II) and hence any error due to the non-uniformity of
the samples is cancelled. Since in the final values of $\Delta V/V$,
the total voltage V was much higher (~ 100 mV) than the flu-
ctuations in the measurement of $\Delta V(\sim 0.1~\mu V)$, the uncertainty
in the results varied between 1 ppm and 6 ppm for the whole
series.

4.3.1 Ferromagnetic Anisotropy of Resistivity

Though qualitatively the variations of magnetoresistance with external field for amorphous and crystalline ferromagnets are quite similar, the ferromagnetic anisotropy of resistivity, i.e., FAR values of amorphous ferromagnets are much smaller than those of their crystalline counterparts. The values of longitudinal and transverse magnetoresistances $\Delta\rho_{\parallel}/\rho$, $\Delta\rho_{\perp}/\rho$, $(\rho_{\parallel}-\rho_{\perp})$ and FAR for all the samples at 300 and 77K are given in Table 4.4. FAR vs x plots at room temperature and 77K are shown in Fig. 4.11. At room temperature this plot shows a broad maximum at x = 16. This maximum, still at x = 16, becomes more prominent at 77K. The FAR values for all the samples in this Fe-B series are positive and range between 0.2% and 0.4% at 300K and 0.3% and 0.7% at 77K. Fig. 4.11 also shows the variation of the anisotropic magnetoresistance $(\rho_{\parallel}-\rho_{\perp})$ with boron concentration x.

4.3.2 Variation of $\frac{1}{\rho}\frac{\partial\rho}{\partial H}$ with Boron Concentration x

The high field slopes of the magnetoresistance vs H plots are calculated from Fig. 4.10. These values for longitudinal and transverse magnetoresistances at 300 and 77K are all tabulated in Table 4.5. The values of $(\frac{1}{\rho}\frac{\partial\rho}{\partial H})_{\parallel}$ and $(\frac{1}{\rho}\frac{\partial\rho}{\partial H})_{\perp}$ are quite close to each other and hence the average values of $\frac{1}{\rho}\frac{\partial\rho}{\partial H}$ at 300K and 77K against the boron concentration x are plotted in Fig. 4.12. The above mentioned table and the figure clearly show that $\frac{1}{\rho}\frac{\partial\rho}{\partial H}$ values at 77K are all negative and

Table 4.4

Values of $\Delta\rho_{||}/\rho$, $\Delta\rho_{\perp}/\rho$, $(\rho_{||}-\rho_{\perp})$ and FAR at 300K and 77K
for $Fe_{100-x}B_x$ series $(13 \leq x \leq 26)$

Samples	300K			$\rho_{||}-\rho_{\perp}(10^{-10}\Omega\,m)$	77K		
	$\Delta\rho_{||}/\rho(10^{-4})$	$\Delta\rho_{\perp}/\rho(10^{-4})$	FAR(%)		$\Delta\rho_{||}/\rho(10^{-4})$	$\Delta\rho_{\perp}/\rho(10^{-4})$	FAR
$Fe_{87}B_{13}$	13.2	-20.8	0.34	40.2	19.6	-46.2	0.6
$Fe_{84}B_{16}$	18.2	-24.6	0.43	62.1	31.0	-43.0	0.74
$Fe_{82}B_{18}$	13.9	-28.4	0.42	73.5	22.6	-44.7	0.67
$Fe_{80}B_{20}$	12.3	-26.3	0.39	56.0	19.9	-36.1	0.56
$Fe_{78}B_{22}$	11.2	-23.5	0.35	70.4	15.2	-31.2	0.46
$Fe_{74}B_{26}$	5.5	-18.6	0.24	49.8	7.5	-20.6	0.28

VARIATION OF FERROMAGNETIC ANISOTROPY
OF RESISTIVITY (FAR) AND ANISOTROPIC
MAGNETORESISTANCE WITH BORON
CONCENTRATION.
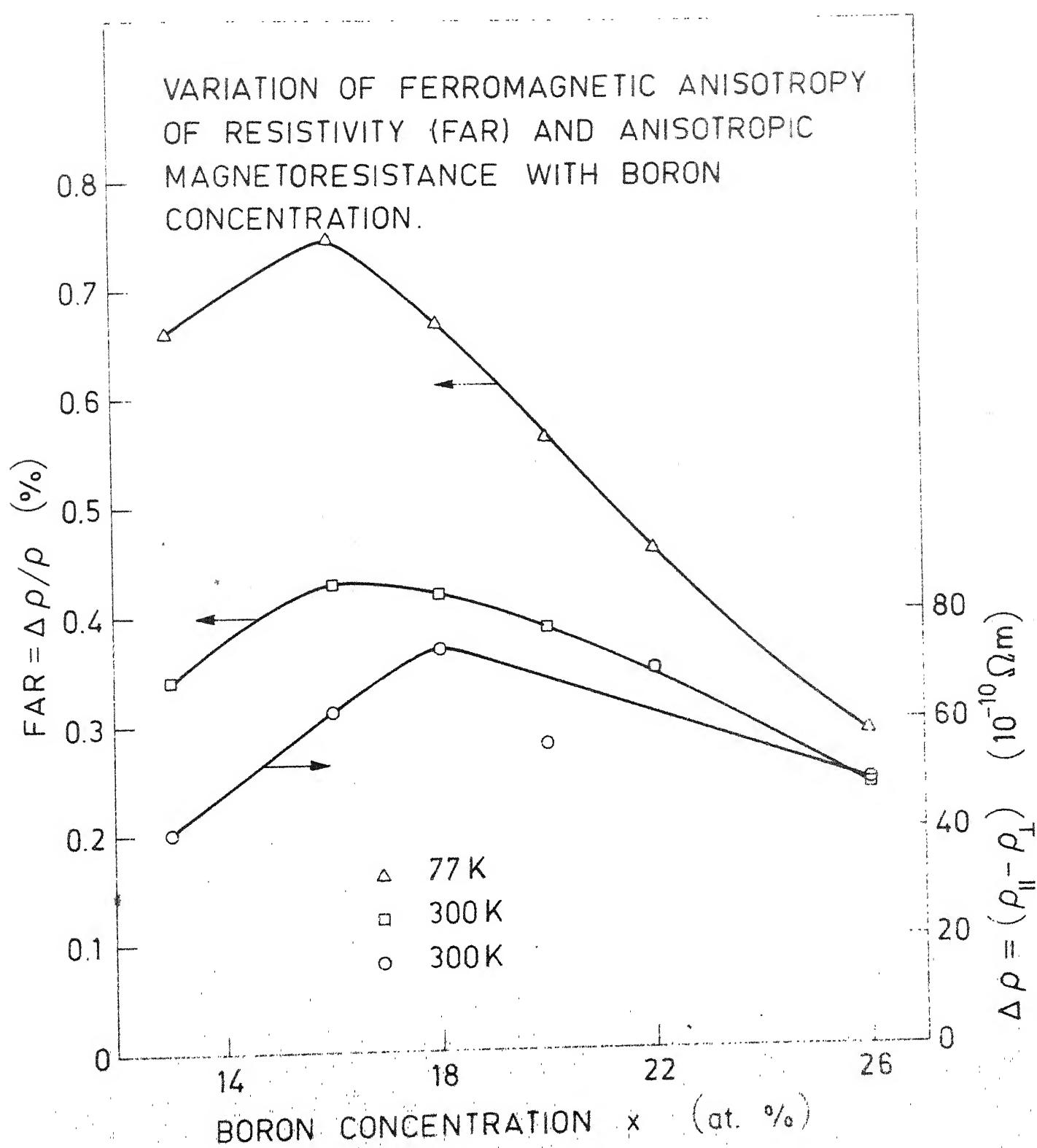
FIG. 4.11

Table 4.5

High-field slopes of magnetoresistance plots at 300K and 77K in $Fe_{100-x}B_x$ (13 ≤ x ≤ 26) series

x	300K			77K		
	$\frac{1}{\rho}\frac{\delta\rho_{||}}{\delta H}$ (10^{-4}T^{-1})	$\frac{1}{\rho}\frac{\delta\rho_{\perp}}{\delta H}$ (10^{-4}T^{-1})	$\frac{1}{\rho}\frac{\delta\rho}{\delta H}$ (10^{-4}T^{-1})	$\frac{1}{\rho}\frac{\delta\rho_{||}}{\delta H}$ (10^{-4}T^{-1})	$\frac{1}{\rho}\frac{\delta\rho_{\perp}}{\delta H}$ (10^{-4}T^{-1})	$\frac{1}{\rho}\frac{\delta\rho}{\delta H}$ (10^{-4}T^{-1})
13	1.25	0.91	1.08	-1.1	-0.88	-0.99
16	-0.5	-0.83	-0.67	-1.9	-2.00	-1.95
18	-0.63	-0.95	-0.75	-1.3	-1.55	-1.43
20	-0.60	-0.70	-0.65	-1.25	-1.30	-1.28
22	-	-0.6	-0.60	-	-0.60	-0.60
26	-0.50	-0.25	-0.38	-0.50	-0.13	-0.32

$1/\rho \dfrac{\partial \rho}{\partial H}$ vs. BORON CONCENTRATION x IN $Fe_{100-x}B_x$
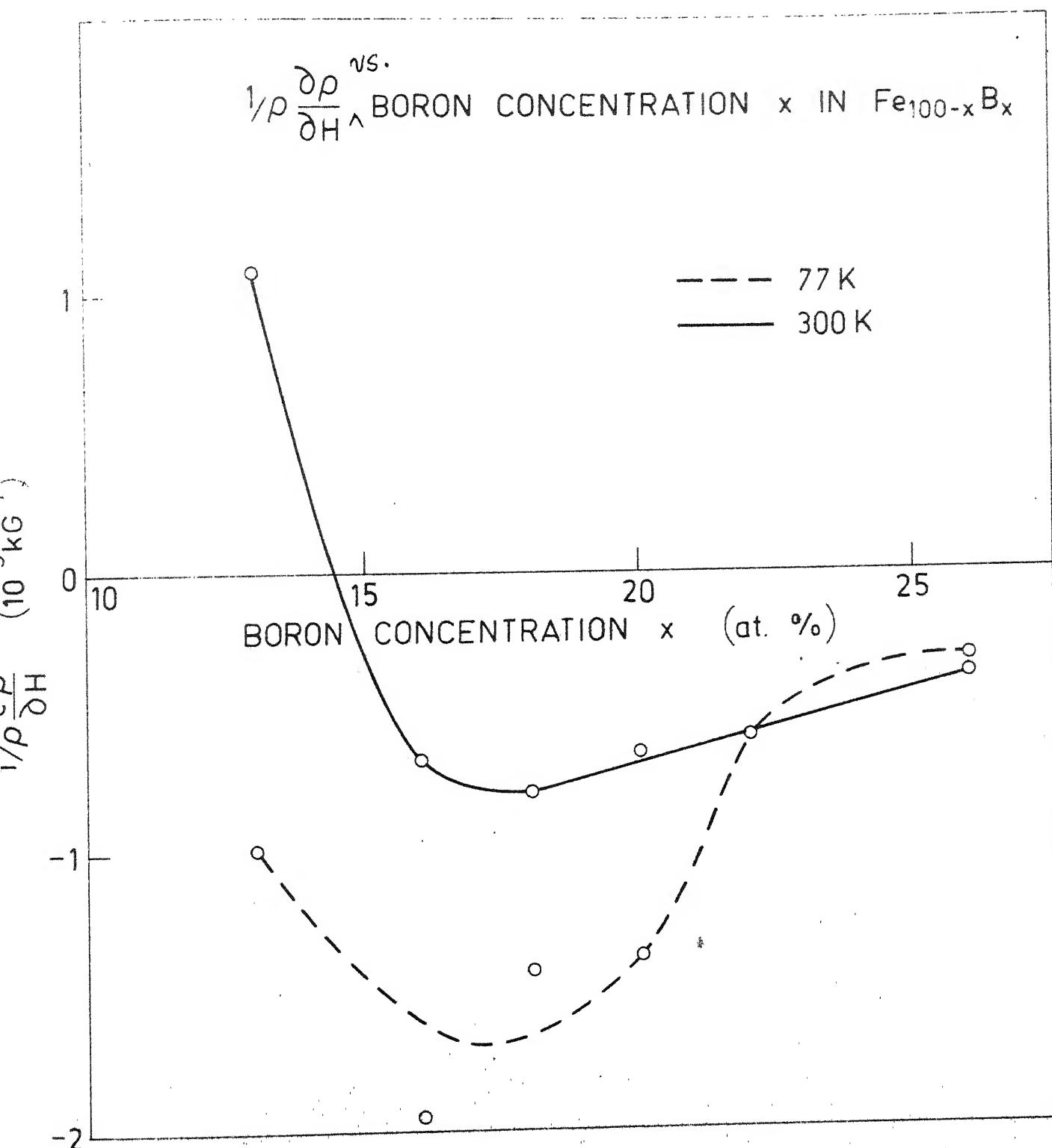
FIG. 4.12

Table 4.6

The values of Θ, the angle between current and magnetization (from magnetoresistance measurements) and β, the tangent of the Hall angle (from Hall effect and resistivity measurements) of $Fe_{100-x}B_x$ $(13 \leq x \leq 26)$ samples

Samples	$\beta = \tan \emptyset_H = \rho_H/\rho \ (10^{-2})$	Θ
$Fe_{87}B_{13}$	3.86	38.9°
$Fe_{84}B_{16}$	3.65	40.7°
$Fe_{82}B_{18}$	4.11	34.9°
$Fe_{80}B_{20}$	3.81	34.4°
$Fe_{78}B_{22}$	1.42	34.6°
$Fe_{74}B_{26}$	1.70	28.6°
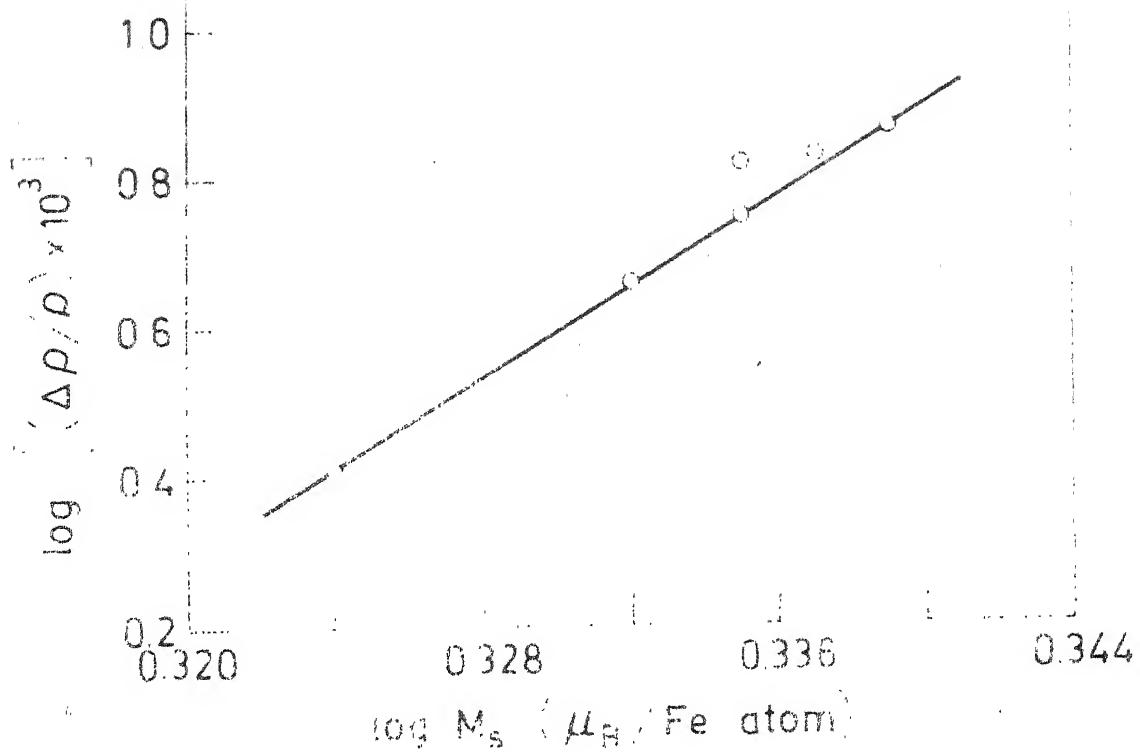
FIG 4.13

4.4 HALL EFFECT

A typical plot of the Hall effect measurements, i.e., the Hall resistivity ρ_H versus field H_{ext} at room temperatures and 77K of $Fe_{80}B_{20}$ sample is shown in Fig. 4.14. The samples of this series have high values of saturation magnetization and hence the Hall resistivity ρ_H saturates at much higher fields. The values of the spontaneous Hall coefficient R_s of this series, are therefore, calculated from the low field slopes of ρ_H vs H data and are given in Table 4.7. In Fig. 4.15, we have plotted the spontaneous Hall coefficient R_s and the Hall conductivity γ_{H_s} at room temperature as functions of boron content x. It is clear, that R_s like many other properties of Fe-B glassy alloys shows a peak around x = 18, whereas γ_{H_s} falls monotonically with x between $13 \leq x \leq 26$. It is also seen from Table 4.7 that qualitatively the variation of R_s with x is similar at room temperature and 77K.

The error in the values of ρ_H and hence in R_s, ranging between 4% ∼ 11%, is mainly introduced by the irregularity of the shape of the samples. The thickness t of the samples, which is needed to calculate $(\rho_H = \frac{V_H t}{I})$, was measured directly at different places of the sample pieces used for the measurement. The thickness was also indirectly calculated from the formula density = $\frac{m}{wlt}$ by measuring the width w at different places, length l and mass m of the same pieces. For the density of the

Table 4.7

Values of R_s, M_s and γ_{Hs} at 300K and R_g at 77K for $Fe_{100-x}B_x$ samples

($13 \leq x \leq 26$)

Samples	300K			77K
	R_s (10^{-9} m^3/C)	M_s (T)	γ_{Hs} (10^2 (Ωm)$^{-1}$)	R_s (10^{-9} m^3/C)
$Fe_{87}B_{13}$	33 ± 1	1.52	297	-
$Fe_{84}B_{16}$	36 ± 1	1.47	252	34 ± 1
$Fe_{82}B_{18}$	50 ± 5	1.43	236	56 ± 5
$Fe_{80}B_{20}$	40 ± 2	1.38	263	41 ± 2
$Fe_{78}B_{22}$	21 ± 2	1.37	70	17 ± 2
$Fe_{74}B_{26}$	27 ± 3	1.30	82	25 ± 3

ρ_H vs H_{ext} PLOT FOR $Fe_{80}B_{20}$

x 77K
o 300K

H_{ext} (kG)

ρ_H $(10^{-8} \Omega m)$
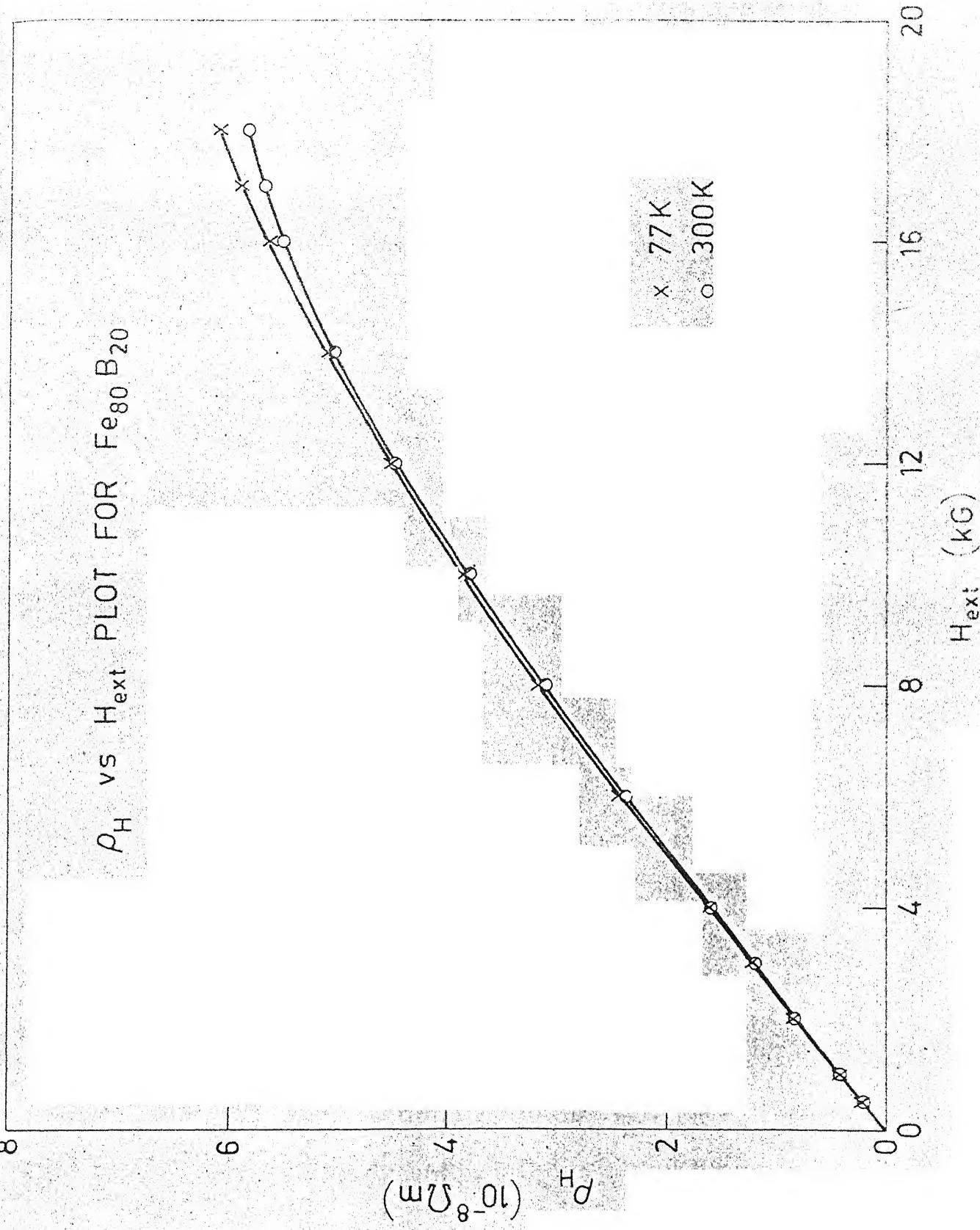
FIG. 4.14

VARIATION OF SPONTANEOUS HALL CONSTANT (R_s) AND HALL CONDUCTIVITY (γ_{H_s}) WITH BORON CONCENTRATION.
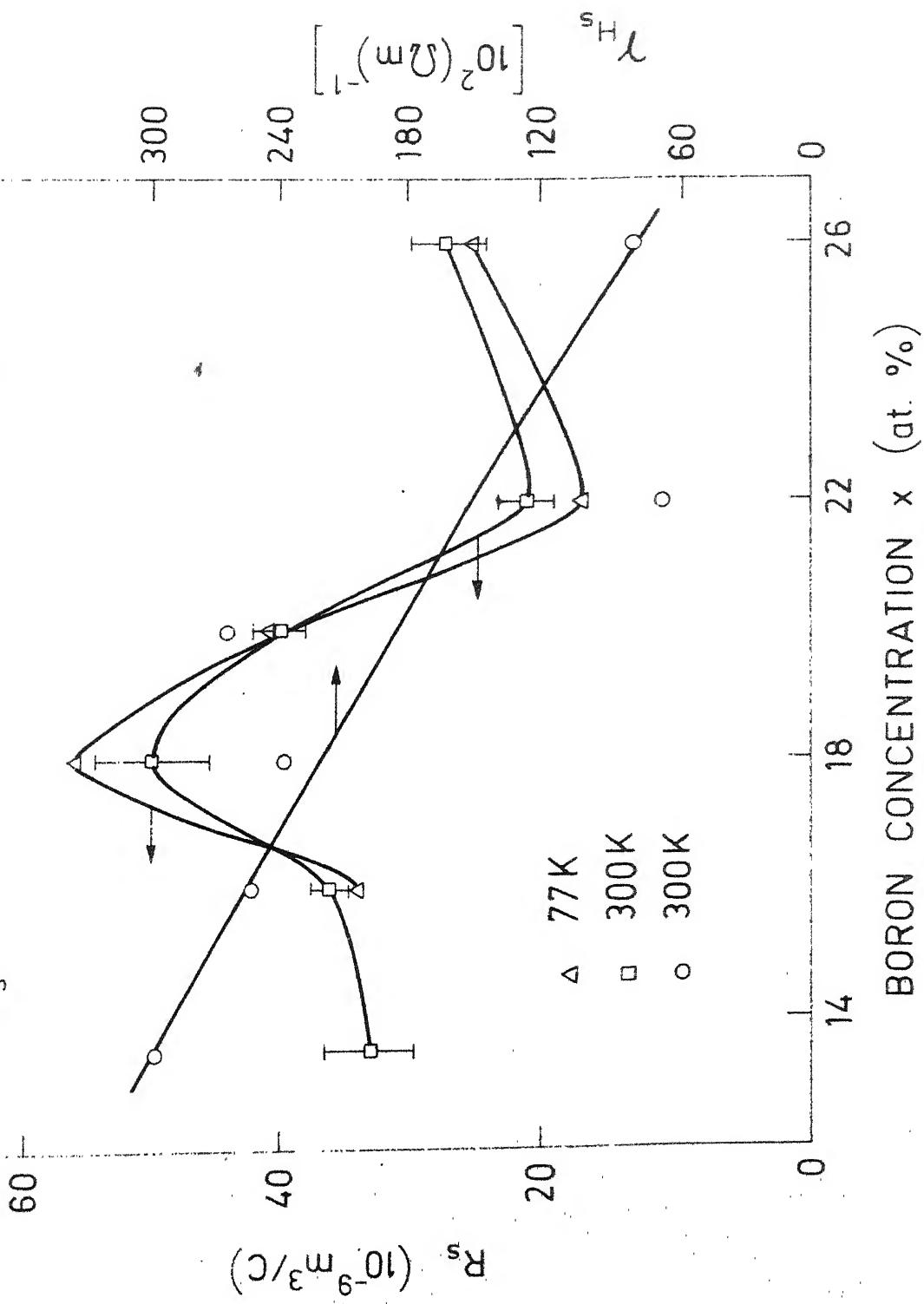
samples the data[109] of Hasegawa and Ray were used. The current stability in the circuit used was better than a few ppm and the accuracy of V_H was ~ 0.1%. Due to the irregularity of the shapes of the samples, the error in the thickness measurement was ~ 4% - 10%. Thus the error in final values of ρ_H was introduced mainly through the error in the measurement of thickness.

A brief discussion on the validity of the relation between R_s and ρ [eqn.(2.37)] is due in the next chapter. The tangent of the Hall angle, β, is directly found out from the experimental ρ and ρ_H data with the help of eqn. (2.38). These β values are tabulated in Table 4.6. Using the β value of $Fe_{80}B_{20}$ from this table we calculated Θ from eqn. (2.46). The Θ value of $Fe_{80}B_{20}$ thus calculated was ~ 46°, which was obviously higher than the expected[79,111] value. This lack of correlation between Hall effect and magnetoresistance is discussed in Chapter V.

CHAPTER V

DISCUSSION *

In this chapter we have discussed the results given in Chapter IV. The theories used to interpret these results are already given in Chapter II.

5.1 ELECTRICAL RESISTIVITY: VARIATION WITH TEMPERATURE

In this section we have studied the temperature variation of electrical resistivity of two series of metallic glasses, namely, Fe-B and Fe-B-Si.

5.1.1 Variation of ρ_T/ρ_{RT} with T ($77K \leq T \leq 300K$) for $Fe_{100-x}B_x$ ($13 \leq x \leq 26$)

The range of possible error in α, $\Delta\alpha$, calculated for this series are given in Table 4.1. These include errors coming from (a) repeated measurements on a given piece of alloy (b) measurement on the different samples of the same composition. The average value of $\Delta\alpha$ over the entire composition range is $\simeq 0.05 \times 10^{-4} K^{-1}$, except for x = 16. Thus $\Delta\alpha$ due to any sample to sample variation is not more than $0.05 \times 10^{-4} K^{-1}$. As a matter of fact, in case of $Fe_{82}B_{18}$ we could exactly reproduce the result in two different pieces. This fact clearly shows that these samples are quite homogeneous.

We will discuss our results in the light of the extended Ziman theory given in Chapter II. In the Fe-B series the sign

of α is found to be positive in the whole range of amorphosity. As shown in Chapter II [eqn. 2.6)], α is expected to be negative only for materials with the structure factor $S_T(2k_F) > 1$. We calculated the value of k_F in the free-electron model, from the number of conduction electrons per unit volume, n, as

$$k_F = (3\pi^2 n)^{1/3} \qquad (5.1)$$

For Fe we have taken[83] $n_{Fe} \simeq 2 \times 10^{28} m^{-3}$, atomic weight = 56, and density = 7.8 g/cm^3, with these data Z_{Fe} is calculated to be $\simeq 0.24$, where Z is the effective number of conduction electrons per atom. Further, using atomic weight of boron = 10, density of the particular metallic glass, say $Fe_{80}B_{20}$ = 7.4 g/cm^3 and $Z_B = 1.6$[83], we have calculated n for $Fe_{80}B_{20}$ as $4.75 \times 10^{28} m^{-3}$. Hence, from eqn. (5.1), k_F is found to be $\simeq 1.1 \times 10^{10} m^{-1}$. The corresponding S(k) value (for k = $2k_F$ = $2.2 \times 10^{10} m^{-1}$) is found to be $\simeq 0.15$ from the S(k) vs k graph[112]. The k_F values for the entire series were calculated and $2k_F$ value was found to lie between 2.01×10^{10} and $2.4 \times 10^{10} m^{-1}$ increasing with increasing x. The corresponding $S(2k_F)$ were also found to increase monotonically within this range of $2k_F$. Although precise estimation of S(k) is rather difficult from this graph, they are definitely much less than 1 and hence theoretically the values of α for the entire series is expected to be positive; this matches well with our

experimental data. An order-of-magnitude calculation of α for $Fe_{80}B_{20}$ was made by using eqn. (2.6) and eqn. (2.8) taking $M \simeq 50$ and $\Theta_D = 400K$. From theory, α comes out to be $\simeq$ $1.4 \times 10^{-4} K^{-1}$, which is in good agreement with our experimental α ($\simeq 1.6 \times 10^{-4} K^{-1}$).

The variation of α with x is shown in Fig. 4.6. The temperature coefficient of resistivity falls abruptly from x = 13 to x = 16, and in the range $16 \leq x \leq 26$, α is almost independent of concentration. The latter is in agreement with the results of Mogro-Campero and Walter[113]. This fall in α from x = 13 to x = 16 points to a structural difference between $Fe_{87}B_{13}$ and other glasses of the series. Similarly, in the region $16 \leq x \leq 26$, a nonvarying α indicates that there is no serious change in the structure. In fact, the concentration dependence of α comes from two factors, namely, the structure factor term and the Debye-Waller factor [see, for example, eqn. (2.6)]. As x increases the $2k_F$ value, and hence $S_T(2k_F)$ increases monotonically. Thus the positive value of α should decrease with x, if $S_T(2k_F)$ was the only factor governing it. But α depends on the Debye-Waller factor as well. As can be seen from eqn. (2.8), the x dependence of $\partial W(T)/\partial T$ mainly comes from the dependence of $W(o)$ and the latter increases with x. Thus, qualitatively it can be argued that the decreasing effect of α from $S_T(2k_F)$ overrides the increasing effect of α from $\partial W(T)/\partial T$ for x = 13 sample and in

the region $16 \leq x \leq 26$ these two effects are competitive and hence α becomes approximately independent of concentration x. Such type of variation of α with x can be correlated with the variation of the crystallization temperature T_{cr} of these alloys with x, as studied by Hasegawa and Ray[109]. They found that T_{cr} abruptly increases from x = 13 to x = 16 and then there is a constant region in the range between $18 \leq x \leq 22$ and after that it slowly increases with x. Such a correlation gives rise to a stability criterion in terms of α. One should note that the effect of magnetic scattering, which might give an additional positive contribution to α, is ignored here.

In the temperature range $80K \leq T \leq 300K$, $\Delta\rho/\rho$ is calculated from eqn. (2.10) by evaluating C and using the values of Θ_D, M and k_F for $Fe_{80}B_{20}$. It is found that $\Delta\rho/\rho$ should approximately be $\simeq$ 4.2% . As shown in Fig. 4.5 the values of $\Delta\rho/\rho$ in the temperature range $80K \leq T \leq 300K$ is independent of the concentration in the range $16 \leq x \leq 26$, with values lying between 2.8 and 3.3%. However, for x = 13 this percentage change is higher (viz., 4.9%).

The Debye temperature of all the six samples were calculated from eqn. (2.11). The Θ_D values for $18 \leq x \leq 22$ are (390 $\pm$ 50)K (similar to those found by Mogro-Campero)[114], but for x = 13 and 16 it shows higher values of 540 $\pm$ 90K, and for

x = 26 again it is around 520K. The exact values can be seen in Table 4.1 and all these Θ_D values have large error bars due to uncertainty in the slope S of the quadratic portion of the ρ_T/ρ_{RT} vs T graph. This was due to the experimental limitations of restricting the measurements in the top portion of the intermediate temperature range, i.e., 20K $\leq$ T $\leq$ 300K. In fact the range of temperature which we have chosen for finding out S, i.e., 80K $\leq$ T $\leq$ 150K, is the portion of ρ_T/ρ_{RT} vs T plot where ρ_T/ρ_{RT} already starts deviating from the quadratic behaviour and moves towards linearity. Hence, uncertainty in the values of S could be expected. Nevertheless, as shown in Fig. 4.7, Θ_D has a minimum around x = 20 in quali-tative agreement with the plots given by other workers[54,115] who have found out Θ_D accurately from independent specific heat measurements. Onn et al[116] had found from heat-capacity mea-surements in $Fe_x Ni_{80-x} P_{14} B_6$ metallic glasses that Θ_D is invariably lower in the amorphous alloys as compared to their nearest available crystalline counterparts. But, as it is clear from our measurements, for $Fe_{100-x}B_x$ alloys with x = 13, 16 and 26, Θ_D values are higher than that of pure Fe ($\simeq$ 420K). This result is supported by the data of Japanese workers[54,115].

Since high Debye temperature means low thermal expansion coefficient, which in turn indicates Invar characteristics, we explain these high values of Θ_D in $Fe_{87}B_{13}$ and $Fe_{84}B_{16}$ by Invar anomaly. For $Fe_{100-x}B_x$ series it is well established[25,26,117]

that around $13 \leq x \leq 17$ atomic percent boron, alloys show
Invar characteristics. This is the same range in which Θ_D
values are higher than that of pure Fe. Hence, these two
facts can be correlated. Matsuura et al[54] have also explained
the high Debye temperature values of this series in terms of
Invar anomaly. However, the reason for getting high Θ_D
values (for $x = 18, 20, 22$ comparable to Θ_D of pure Fe and
for $x = 26$ higher than that of pure Fe) in the range
$18 \leq x \leq 26$, in contrast to the results of Onn et al, is
not understood. Matsui and Adachi[118] and Caudron et al[119]
have shown that in Fe-Ni alloys there is a drastic reduction
in Θ_D values towards the Invar region. This reduction has
been interpreted as 'softening' of phonon modes and the
resulting instability of the Invar phase. From our data
of Θ_D, it could perhaps be said that the phonon softening
does not take place in the amorphous Fe-B alloys.

Lastly, a comment is due on the applicability of Ziman's
theory in these metallic glasses. From eqns. (2.5), (2.7) and
(2.8), one can easily find that[93]

$$\rho(T) = \begin{cases} a\pi^2 T^2/6\ \Theta_D^3 & \text{for } T \ll \Theta_D \quad (5.2) \\ aT/\Theta_D^2 & \text{for } T \geq \Theta_D \quad (5.3) \end{cases}$$

Eqn. (5.3) clearly shows that the variation of $\rho(T)$ with T
should deviate from linearity for temperatures below Θ_D.
In contrast to this we find that ρ_T/ρ_{RT} versus T graphs

(Fig. 4.1) are linear down to temperatures much less than the corresponding Debye temperatures, Θ_D. As pointed out in Chapter I, many workers[56-58] have discussed the limitations of applying Ziman's theory to such strong scattering liquid or glassy metals and recently this has been a subject of interest for theoreticians. Thus, the values of α and $\Delta\rho/\rho$, calculated here on the basis of the above theory should be taken as only order-of-magnitude estimates.

5.1.2 Electronic Stability Criterion

Next, we come to the question of the electronic stability criterion. A system is most stable when the Fermi energy E_F lies at a minimum of the density-of-states curve, $D(E)$. To solve for the density of states of the glassy system, an expression using the free electron perturbation theories, is given by[20]

$$E = E^0_{k'} + V(o) + \frac{\Omega}{8\pi^3} \int \frac{|V(k)|^2 \, S(k)}{E^0_{\vec{k'}} - E^0_{\vec{k'}+\vec{k}}} \; d^3k \; ; \qquad (5.2)$$

where $V(k)$, $S(k)$ and Ω have been defined in Chapter II and $E^0_k = \hbar^2 k^2/2m$. This expression fails when $|\vec{k'}+\vec{k}_p| = |\vec{k'}|$ just as it does in the crystal where a gap opens up in the energy band at the zone boundary. In the case of glasses we do not expect a gap but we expect a similar decrease in the density of states at the energy $E = \frac{\hbar^2}{2m} (1/2 \; k_p^2)$. In the glassy state when $S(k)$ remains spherically symmetric, we expect that all the states at $|k| = 1/2 \; k_p$ are affected. Hence, at the concentrations where $k_F = 1/2 \; k_p$ or $2k_F = k_p$ the Fermi energy E_F will

lie at a minimum of the density of states curve. As stated in

Sec. 2.1.3, the effective number of conduction electrons per

atom Z_{eff} corresponding to $2k_F = k_p$ is around $Z_{eff} = 1.7$. For

the present $Fe_{100-x}B_x$ series, in eqn. (2.14) using $Z_{Fe} = 1$

and $Z_B = 3$ (valency of Boron) we get a stability around $x = 35$.

This value is far away from the actual stable region of this

series (which is around $x \simeq 20$). We have calculated the Z_{eff}

at k_p for this particular series. Using $k_p = 3 \times 10^{10} m^{-1}$ [112], it

can be easily shown that Z_{eff} corresponding to the peak of the

$S(k)$ vs k graph of the Fe-B series is $\simeq 1.2$ electrons per atom.

The Z_{eff} values for this series of stable alloys lie between

0.4 and 0.6 [calculated from eqn. (2.16)] using $Z_{Fe} = 0.24$

and $Z_B = 1.6$ [Ref. 83)] and hence they are obviously far away

from 1.2. Thus, we find that one could still have stable alloys

with $2k_F \ll k_p$. This conclusion is also corroborated by the

interpretation we have given to justify the positive α for the

Fe-B series. Since $0.4 \leq Z_{eff} \leq 0.6$ is much less than the Z_{eff}

corresponding to the peak of $S(k)$ versus k graph, we get

$S(k) \ll 1$, giving rise to a positive α. Also, taking these

values of Z_{eff} in our theoretical calculations, we could

reproduce all our experimental data, within reasonable error

limits. Thus, one could say that the stability criterion of

Nagel and Tauc is not applicable to the stable amorphous alloys

with positive α, although it holds quite well for those having

negative α values.

5.1.3 Variation of Resistivity with Concentration x

The resistivity values of all the six samples were theore-
tically estimated from eqn. (2.15)[120]. The values of W(o) for
the $Fe_{100-x}B_x$ series are obtained from eqn. (2.9) using k_F, M
and Θ_D as given in Sec. 5.1.1. Although it is not easy to get
a precise estimate of $S(2k_F)$ from S(k) versus k graph[112] we
still have to take into account its variation with x because it
plays a significant role in eqn. (2.15). The ρ values are first
calculated in terms of the constant C' of eqn. (2.15) and by
comparing one of these values to the corresponding experimental
value, we can have a rough estimate of the trend of the
variation of ρ with boron concentration x. As stated in
Chapter IV, ρ shows a tendency to increase with increasing
x, both theoretically and experimentally. The experimental
plot (Fig. 4.9) shows that the percentage change of resistivity
between x = 13 and x = 26 samples is ~ 30%.

Fukamichi et al[81] have also studied the variation of
absolute resistivity with concentration x in $Fe_{100-x}B_x$
(14 ≤ x ≤ 22) metallic glass series. They too have found an
increase in resistivity with increasing x, but in their samples
total variation (between x = 14 and x = 22) of ρ is only
~ 10%. As it is clear from Fig. 4.9, the theoretical curve
shows a rather sharp change over the entire range of composition.
This overestimation of ρ might be a result of overestimating

the structure factor $S(2k_F)$, which is very difficult to estimate precisely from the available plots. The error in calculating ρ was also introduced because we have taken the values of $S(2k_F)$[112] of a different set of samples, prepared under different conditions (Fukunaga et al[112] measured $S(k)$ on splat-cooled Fe-B amorphous alloys, whereas our samples are melt-spun). Also, according to eqn. (2.15), we needed the values of $S_0(k)$, i.e. $S(k)$ at 0 K, but the available data were taken at room temperature. Still, in the absence of the exact values of $S_0(2k_F)$, we have used these structure factor plots to get an idea of the behaviour of ρ , theoretically. Hence, our theoretical plot of ρ versus x should be taken just as a guide to show whether ρ decreases or increases with x.

The main contribution to the electrical resistivity of pure transition metals arises from resonance scattering. The addition of metalloid atoms effectively increases the number of conduction electrons and thus in turn increases k_F. Because of this addition the structure factor $S(k)$ plays a significant role in the resistivity of metallic glasses. With increasing x, $2k_F$ moves towards k_p (the most probable nearest neighbour distance in k-space) and thus increase the value of the resistivity.

5.1.4 Variation of Resistivity $\rho(T)$ with T in the Range $4.2K \leq T \leq 300K$ for $Fe_{80}B_{20-x}Si_x$ (o $\leq$ x $\leq$ 12) Series

As shown in Fig. 4.2, for this series too, the ρ_T/ρ_{RT}

versus T plots are linear down to ~ 150K. In the temperature range 20K $\leq$ T $\leq$ 100K ρ_T/ρ_{RT} data fit quite well in a T^2 plot (Fig. 4.4). The Debye temperature Θ_D were calculated from eqn. (2.11), with the help of slopes α and S, found out directly from Figs. 4.2 and 4.4. Fig. 4.8 shows a Θ_D versus x plot for $Fe_{80}B_{20-x}Si_x$ (o $\leq$ x $\leq$ 12) series. It is clear that the addition of silicon to the parent series (Fe-B), brings down the Debye temperature of these glasses. In fact, as stated earlier (Ref. 116), Θ_D values of these amorphous alloys are expected to be smaller than those of pure Fe (~420K). Unlike in Fe-B series, Θ_D of Fe-B-Si series are found to be < 420K, as expected. Probably, the addition of silicon removes the Invar characteristics of Fe-B alloys and hence the values of Debye temperature come down. About the varying nature of the Debye temperature beyond x = 1, one could say two things :

i) it is a real effect and might indicate some structural changes in these alloys

ii) it might be a result of the limitations of applying Ziman's theory to these alloys and the oscillatory curve might be replaced by a straight line.

Since the structural data of these alloys are not available, we do not have any means to verify these points.

Ziman's theory takes into account the electron-ion potential scattering and evolves into a T^2 dependence at low temperatures. Another possibility is the electron-magnon scattering

which results in a $T^3/2$ dependence. A detailed analysis of the resistivity data in the temperature range $20K \leq T \leq 100K$, was done to find out the possibility of the presence of magnon contribution to the resistivity. The least-squares fitting procedure was used for this purpose. Resistivity data were fitted to a power law of the form ,

$$\rho = a + bT^{3/2} + cT^2$$

As shown in Table 5.1, the χ^2 of the least-squares fit were smaller when both $T^{3/2}$ and T^2 terms were simultaneously present than when only T^2 was considered. Inspite of this, the possibility of the simultaneous presence of both terms is ruled out because such a fitting gave negative b or c or unrealistically high Debye temperature.

Hence, in the temperature range $20K \leq T \leq 100K$, we have considered the presence of T^2 terms only. To calculate θ_D, we have used the coefficients c (or the slope S of ρ_T/ρ_{RT} vs T^2 plots) from the least-squares fit when only T^2 term was considered.

5.2 MAGNETORESISTANCE

We first discuss an important point about the magneto-resistance measurements, in these thin ribbons. As stated in Chapter III, during both the transverse and longitudinal measurements the sample was oriented in such a way that the applied field was always exactly parallel to the ribbon plane.

Table 5.1

x^2, b, c of least-squares fit when $T^{3/2}$ and T^2 terms are simultaneously present	x^2, c of least-squares fit when only T^2 term is present
For sample with x = o	
x^2 1.24×10^{-9}	x^2 3.21×10^{-9}
b $(-0.15 \pm 0.02) \times 10^{-5}$	
c $(7.24 \pm 0.23) \times 10^{-7}$	c $(5.81 \pm 0.04) \times 10^{-7}$
For sample with x = 1	
x^2 8.57×10^{-8}	x^2 2.74×10^{-7}
b $(1.38 \pm 0.24) \times 10^{-5}$	
c $(-6.52 \pm 2.2) \times 10^{-7}$	c $(6.31 \pm 0.38) \times 10^{-7}$
For sample with x = 2	
x^2 7.4×10^{-10}	x^2 7.75×10^{-8}
b $(1.08 \pm 0.025) \times 10^{-5}$	
c $(0.62 \pm 0.2) \times 10^{-7}$	c $(10.9 \pm 0.21) \times 10^{-7}$
For sample with x = 4	
x^2 2.11×10^{-8}	x^2 4.12×10^{-8}
b $(0.52 \pm 0.12) \times 10^{-5}$	
c $(2.97 \pm 1.09) \times 10^{-7}$	c $(7.85 \pm 0.13) \times 10^{-7}$

x^2,b,c of least-square fit when $T^{3/2}$ and T^2 terms are simultaneously present		x^2, c of least-squares fit when only T^2 term is present	

For sample with x = 6

x^2	6.11×10^{-9}	x^2	3.21×10^{-8}
b	$(0.64 \pm 0.07) \times 10^{-5}$		
c	$(3.78 \pm 0.68) \times 10^{-7}$	c	$(9.88 \pm 0.13) \times 10^{-7}$

For sample with x = 8

x^2	2.69×10^{-8}	x^2	1.54×10^{-7}
b	$(1.43 \pm 0.15) \times 10^{-5}$		
c	$(-1.3 \pm 1.46) \times 10^{-7}$	c	$(12.5 \pm 0.31) \times 10^{-7}$

For sample with x = 12

x^2	3.34×10^{-9}	x^2	1.37×10^{-8}
b	$(0.37 \pm 0.05) \times 10^{-5}$		
c	$(5.06 \pm 0.44) \times 10^{-7}$	c	$(8.51 \pm 0.08) \times 10^{-7}$

We point out here why this precaution should be taken! In fact, while making transverse magnetoresistance measurements two types of orientation of the field with respect to the ribbon plane are possible.   Fig. 5.1 shows these two orientations.

As it is clear from this figure, in both these orientations the condition of transverse magnetoresistance $(\vec{H} \perp \vec{J})$ is met. But, we have always chosen the particular orientation $\vec{H} \, ||$ ribbon plane for our measurements. The reason for doing so is to minimise the effect of demagnetizing field. When the applied magnetic field $\vec{H}$ is directed perpendicular to the ribbon plane, at low fields, the influence of demagnetizing field is very prominent (see Appendix 2)[121], since these samples have large width/thickness ratio. Because of this the saturation magnetization and hence the saturation of $\Delta \rho_{\perp}/\rho$ of these samples are reached only at considerably higher fields thereby causing the fall in negative magnetoresistance with field to be much slower. At high fields this influence is not present. We would like to point out here that, in the case of transverse magnetoresistance measurements, not only the sample orientation but also the sample alignment with respect to the magnetic field plays an important role at low fields. If the sample is misaligned, the transverse magnetoresistance at low fields will show positive values, as observed by Fukamichi et al[75] and Kern and Gönser[77]. They have attributed this
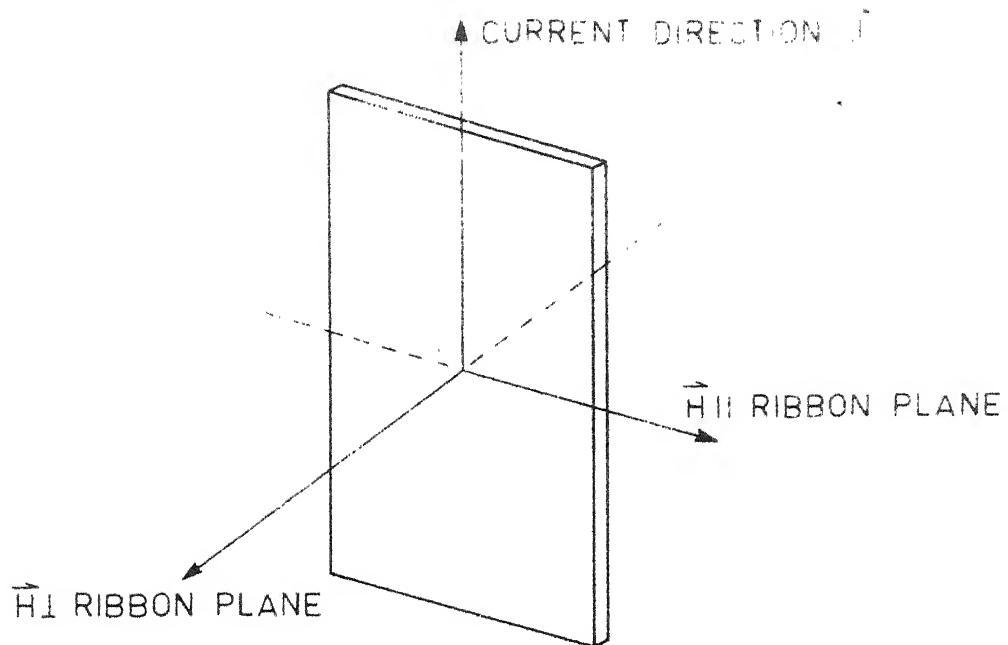
FIG. 5.1
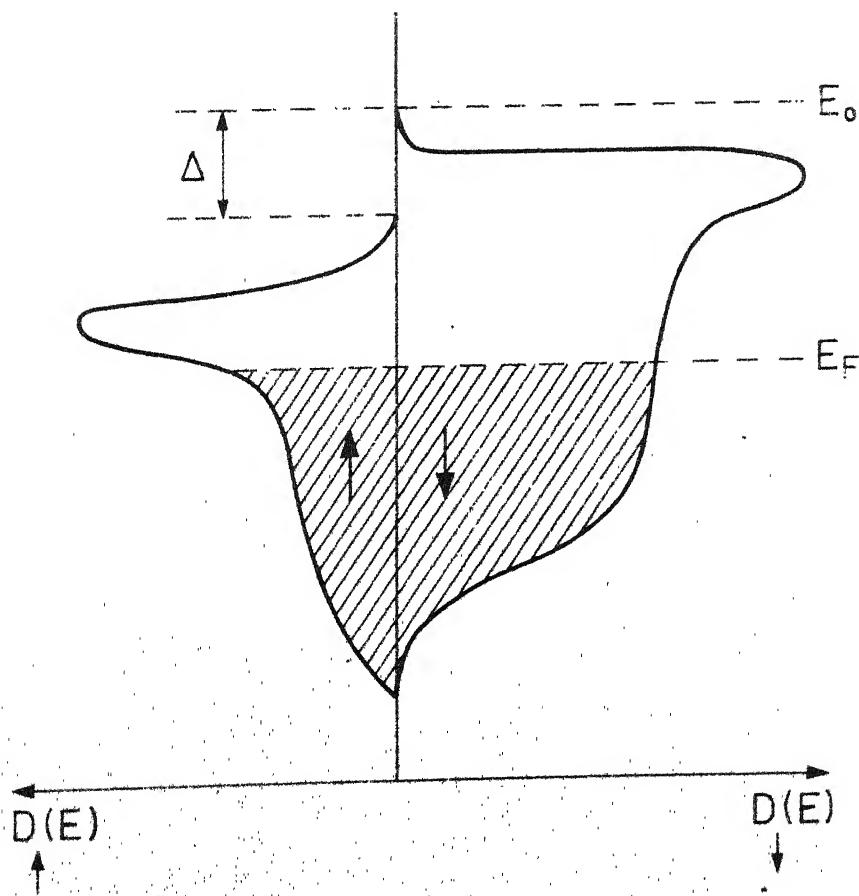
IG 5.2

positive value to the initial orientation of some of the domains in the direction perpendicular to the field and parallel to the current. However, according to our observations, this sort of positive values of $\Delta\rho_\perp/\rho$ will show up in the magnetoresistance measurements, in both the possible orientations of the field with respect to the ribbon plane, only if the alignment of the sample is wrong. Since longitudinal magnetoresistance, $\Delta\rho_{||}/\rho$, saturates much faster with field than transverse magneto-resistance, $\Delta\rho_\perp/\rho$, even a slight misalignment would introduce a positive value which overshadows the inherent negative value of $\Delta\rho_\perp/\rho$. The only merit of choosing the orientation $\vec{H} \, ||$ ribbon plane is that, any spurious positive transverse magneto-resistance will be much smaller in this orientation because of the small value of the demagnetizing factor. Hence, it is much easier to avoid the misalignment effect in this orientation.

5.2.1 Ferromagnetic Anisotropy of Resistivity (FAR)

As shown in Chapter II, the ferromagnetic anisotropy of resistivity is given by eqn. (2.29). The values calculated from magnetoreistance measurements are given in Chapter IV. The broad maximum of FAR vs x plot at 300K and a more prominent one at 77K are in agreement with the results obtained by Fukamichi et al[75]. This type of variation of FAR with concentration is quite similar to the variation of many other physical properties like density[109,112], magnetostriction[47,122], co-ordination number[112], magnetic moment[25] etc. Kemény et al[124]

have shown that even the crystallization process changes from a 2-step mechanism to a 1-step one as the boron content x changes from $x \leq 15$ to $x \geq 15$. From eqn. (2.36) it is clear that a peak in magnetic moment versus x plot implies a peak in FAR versus x graph. In these metallic glasses the peak in μ versus x plot gets smeared out with increasing temperature (in fact μ vs x plot at 4.2K itself is quite smeared out and when the room temperature μ values are calculated from eqn. (1.3), using the data of Hasegawa and Ray[26] the μ becomes independent of x at 300K). So, again from eqn. (2.36), a similar behaviour is expected in FAR vs x graph too with a more prominent peak at 77K. It is clear from Fig. 4.11 that our FAR versus x plot at room temperature is broader as compared to that at 77K.

Another interesting feature which merits some discussions is the small values of FAR in these metallic glasses as compared to that of their crystalline counterparts. For crystals, as given by Jan[102], FAR values might be as high as 20%, whereas our data show that FAR for this series varies only between 0.2% and 0.6%. Nigam and Majumdar[82] have tried to explain this in the light of Berger's split-band model. According to them glasses of Fe-B series lie far away from the $\lambda_s = o$ line on the $(Fe_xNi_{1-x})_{80}B_{20}$ ternary diagram (λ_s = coefficient of linear magnetostriction) and hence the FAR values are small for these alloys. But, as pointed out by Fukamichi et al[75], Berger's model is applicable to strong ferromagnets, whereas Fe-B

amorphous alloys are weak ferromagnets. This view is supported by the band model[125] [$\Delta < (E_0 - E_F)$] too (see Fig. 5.2). In fact[125] $Fe_{80}B_{20}$ is a typical example of a weak ferromagnet. Also, d-type band splitting in Fe-B alloys is definitely not possible because boron does not have any d-electron state ($2s^2$, $2p^1$). Hence, it is not justified to use Berger's model to explain the small FAR values of Fe-B alloys. The small FAR values of metallic glasses can be attributed to the fact that though the anisotropic magnetoresistance i.e. $\rho_{||} - \rho_{\perp}$ of amorphous and crystalline materials are comparable (it does not depend on the initial magnetic domain structure), the resistivity of crystalline materials is much smaller than that of amorphous alloys.

From Fig. 4.9 and Fig. 4.11, we have tried to predict at 300K, the FAR and the resistivity of amorphous Fe, by extrapolating these plots to x = o. Our results show that the FAR of amorphous Fe is negative ~ -0.4% (whereas for crystalline Fe it is +0.5%) and the resistivity of amorphous Fe, ρ_{am-Fe} is found to be $\cong$ 1×10^{-6} Ω m which is an order of magnitude larger as compared to $\rho_{cryst.Fe} = 10^{-7}$ Ω m .

5.2.2 Θ, the Angle between $\vec{J}$ and $\vec{M}$

Metallic glasses have uniaxial anisotropy. Hence, the domains in these alloys are preferntially oriented at some angle Θ with the ribbon axis. Generally, metallic glasses

are in the form of thin ribbons and so the most natural choice of current direction $\vec{J}$ is along the ribbon axis Many workers[28,79,111] have tried to find out this angle between $\vec{J}$ and $\vec{M}$ through various methods. As given by eqn. (2.35), we have tried to formulate an expression for Θ in terms of our measured quantities from the fundamental concepts of magnetoresistance.

5.2.3 Variation of the Forced Magnetoresistivity $\frac{1}{\rho}\frac{\partial\rho}{\partial H}$ with x

As pointed out in Chapter IV, the magnetoresistance plots ($\Delta\rho/\rho$ vs H) show negative slopes at high fields. These slopes, i.e., the forced magnetoresistivity $\frac{1}{\rho}\frac{\partial\rho}{\partial H}$ were directly found out from these graphs. A plot of $\frac{1}{\rho}\frac{\partial\rho}{\partial H}$ vs x (Fig. 4.12), at 300K shows that it decreases from a positive value at x = 13 to negative values beyond x = 14.5 giving a minimum at x = 18 and then it increases slowly with x. At 77K it is always negative and has a minimum around x = 17.

Actually, the negative slopes in these plots are due to reduced electron-magnon scattering at higher fields. It is well known that in Fe-B amorphous alloys the magnetic moment decreases with decreasing boron content[25,75,117]. Hence, in the range of lower boron content, less electron-magnon scattering is expected and correspondingly the slope should be more negative. As it is clear from eqn. (2.30) in Chapter II ($\frac{1}{\rho}\frac{\partial\rho}{\partial H}$) should be more negative with increasing high-field

susceptibility. Also, the samples with low boron content have large high field susceptibility values (Invar property) and hence eqn. (2.30) implies that lower the boron content more negative should be the value of $\partial\rho/\partial H$. But as stated in the last paragraph, in the range $13 \leq x \leq 18$ at 300K and $13 \leq x \leq 16$, at 77K, in contradiction to our expectations the value of $\frac{1}{\rho}\frac{\partial\rho}{\partial H}$ becomes less negative with decreasing x. However, in the range $18 \leq x \leq 26$ (for 300K) and $16 \leq x \leq 26$ (for 77K) the trend of the plots is consistent with our expectations. The behaviour in the range $13 \leq x \leq 18$ can be explained by the Invar anomaly. A similar behaviour has been observed[126] in Fe-Ni crystalline Invar alloys. Soumura[126] has explained this behaviour by taking into account the contribution due to large forced volume magnetostriction. In fact Fukamichi et al[117] have observed large values of volume magnetostriction ($\partial\omega/\partial H$) for these alloys in the Invar region ($13 \leq x \leq 18$); therefore, this large value of $\partial\omega/\partial H$ could be expected to contribute to the magnetoresistance of these alloys. Assuming that $\frac{1}{\rho}\frac{\partial\rho}{\partial H}$ is a function of volume V and magnetic field H, at constant pressure we can write,

$$\frac{1}{\rho}\left(\frac{\partial\rho}{\partial H}\right)_P = \left(\frac{\partial \ln\rho}{\partial \ln V}\right)_H \left(\frac{\partial\omega}{\partial H}\right)_P + \frac{1}{\rho}\left(\frac{\partial\rho}{\partial H}\right)_V \qquad (5.3)$$

where

$$\frac{\partial\omega}{\partial H} \; \alpha \; M \; \chi_{hf} \qquad (5.4)$$

where κ is the compressibility, M the magnetization and χ_{hf} is the high field susceptibility. In eqn. (5.3) generally the first term is negligibly small but for Invar alloys, as stated earlier $\partial\omega/\partial H$ is large and one cannot ignore this term. The room temperature value of $\partial\omega/\partial H$ for Fe-B alloys is remarkably large[127] and as stated by Fukamuchi et al[75] the calculated value at 4.2K by using eqn. (5.4) is also large, hence $\partial\omega/\partial H$ at 77K is also expected to be considerably large lying between these two values. Since $\partial\omega/\partial H$ increases with decreasing boron content and this effect seems to override the effect of electron-magnon scattering on forced magnetoresistivity, we get a less negative $\frac{1}{\rho}\frac{\partial\rho}{\partial H}$ with decreasing boron content in the Invar range of Fe-B alloys, namely, $13 \leq x \leq 18$. It is clear from Fig. 4.12 that the values of $\frac{1}{\rho}\frac{\partial\rho}{\partial H}$ decrease, i.e., become more negative with decreasing temperature. This is an unexpected result, because at low temperatures magnons are very few in number, hence saturation is reached and consequently $\partial M_s/\partial H$ tends to zero. Thus negative slope at high fields is expected to vanish in contrast to our results.

5.3 HALL EFFECT

In amorphous ferromagnetic alloys, just as in the case of polycrystalline materials, Hall resistivity is given as,

$$\rho_H = \frac{V_H t}{I} = R_o B_{in} + R_s M_s \qquad (5.5)$$

where the magnetic induction B and magnetization M are both expressed in Tesla. The spontaneous Hall coefficient R_s is generally found out by extrapolation of the high field data of ρ_H versus B_{in} to $B_{in} = 0$. But as stated in Chapter IV, in case of metallic glasses ρ_H versus B_{in} ($B_{in} = H_{ext}$) plot saturates so slowly that it is very difficult to find out R_s by this direct method. R_s in such alloys with high M_s values are calculated from the low field slope of ρ_H versus B_{in} plots. Justification of calculating R_s by this latter method is given below[128].

We can express eqn. (5.5) in terms of R_1 and R_o as,

$$\rho_H = R_o B_{in} + (R_1 - R_o)M_s$$

$$= R_o(B_{in} - M_s) + R_1 M_s$$

As shown in Sec. 3.7, we can write $B_{in} = H_{ext}$ and thus ρ_H can be written as,

$$\rho_H = R_o(H_{ext} - M_s) + R_1 M_s \tag{5.6}$$

Below the Curie temperature T_c and well below saturation $H_{ext} = M_s$. Then, eqn. (5.6) becomes

$$\rho_H = R_1 M_s \tag{5.7}$$

Since in amorphous ferromagnets $R_s \gg R_o$, $R_1 \simeq R_s$ and hence

$\frac{\partial \rho_H}{\partial H_{ext}}\Big|_{H_{ext}=0}$ will give the spontaneous Hall coefficient R_s.

We will, therefore, discuss the spontaneous Hall coefficient R_s thus calculated from the low field slope of ρ_H versus H_{ext} graph. O'Handley[83] has discussed R_s of amorphous $Fe_{80}B_{20}$. He has explained his results in terms of Berger's scattering mechanism as explained in Chapter II. It is argued that R_s of $Fe_{80}B_{20}$ is proportional to ρ^2 because it falls on an universal R_s vs ρ graph. It also seems to satisfy the relation $\Delta y \propto R_s/\rho^2$ (where Δy is the magnitude of the side jump) by giving $\Delta y \simeq 1 \times 10^{-10}$ m [calculated from eqn. (2.41)], comparable to that of crystalline transition metal alloys (also $\simeq 10^{-10}$ m). This agreement between Δy values and the point for $Fe_{80}B_{20}$ falling on the R_s versus ρ graph for crystalline materials seem to be a mere coincidence. As can be seen from Figs. 4.9 and 4.15, R_s does not vary as ρ^n. In fact, this relation given by eqn. (2.37) ($R_s = A \rho^n$) makes the assumption that any band structure differences due to the additives are negligible, the alloys are dilute ($\sim 5\%$) and R_s is governed mainly by scattering. As shown by Suzuki et al[112], the composition dependence of the coordination number, the density and the binding energy of Fe 3d-band clearly show that around the composition range from 14 to 16 atomic percent boron, there is a drastic modification in the topological arrangement of the Fe atoms in the Fe-B glassy alloys. These studies

suggest that the B atoms occupy interstitial position in the
low boron content alloys and with increasing boron content,
those atoms take the substitutional positions in the alloy.
Thus the band structure is severely altered around the eutectic
composition, and hence eqn. (2.37) should not hold for these
alloys.

For the $Fe_{100-x}B_x$ series, boron is non-magnetic and hence
with decreasing boron concentration we expect an increase in
R_s value. It is clear from Fig. 4.15, that between x = 26 and
x = 18, R_s increases with decreasing x as expected, but for
$13 \leq x \leq 18$, there is a fall in the R_s values. This sort of
unexpected behaviour of R_s for alloys with $x \leq 18$ can be
attributed to the Invar anomaly of Fe-B glassy alloys. Also,
the specific heat study of these alloys by Matsuura et al[54]
shows an unusually large value of γ (the electronic specific
heat coefficient) far exceeding the band structure contribution.
They attribute this unexpectedly large γ value for the low B
alloys to the ferromagnetic instability or magnetic inhomogenei-
ty closely related to the occurrence of Invar effect. Keeping
in view our R_s versus x plot, we suggest that due to the
occurrence of Invar characteristics in this series of alloys
around $x \leq 18$, the R_s values start falling.

The unexpectedly large monotonic fall of the Hall conducti-
vity γ_{H_s} ($R_s M_s/\rho^2$) could be understood in the following way.

In the range of composition $18 \leq x \leq 26$, R_s decreases and ρ increases with increasing x and thus both contribute to decrease γ_{H_s} with increasing x. However, in the range below x = 18, R_s and ρ both decrease with decreasing x and it becomes difficult to predict the behaviour of γ_{H_s}. As it is clear from Figs. 4.9 and 4.15, and also from Tables 4.3 and 4.7 the percentage variation of R_s and ρ in the range $13 \leq x \leq 18$ are more or less the same but since γ_{H_s} is inversely proportional to ρ^2, the effect of ρ is more and hence γ_{H_s} increases with decreasing x in this range.

5.4 CORRELATION BETWEEN HALL EFFECT AND MAGNETORESISTANCE

The correlation indicated by eqn. (2.46) could not be established in these metallic glasses. However, the reason behind this failure is very clear now. In $Fe_{80}B_{20}$, scanning electron microscope studies show[28,111] that the principal domains (~ 600 μm in width) lie parallel to the ribbon axis with the magnetization oriented at $20^{o} \sim 30^{o}$ off the ribbon axis in the plane of the sample. Due to the typical shape of these samples (thin, long ribbons), measurements of magnetoresistance and Hall effect are carried out in the orientation where the current flows parallel to the ribbon axis. It is clear from Sec. 2.4, that when current flows parallel to the domain walls, Berger's mechanism[107] does not come into the picture. Hence, the normal ferromagnetic anisotropy of resistivity is the only dominant mechanism for the magnetoresistance, as measured in the present orientation.

CHAPTER VI

ROLE OF Si AND C IN METGLAS 2605 SC[*]

6.1 INTRODUCTION

Metglas 2605 SC ($Fe_{81}B_{13.5}Si_{3.5}C_2$) is the successor of
Metglas 2605 ($Fe_{80}B_{20}$)[130]. It has a superior combination of
magnetic properties and low cost. In this chapter we report
a detailed study of thermomagnetic and transport properties
of these two amorphous ferromagnets in order to understand the
role, if any, of the partial replacement of boron (B) by
silicon (Si) and carbon (C). The low-field magnetic moment
was measured as a function of temperature from 300 to 1050K
to   investigate the whole process of magnetic and structural
phase transitions. Differential thermal analysis in the same
temperature range provided the crystallization temperatures.
Mössbauer and X-ray studies on annealed Metglas 2605 SC esta-
blished the equilibrium crystalline phases. The electrical
resistivity was measured from 300K down to 77K while the
magnetoresistance was measured at 300 and 77K. The Hall
resistivity was measured at 300K only. An attempt is made to
interpret the data in terms of existing ideas about amorphous
systems.

6.2 EXPERIMENTAL TECHNIQUE

The metallic glasses 2605 and 2605 SC were obtained from

Allied Chemical Corporation, New Jersey, USA. The thermo-
magnetic studies in the temperature range of 300 to 1050K
were made by using a PAR vibrating sample magnetometer
(Model 155) and a high temperature oven assembly (Model 151),
placed in the residual field ($\simeq$ 30G) of an electromagnet.
The magnetometer was calibrated with the help of a standard
Ni sample. The temperature of the sample was determined by a
Chromel-Alumel thermocouple and was correct to $\pm$ 2K. The
sample was kept in such a way that the magnetic field lay in
the plane of the sample (to minimise the demagnetizing field).
The typical heating rate used in the experiment was $\simeq$ 5K/min.
The rate was lowered to $\simeq$ 1K/min near the transition tempera-
tures.

For X-ray diffraction and Mössbauer studies we had
annealed a piece of 2605 SC for $\simeq$ 2 hrs. at 1200K. The sample
was completely crystallized by this heat treatment. Mössbauer
spectrum of this sample was taken by using a [57]Co-Rh source.
X-ray diffraction pattern of the same piece was taken in an
ISODEBYEFLEX 2002 diffractometer using a Cr source. The
differential thermal analysis was performed at a heating rate
of 5K/min using a Mom (Budapest) derivatograph.

The electrical resistivity, the magnetoresistances and the
Hall effect were measured using the procedures already described
in Chapter III.

6.3 RESULTS AND DISCUSSION

6.3.1 Curie Temperature T_c

The results of our studies of the low-field ($\simeq$ 34 G) magnetic moment μ (in arbitrary units) of Metglas 2605 SC as a function of temperature T are plotted in Fig. 6.1. The kink-point method gives a T_c of 646 K. The inset shows that the maximum of $-d\mu/dT$ vs. T plot is at 649 K. Thus the average T_c of the sample could be taken as (647 $\pm$ 2)K. Curie temperatures, T_c for all the $Fe_{100-x}B_x$ sample (13 $\leq$ x $\leq$ 26), were also measured. As shown in Fig. 6.2, T_c increases with increasing x. The Curie temperature of $Fe_{81}B_{19}$ from this graph is found to be $\simeq$ 645 K. This agrees well with the data of Kemény et al[124]. Thus, one can say that T_c is not much affected by partial replacement of B by Si and C. This implies that the near neighbour environment of the Fe-atoms is not very different in these two metallic glasses.

6.3.2 Thermomagnetic Studies

Fig. 6.3 shows an X-Y recorder plot of the low-field moment μ as a function of temperature T. A thermal cycling (from 300 to $\simeq$ 1050 K) of both Metglas 2605 SC and 2605 is shown in this figure. In the process of measurement Metglas 2605 has also been annealed at 915 K for 2 h.

The continuous curve of Fig. 6.3 represents the magnetization behaviour of 2605 SC. The first fall (645 K) corresponds to the transition from an amorphous ferromagnetic (a_f)

LOW FIELD (≈30 gauss) MAGNETIZATION OF METGLAS 2605 SC
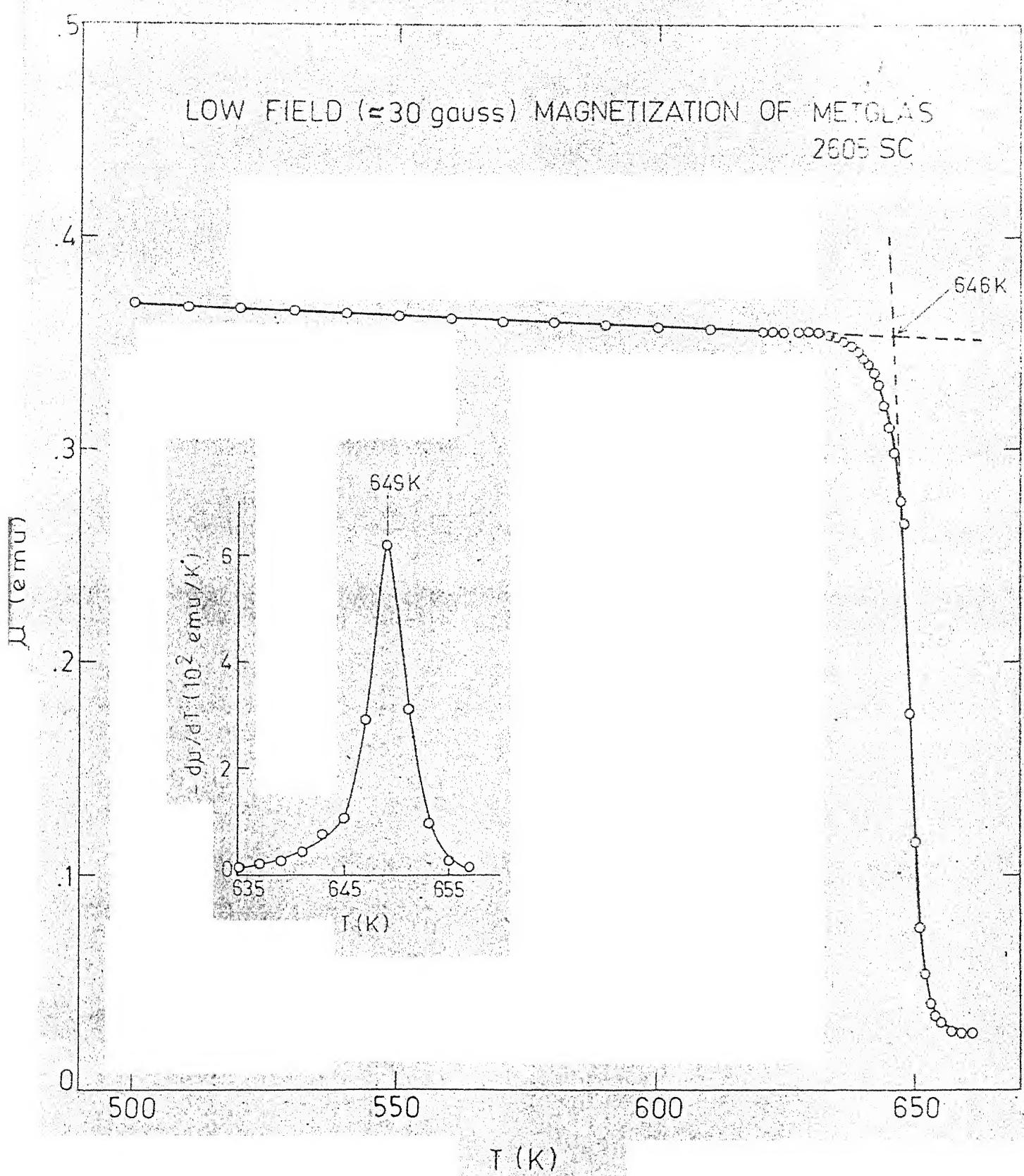
FIG. 6.1
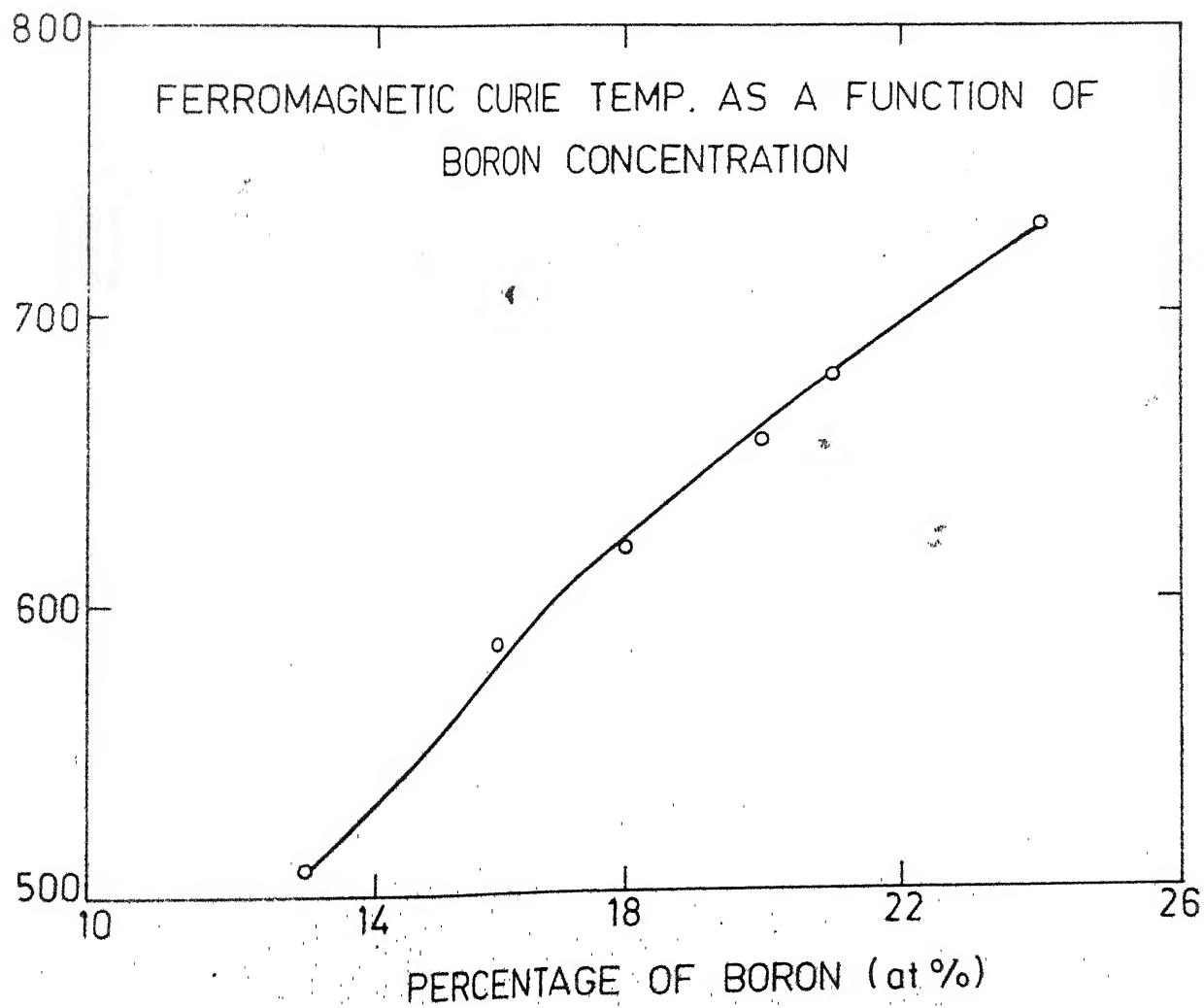
FIG. 6.2

CRYSTALLIZATION IN METGLAS

- - - - 2605
———— 2605 SC

μ (arbitrary units)

T (K)

FIG. 6.3

138
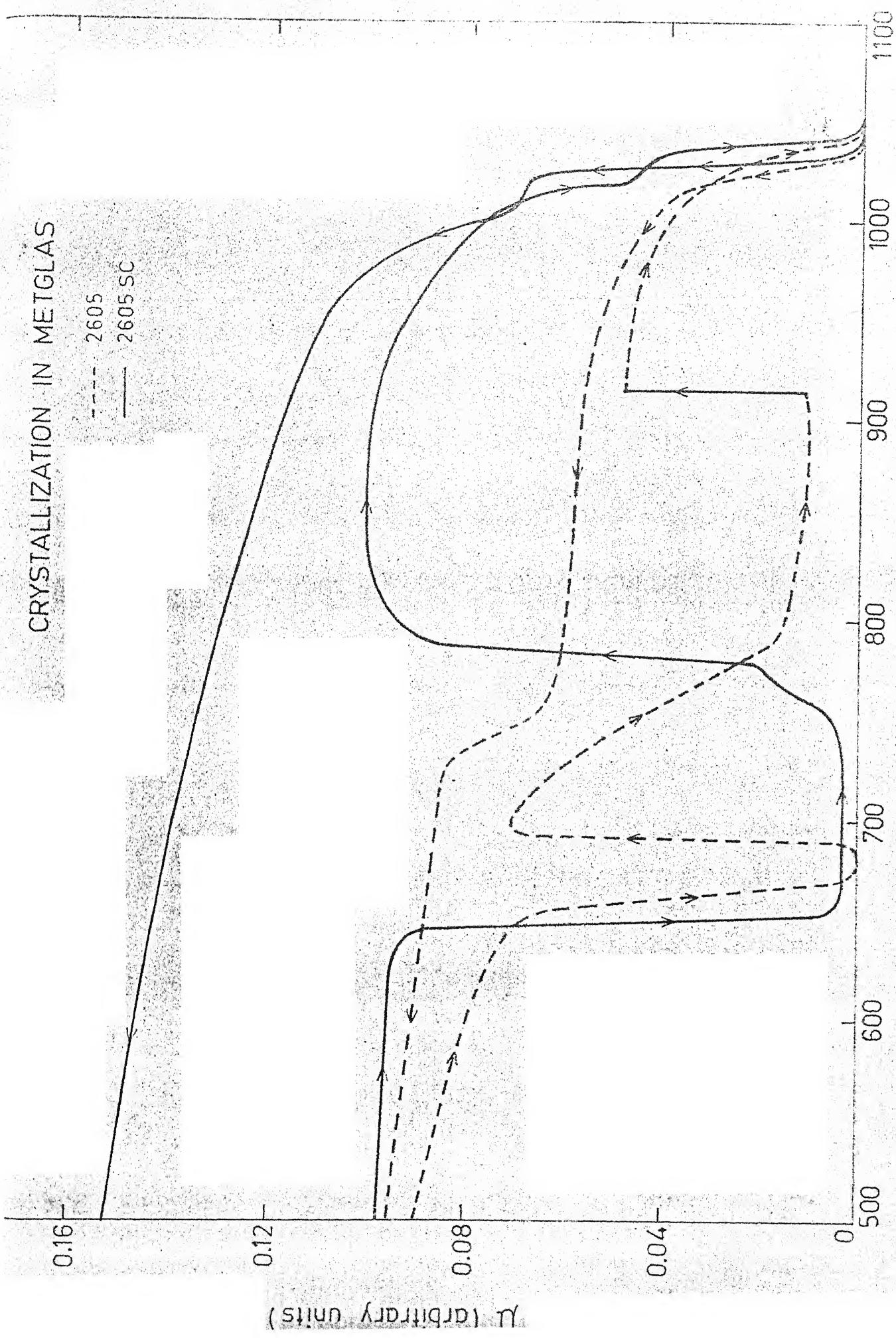
to an amorphous paramagnetic (a_p) state. At 750 K, α-Fe
starts precipitating and then at 780 K Fe_3B is getting
crystallized. The thermomagnetic data shows an unexpected
sharp rise in moment at 780 K, which is reproducible in
many runs. Such a rise in the moment could not be due to
α-Fe precipitation only. The moment of Fe_3B phase, on the
other hand, cannot be so large near its Curie temperature
which is around 800 K[131]. However, this is possible if
there appears other crystalline phases having high enough
T_c, e.g., Fe_3B decomposing into Fe_2B and α-Fe. Thus, most
probably, this sharp rise indicates that at 780 K, Fe_3B has
crystallized as well as has decomposed into Fe_2B and α-Fe
in their ferromagnetic states. Chien et al. had reported the
decomposition temperature of Fe_3B as $\geq$ 825 K[131], whereas we
find it to be around 780 K. This difference in decomposition
temperature could be due to very different heating rates in
the two cases, namely, 20 and 5 K/min, respectively. At much
higher temperatures there are two sharp falls, one at 1015 K
and the next at 1045 K. This very clearly shows the presence
of Fe_2B (T_c = 1015 K)[131] and α-Fe (T_c = 1043 K). Since the
magnetic moment becomes almost zero around 1045 K, it is clear
that no other ferromagnetic phase is present having still
higher T_c. While cooling we see a two-step rise in the
moment near 1040 and 1010 K corresponding to the two
equilibrium phases α-Fe and Fe_2B. The crystallization
sequence of 2605 SC can be schematically represented as :

at 645 K $\qquad$ $a_f(2605\ SC) \rightarrow a_p(2605\ SC)$,

at 750 K $\qquad$ $a_p(2605\ SC) \rightarrow C_f(\alpha\text{-}Fe) + a_p(rest)$,

at 780 K $\qquad$ $a_p(rest) \rightarrow C_f(\alpha\text{-}Fe) + C_f(Fe_3B)$

$$\text{and}$$

$$C_f(Fe_3B) \rightarrow C_f(Fe_2B) + C_f(\alpha\text{-}Fe),$$

at 1015 K $\qquad$ $C_f(Fe_2B) + C_f(\alpha\text{-}Fe) \rightarrow C_p(Fe_2B) + C_f(\alpha\text{-}Fe)$,

at 1045 K $\qquad$ $C_f(\alpha\text{-}Fe) + C_p(Fe_2B) \rightarrow C_p(\alpha\text{-}Fe) + C_p(Fe_2B)$.
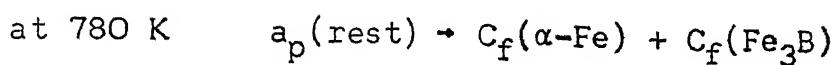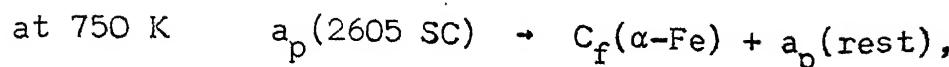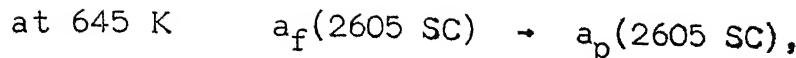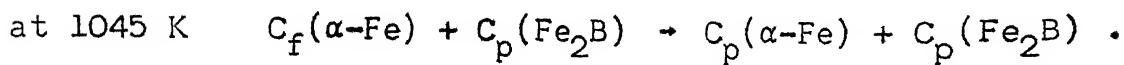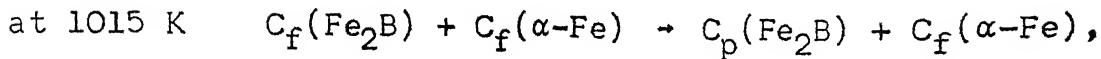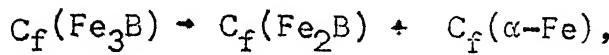
The dotted curve of Fig. 6.3 represents the magnetization of 2605. The first fall (655 K) is again due to the transition from an amorphous ferromagnetic to an amorphous paramagnetic state. In contrast to 2605 SC, the sharp rise in moment at 690 K shows the simultaneous crystallization of α-Fe and Fe_3B, both in their ferromagnetic states. Near 800 K, a smeared out fall occurs as one of the above two phases, namely, Fe_3B becomes paramagnetic. Note that the magnetic moment still does not fall to zero which verifies the presence of α-Fe, the second ferromagnetic phase. Around 915 K, the magnetic moment has a tendency to rise due to the crystallization of remaining Fe and here the sample was kept at a constant temperature for 2 h for complete crystallization. The next fall near 1040 K is clearly due to α-Fe. Here the magnetic moment becomes zero, showing the absence of any other ferromagnetic phase with higher T_c. While coming back in this thermomagnetic cycle

the rise in moment near 1040 and 800 K, proves the presence of α-Fe and Fe_3B as the two equilibrium phases. Schematically the crystallization sequence of 2605 is given by :

at $\simeq$ 655 K $\qquad a_f(2605) \rightarrow a_p(2605)$,

at $\simeq$ 690 K $\qquad a_p(2605) \rightarrow C_f(\alpha\text{-Fe}) + C_f(Fe_3B)$,

at $\simeq$ 800 K $\qquad C_f(\alpha\text{-Fe}) + C_f(Fe_3B) \rightarrow C_f(\alpha\text{-Fe}) + C_p(Fe_3B)$,

at $\simeq$ 1040 K $\qquad C_f(\alpha\text{-Fe}) + C_p(Fe_3B) \rightarrow C_p(\alpha\text{-Fe}) + C_p(Fe_3B)$.
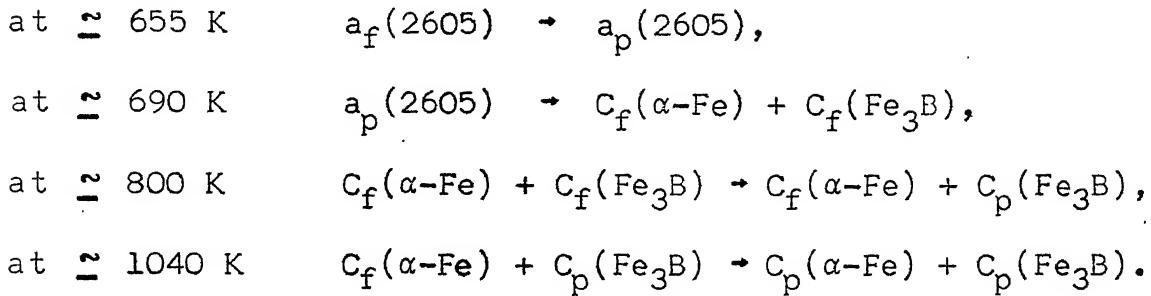
From the above discussion we find that in the case of 2605 α-Fe and Fe_3B crystallize in a single step whereas for 2605 SC there are two well-resolved steps of crystallization. The results of differential thermal analysis (DTA) support the above conclusion and are shown in Fig. 6.4. For Metglas 2605 SC the two major crystallization peaks are separated by about 30 K while Metglas 2605 has one major peak at $\simeq$ 710 K and two minor peaks around 920 K. A similar two-step crystallization for small B content samples and a single-step process for high B contents ones had been observed by Kemeny et al[124]. According to them, α-Fe precipitates until the composition of the remaining glass reaches $Fe_{75}B_{25}$ and then Fe_3B starts crystallizing. In 2605 SC Fe and B are present in the ratio 6:1, hence α-Fe precipitates first until this ratio becomes 3:1 and only then crystallization of Fe_3B starts. In 2605 the ratio, being 4:1, is already very close to 3:1 and

DIFFERENTIAL THERMAL ANALYSIS
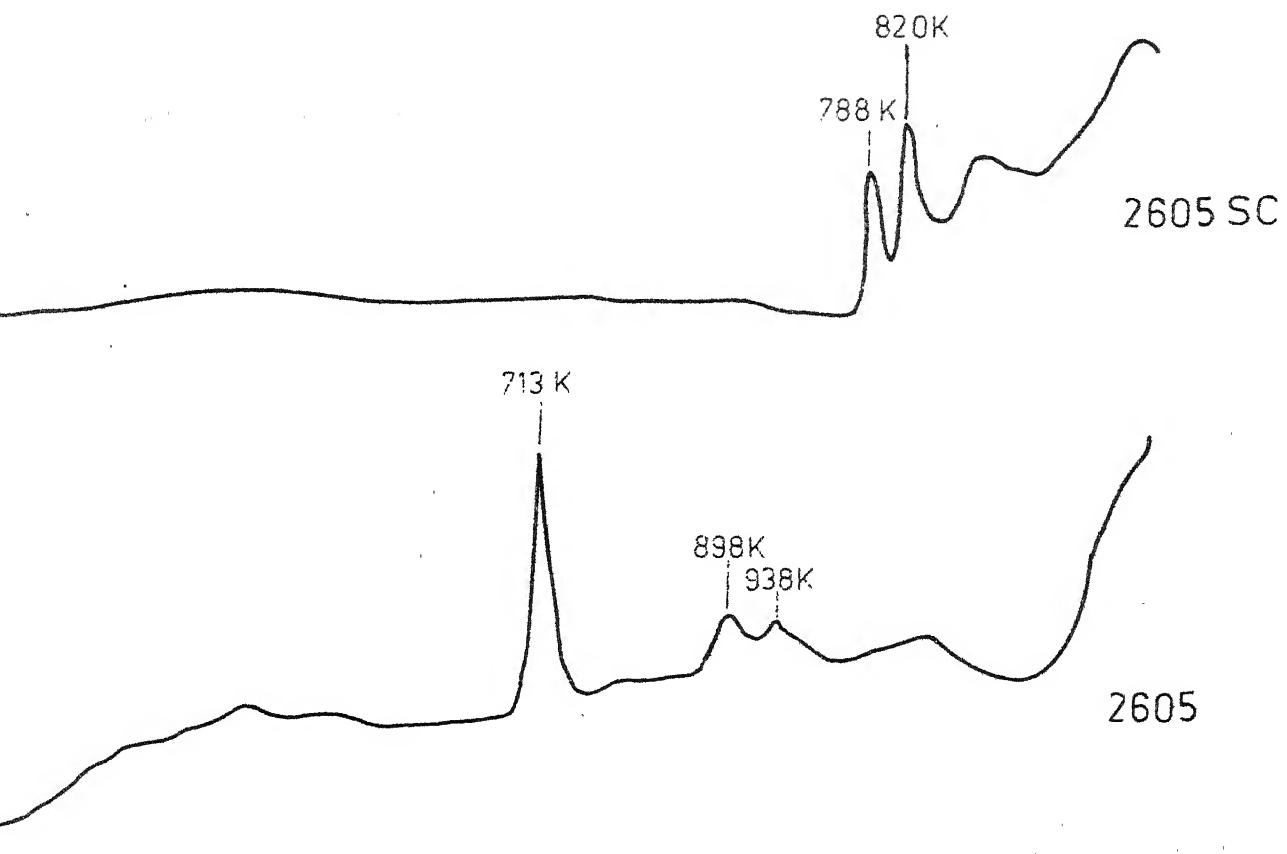
FIG. 6.4
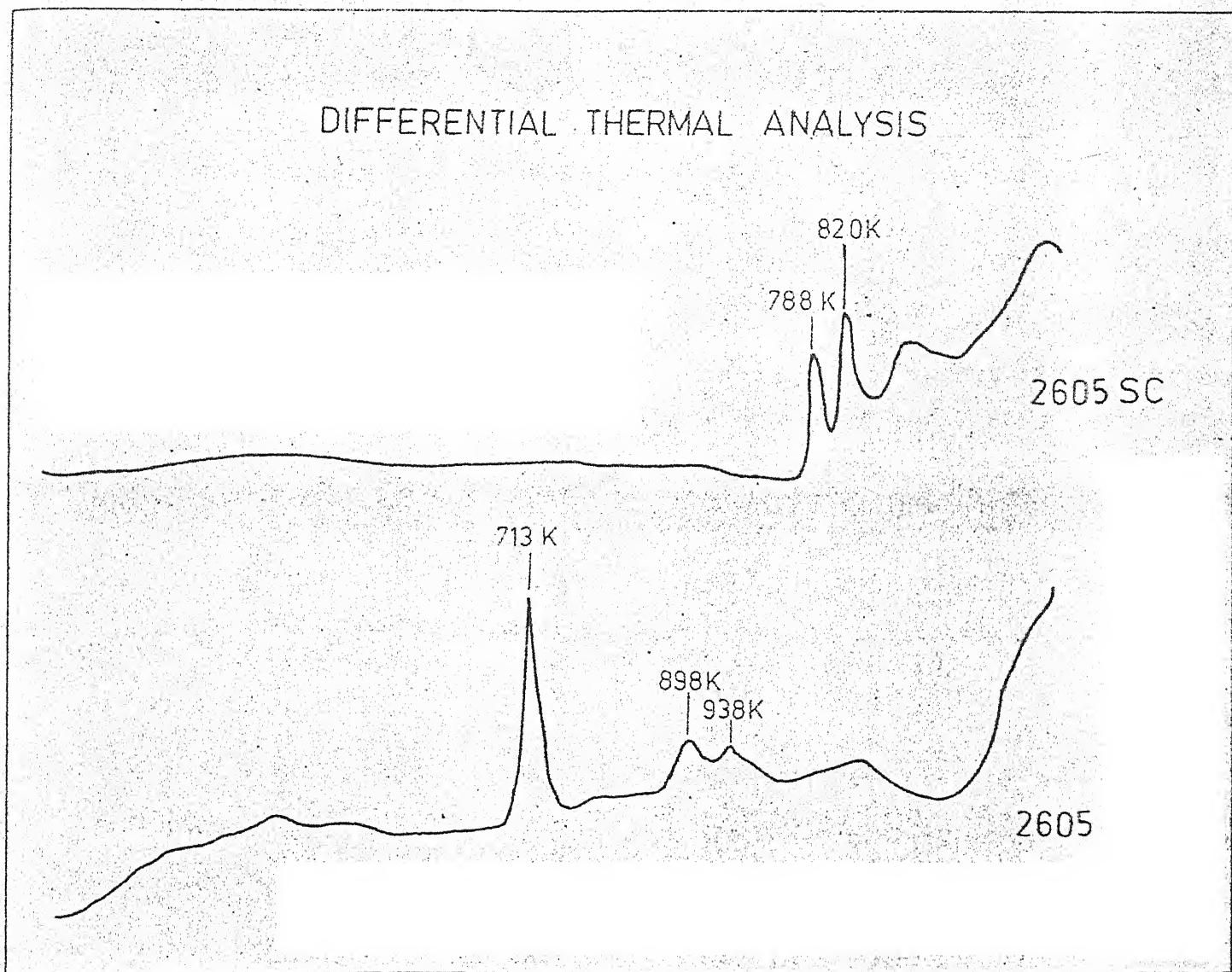
FIG. 6.4

MÖSSBAUER SPECTRUM OF METGLAS 2605 SC (annealed)
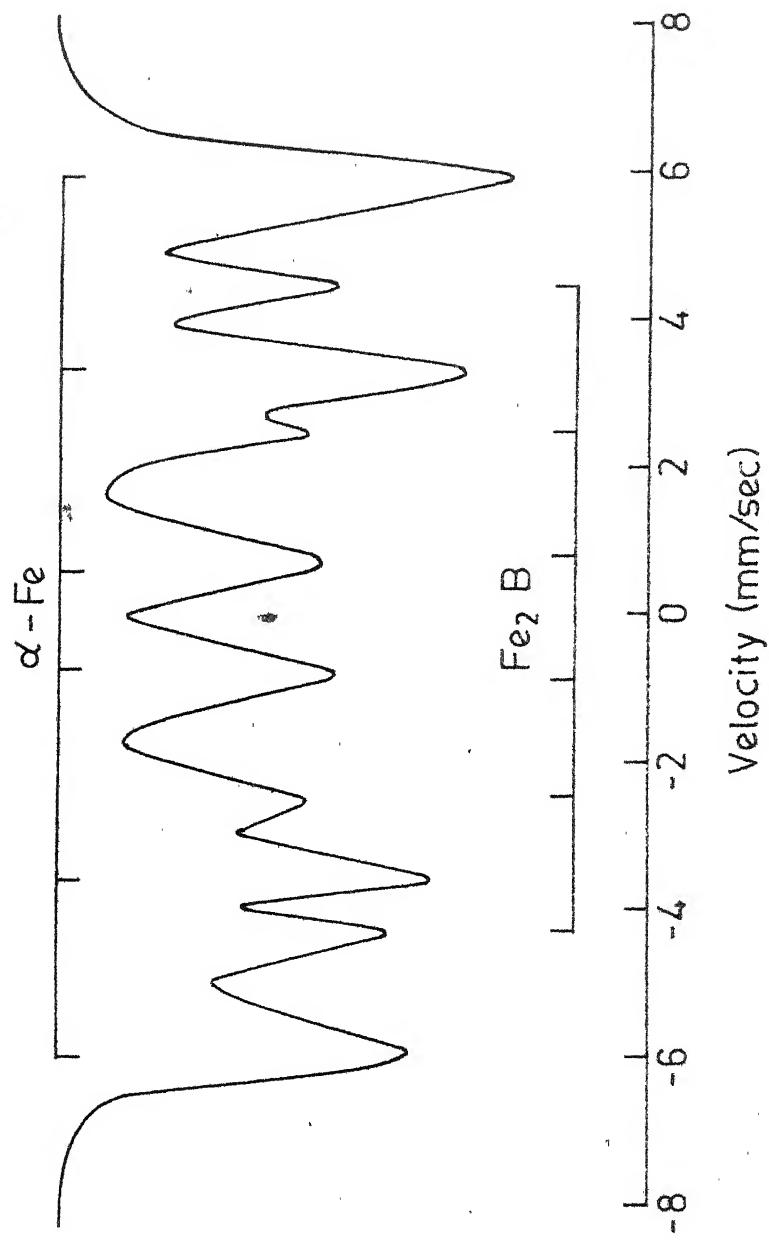
FIG. 6.5

isomer shift, within the error limit is found to be of α-Fe. Thus, Mössbauer study confirms the presence of α-Fe and Fe_2B as the equilibrium phases in 2605 SC.

6.3.4 X-ray Analysis

The X-ray analysis of the annealed 2605 SC sample shows a number of lines whose d-spacings are given in Table 6.1 as d_{obs}. Also, the characteristic lines of α-Fe, Fe_2B and Fe_3B are tabulated as d_{std}. A comparison immediately confirms the presence of α-Fe and Fe_2B phases. The X-ray diffraction pattern of 2605 SC had clearly shown the dominance of metal-metal pair contributions. This is due to the fact that the metal atoms have larger X-ray scattering factors than the metalloid (B) atoms and also, the alloy contains only about 13.5 at.% B.

The diffraction pattern had also shown some other lines which are yet to be identified. However, it is clear from the magnetization studies that they do not correspond to any magnetic phase.

6.3.5 Transport Properties

In Fig. 6.6 we have plotted ρ_T/ρ_{RT} vs. T (heating rate of $\simeq$ 2 K/min) for both Metglas 2605 SC and 2605. The resistivity varies linearly at higher temperatures and shows a quadratic behaviour at lower temperatures. The resistivity changes by about (2-3)% between 300 to 77 K. The temperature

Table 6.1

X-ray data of annealed Metglas 2605 SC

α-Fe		Fe$_2$B		Fe$_3$B	
d_{obs} (A^O)	d_{std}^{135} (A^O)	d_{obs} (A^O)	d_{std}^{135} (A^O)	d_{obs} (A^O)	d_{std}^{135} (A^O)
2.026	2.027	2.119	2.12	not present	2.090
1.430	1.433	2.011	2.01	not present	2.040
1.170	1.170	1.829	1.83	not present	2.034
		1.630	1.63		
		1.202	1.20		
		1.138	1.19		

coefficients of resistivity, $\alpha = (1/\rho_{RT})\partial\rho_T/\partial T$ for 2605 SC and 2605 are $(1.20 \pm 0.05) \times 10^{-4}$ K^{-1} and $(1.65 \pm 0.05) \times 10^{-4}$ K^{-1}, respectively. As stated earlier in Chapter II, the variation of ρ with temperature is governed by two factors :(1) The electron-phonon scattering which gives a positive α and(2) The decrease at higher temperatures in the height of the first peak of the structure factor S(k) vs. wave vector k graph which gives rise to a negative α. The latter is larger for
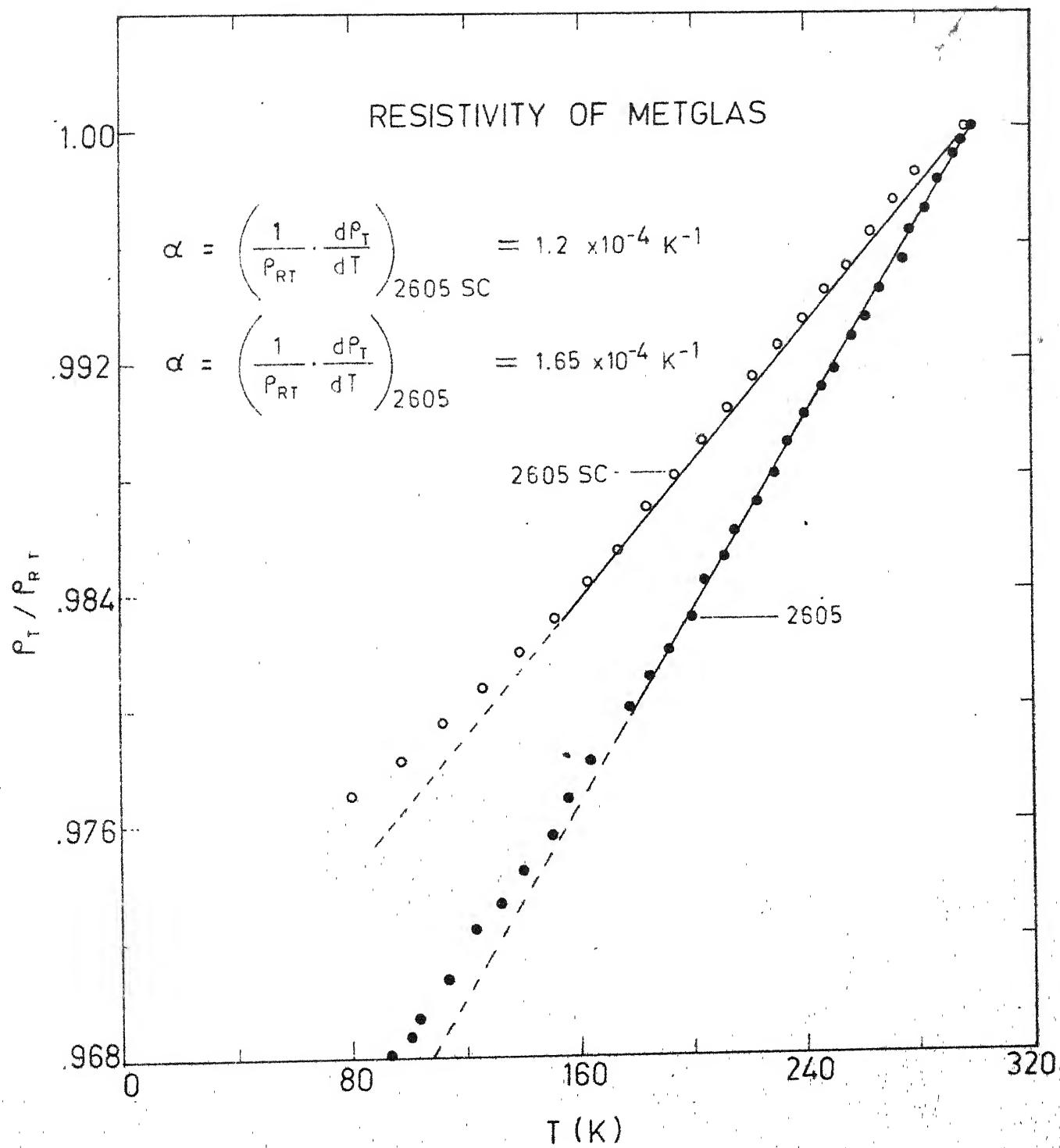
FIG. 6.6

metalloids with valency 4 (for x = 20) (see e.g., ref. [98]).
When B (valency 3) is partially replaced by Si and C (valency 4
for both) the effective valency increases beyond 3 and so the
negative contribution is more which makes the overall tempera-
ture coefficient of resistivity less positive in 2605 SC. The
temperature coefficient of resistivity is large if the total
resistivity is dominated by electron-phonon scattering. In
metallic glasses scattering from structural disorder is the
dominant mechanism and hence α is found to be much less than
that of the crystalline alloys. Thus, the lower value of α
for 2605 SC as compared to that of 2605 suggests more
structural disorder in the former. Hence, partial replacement
of B by Si and C makes 2605 SC comparatively more stable than
2605 as an amorphous alloy. The higher value of resistivity ρ
(by $\simeq$ 6%) in 2605 SC also supports the above conclusion about
their stability. The Debye temperature θ_D, calculated from
eqn. (2.11) for 2605 SC and 2605 are 470 and 390K, respectively.
However, we observe that the linearity (down to 160 and 180K
for 2605 SC and 2605, respectively, see Fig. 6.1) of ρ_T/ρ_{RT} vs.
T continues much below the Debye temperature in contradiction
to eqn. (2.8).

Fig. 6.7 shows plots of magnetoresistance $\Delta\rho/\rho$ of
Metglas 2605 SC against the external magnetic field H_{ext} for
both longitudinal ($\vec{J} \parallel \vec{M}$) and transverse ($\vec{J} \perp \vec{M}$) orientations
at 300 and 77K. The behaviour at low fields is very similar

MAGNETORESISTANCE OF METGLAS 2605 SC

$\vec{J} \parallel \vec{M}$ 77 K

$\vec{J} \parallel \vec{M}$ 300 K

$\vec{J} \perp \vec{M}$ 300 K

$\vec{J} \perp \vec{M}$ 77 K

$\overline{\Delta P / P} \times 10$

Hext (KG)
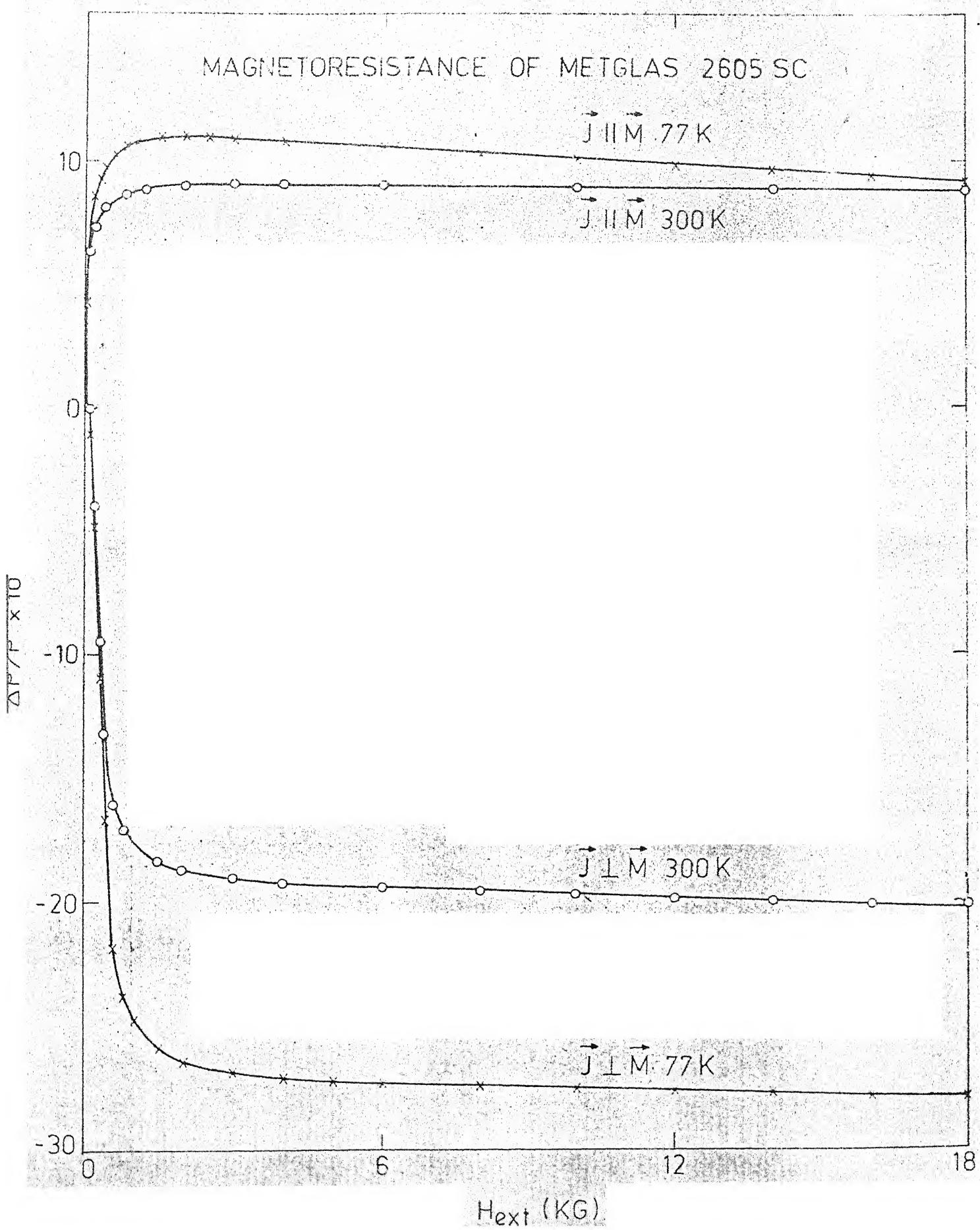
FIG. 6.7

to that of crystalline ferromagnets with domain structures.
The FAR is 0.28 and 0.38% at 300 and 77 K, respectively, while
for 2605 they are 0.38 and 0.54% at 300 and 77 K, respectively.
These values are much smaller than those of their crystalline
counterparts. The high field slopes are negative and are due
to less electron-magnon scattering at higher fields. The Hall
effect data of 2605 SC is shown in Fig. 6.8. R_s is here cal-
culated in the usual manner. From the Hall resistivity (ρ_H)
data of Metglas 2605 SC we have calculated the extraordinary
Hall constant R_s and the Hall conductivity $\gamma_{H_s} = R_s M_s / \rho^2$
where M_s is the saturation magnetization (see Table 6.2).

In Table 6.2 we have compared the values of ρ , α,
$\Delta\rho_{||S}/\rho$, $\Delta\rho_{\perp S}/\rho$, FAR, high-field slopes $[(1/\rho)\ \partial\rho/\partial H]_{||}$
and $[(1/\rho)\partial\rho/\partial H]_{\perp}$, M_s, R_s and γ_{H_s} for 2605 SC and 2605. One
finds from this table that the magnetoresistance and the Hall
effect do not show any qualitative difference in these two
metallic glasses.

6.4 CONCLUSIONS

The present work could be summarized as follows :

i) The Curie temperature is little affected by the partial
replacement of B by Si and C. However, the final equilibrium
phases peresent in 2605 SC are Fe_2B and α-Fe while in 2605
they are Fe_3B and α-Fe.

HALL RESISTIVITY AS A FUNCTION OF B_{in} AT ROOM TEMP.
2605 SC

$P_H \times 10^9$ Ω m

B_{in} (KG)
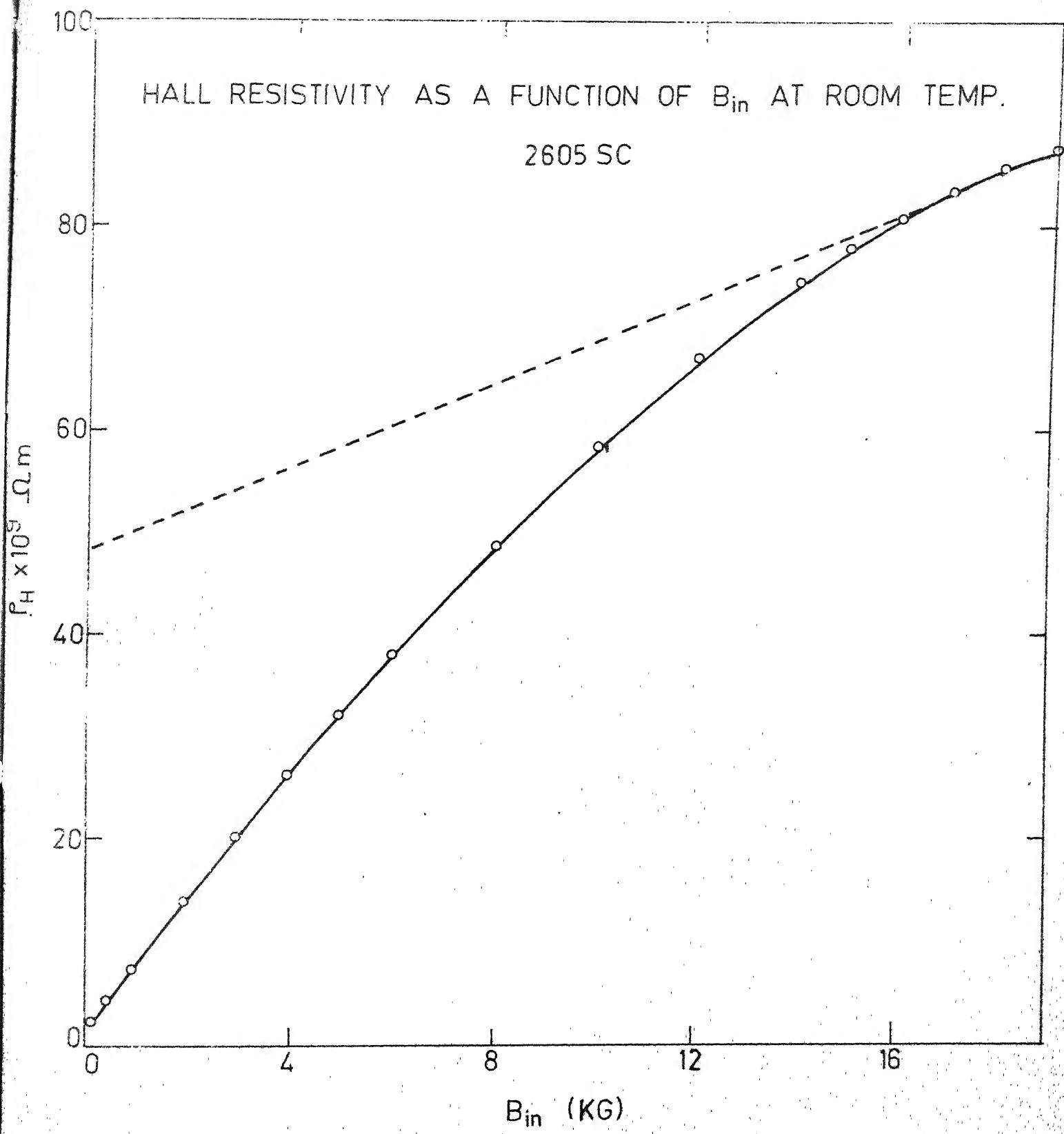
FIG. 6.8

Table 6.2

Comparison of transport properties of Metglas 2605 SC
and 2605

Property	at T(K)	Metglas 2605 SC	Metglas 2605
$\rho(\mu \Omega m)$	300	1.25	1.18
$\alpha(10^{-4}K^{-1})$	–	1.20 ± 0.05	1.65 ± 0.05
$\Theta_D(K)$	–	470	390
$\frac{\Delta\rho_{\parallel S}}{\rho}$ (10^{-4})	300	9	13
	77	11	17
$\frac{\Delta\rho_{\perp S}}{\rho}$ (10^{-4})	300	−19	−25
	77	−27	−37
FAR(%)	300	0.28	0.38
	77	0.38	0.54
$(\frac{1}{\rho}\frac{\partial\rho}{\partial H})_{\parallel}(10^{-8}G^{-1})$	300	−0.13	−0.30
	77	−1.00	−1.00
$(\frac{1}{\rho}\frac{\partial\rho}{\partial H})_{\perp}(10^{-8}G^{-1})$	300	−0.75	−0.50
	77	−0.50	−1.10
$R_s(10^{-3}$ m^3/c)	300	2.90 ± 0.3	5.5 ± 0.3
$M_s(T)$	300	1.61	1.56
$\gamma_{H_s}(10^2$ $\Omega^{-1}m^{-1})$	300	300	616

ii) In 2605 SC, α-Fe and Fe_3B crystallize in two different steps while in 2605 it is a single step process. Differential thermal analysis also supports this fact by showing two peaks for 2605 SC and only one major peak in case of 2605.

iii) The heat effect of the transformation of Fe_3B into α-Fe and Fe_2B is too small to be observed in DTA, but this transformation can be recognised through magnetization studies.

iv) The partial replacement of B by Si and C enhances the crystallization temperature of 2605 SC and thereby increases its stability.

v) A lower value of the temperature coefficient of resistivity and a higher value of the resistivity also confirm the fact that 2605 SC is more stable.

vi) Magnetoresistance and Hall effect are not much affected by the partial replacement of B by Si and C.

Hence, it is concluded that the thermomagnetic properties are seriously affected by the replacement of B by Si and C while the transport properties have changed only quantitatively.

APPENDIX   1

ERROR CALCULATION IN Θ_D OF $Fe_{80}B_{19}Si_1$

$$\Theta_D = \frac{\pi^2}{6}\,\frac{\alpha}{s} \quad [eqn. (2.11)]$$

Hence, error in Θ_D = error in α + error in S,

where α is the slope of linear part of ρ_T/ρ_{RT} vs T plot

S is the slope of ρ_T/ρ_{RT} vs T^2 plot.

It is clear that error in α will be the same whether the measurements are done between 77K $\leq$ T $\leq$ 300K or between 4.2K $\leq$ T $\leq$ 300K. Only the accuracy in calculating S can be increased by making measurements down to 4.2K.

Error in S :

error in y axis of ρ_T/ρ_{RT} vs T^2 plot =

$$\frac{\sqrt{[(0.5)^2+1^2+(1.5)^2+2^2+1^2]}}{\sqrt{16}}\ div = 0.73\ div.$$

0.73 div in y axis = 0.000073 .

Hence, uncertainty in y axis = $\frac{0.000073}{0.003600}$ = $2.03\times10^{-2} \simeq 2\%$

error in x axis of ρ_T/ρ_{RT} vs T^2 plot =

$$\frac{\sqrt{[(0.5)^2+(0.5)^2+1^2+2^2+(2.5)^2+(1.5)^2]}}{\sqrt{16}} = 0.9354\ div$$

0.9354 div on x axis = $93.54K^2$.

Hence, uncertainty in x axis = $\frac{93.54}{4742.91}$ = $1.97 \times 10^{-2} \sim 2\%$

Therefore, error in S $\simeq$ 4% .

Error in α :

Error in y axis of ρ_T/ρ_{RT} vs T plot =

$$\frac{\sqrt{[1^2+(0.5)^2+1^2+(0.5)^2+(0.5)^2+1^2]}}{\sqrt{20}} = 0.43 \text{ div} = 0.000043$$

Therefore, error in y axis = $\frac{.000043}{.016700}$ = 2.575×10^{-3} = 0.26%

Error in x axis = $\frac{\sqrt{[(1)^2+(0.5)^2+(0.5)^2+(0.5)^2+(0.5)^2+(1)^2]}}{\sqrt{20}}$ =

$$= 0.39 \text{ div} = 0.78K$$

Hence, error in x axis = $\frac{0.78}{109.5}$ = $7.12 \times 10^{-3} \simeq 0.7\%$

Therefore, error in α = 1%

Hence, error in θ_D = (4+1)% = 5%

Hence, θ_D = (330+16)K for $Fe_{80}B_{19}Si_1$.

APPENDIX – 2

CALCULATION FOR DEMAGNETIZING FIELD H_{demag}

In a sample in the form of a rectangular plate with length = 2c, width = 2b and the thickness = 2a, the demagnetizing factor α is given by[121] :

When magnetic field H || c,

$$\alpha = \frac{2}{\pi} \cot^{-1} \left[\frac{(a^2+b^2+c^2)^{1/2} \, c}{ab} \right] .$$

When magnetic field H || b,

$$\alpha = \frac{2}{\pi} \cot^{-1} \left[\frac{(a^2+b^2+c^2)^{1/2} \, b}{ac} \right] .$$

When magnetic field H || a,

$$\alpha = \frac{2}{\pi} \cot^{-1} \left[\frac{(a^2+b^2+c^2)^{1/2} \, a}{bc} \right] .$$

For a typical sample used for our transverse and longitudinal magnetoresistance measurements,

$$2c = 1.4 \text{ cm}$$

$$2b = 0.1 \text{ cm}$$

$$2a = 0.0025 \text{ cm} .$$

For transverse magnetoresistance, H $\parallel$ b and therefore

$$\alpha = \frac{2}{\pi} \cot^{-1} \left[\frac{\{(0.7)^2(0.05)^2+(0.00125)^2\}^{1/2} \times 0.05}{0.7 \times 0.00125} \right]$$

$$= \frac{2}{\pi} \cot^{-1} [40.102]$$

$$= 1.588 \times 10^{-2}$$

Therefore, $H_{demag} = \alpha M_s = 1.588 \times 10^{-2} \times 16.1$ [M_s=16.1 kG]

$$= 0.256 \text{ kG}$$

$$= 256 \text{ gauss}$$

For longitudinal magnetoresistance H $\parallel$ c and so,

$$\alpha = \frac{2}{\pi} \cot^{-1} \left[\frac{\{(0.7)^2+(0.05)^2+(0.00125)^2\}^{1/2} \times 0.7}{0.00125 \times 0.05} \right]$$

$$= 8.104 \times 10^{-5}$$

Therefore, $H_{demag} = \alpha M_s = 8.104 \times 10^{-5} \times 16.1$ kG

$$= 1.3 \times 10^{-3} \text{ kG}$$

$$= 1.3 \text{ gauss}$$

Hence, in longitudinal measurements, $H_{demag} \simeq 0.$

REFERENCES

1. P. Duwez, in Topics in Applied Physics, vol. 46, edited by Gunther odt and H. Beck (Springer-Verlag, Berlin, Heidelberg, New York 1981).

2. A.I. Gubanov, Fiz. Tver. Tel. 2, 502 (1960).

3. W. Klement Jr., R.H. Willens and P. Duwez, Nature 187, 869 (1960).

4. M.H. Cohen and D. Turnbull, Nature 189, 131(1961).

5. P. Duwez, R.H. Willens and R.C. Crewdson, J.Appl. Phys. 36, 2267(1965).

6. H.S. Chen and D. Turnbull, J.Chem. Phys. 48, 2560(1968).

7. H.S. Chen and D. Turnbull, Acta Metall. 17, 1021(1969).

8. P. Duwez and S.C.H. Lin, J.Appl.Phys. 38, 4096(1967).

9. I.S. Jacobs, J.Appl.Phys.50, 7294(1979).

10. Polk and Giessen, in Metallic Glasses, edited by Gilman and Leamy (American Society for Metals, Metals Park, Ohio, 1976).

11. E.M. Breinan, B.H. Kear and C.M. Bonas, Phys.Today 29, 45 (1976).

12. R. Clampitt, M.G. Scott, K.L. Aithen and L. Gowland, in Rapidly Quenched Metals III, edited by B. Cantor (The Metals Society, London 1978).

13. Davis, Fischer, Giessen and Polk, in Rapidly Quenched Metals III, edited by B. Cantor (The Metals Society, London 1978).

14. H. Beck and H.J. Guntherodt, in Topics in Applied Phys., vol.46, edited by Guntherodt and Beck (Springer-Verlag, Berlin, Heidelberg, New York 1981).

15. R.W. Cahn, Contemp. Phys. 21, 43 (1980).

16. Spaepen and Turnbull in Proc. of 2nd Int.Conf. Rapidly Quenched Metals, edited by Grant and Giessen (MIT Press, Cambridge, Mass, 1976.

17. J.D. Bernal, Proc.R.Soc. A280, 299(1964).

18. P. Predecki, B. Giessen and N.J. Grant, Trans. Met.Soc. AIME, 245, 407(1969).

19. H.S. Chen and K.A. Jackson, in Metallic Glasses, edited by Gilman and Leamy (American Society for Metals, Metals Park, Ohio 1976).

20. S.R. Nagel and J. Tauc, Phys.Rev.Lett. 35, 380(1975).

21. G.S. Cargill III, in Solid State Phys, vol.30, edited by Ehrenreich, Seitz and Turnbull (Academic Press, New York, 1975).

22. J.L. Finney, Proc. Roy. Soc.(London) 319, 479 (1970).

23. C.H. Benett, J.Appl. Phys. 43, 2727 (1972).

24. G.S. Cargill III and S. Kirkpatrick, AIP Conf.Proc. 31, 339(1976).

25. H. Hiroyoshi, K. Fukamichi, M. Kikuchi, A. Hoshi and T. Masumoto, Phys. Lett. 65A, 163(1978).

26. R. Hasegawa and Ranjan Ray, Phys.Rev. B20, 211(1979).

27. N. Kazama, M. Kameda and T. Masumoto, AIP Conf.Proc. 34, 307(1976).

28. R. Hasegawa, O'Handley, Tanner, Ray and Kavesh, Appl.Phys. Lett. 29, 219(1976).

29. F.E. Luborsky, in Ferromagnetic materials, vol.1, edited by E.P. Wohlfrath (North-Holland Publishing Company, 1980).

30. R. Alben, J.I. Budnick and G.S. Cargill III, in Metallic Glasses, edited by Gilman and Leamy (American Soc. for Metals, Metals Park, Ohio, 1976).

31. T. Mizoguchi, K. Yamauchi and H. Miyajima, in Amorphous Magnetism edited by H.O. Hooper and A.M. deGraaf (Plenum Press, New York, 1973).

32. J. Durand and M. Yung, in Amorphous Magnetism II, edited by Levy and Hasegawa (Plenum Press, New York, 1977).

33. C.L. Chien and R. Hasegawa, AIP Conf. Proc. 31, 366(1976).

34. T.Mizoguchi and K. Yamauchi, J.De.Physique, 35(C4), 287(1974).

35. K. Yamada, Y. Ishikawa and Y. Endoh, Solid State Commun 16, 1335(1975).

36. H.J. Leamy, E.M. Gyorgy, R.C. Sherwood, T. Wakiyama and H.S. Chen, AIP Conf. Proc. 29, 211(1976).

37. G.S. Cargill III, AIP Conf.Proc. 24, 138(1975).

38. C.D. Graham Jr. and T. Egami, Ann. Rev.Mater.Sci. 423(1978).

39. H.S. Chen, R.C. Sherwood and E.M. Gyorgy, IEEE Trans. Magn. MAG-13, 1538(1977).

40. H.S. Chen, R.C. Sherwood, H.J. Leamy and E.M. Gyorgy, IEEE Trans. Magn. MAG-12, 933(1976).

41. J.J. Rhyne, J.H. Schelleng and N.C. Koon, Phys.Rev. B10, 4672 (1974).

42. B.S. Berry and W.C. Pritchet, Phys.Rev.Lett. 34, 1022(1975).

43. S. Ohnuma and T. Masumoto, in Rapidly Quenched Metals III, edited by B. Cantor (Metals Soc.London, 1978).

44. H.A. Brooks, J.Appl.Phys. 47, 344(1976).

45. R.C. Sherwood, E.M. Gyorgy, H.S. Chen, S.D. Ferris, G. Norman and H.J. Leamy, AIP Conf.Proc. 24, 745(1975).

46. N. Tsuya, K.I. Arai, Y. Shiraga, M. Yamada and T.Masumoto, Phys.Stat.Sol(a) 31, 557(1975).

47. K. Narita, J. Yamasaki and H. Fukunaga, J.Appl.Phys. 50, 7591(1979).

48. R.C. O'Handley, in Amorphous Magnetism II, edited by Levy and Hasegawa (Plenum Press, New York, 1977).

49. K.I. Arai, N. Tsuya, M. Yamada, H. Shirac, H. Fujimori, H. Saito and T. Masumoto, in 2nd Int. Conf.Rapidly Quenched Metals, edited by Grant and Giessen (MIT Press, Cambridge, Mass, 1976).

50. R.C. O'Handley, Solid State Commun. 22, 485(1977).

51. T. Jagielinski, K.I. Arai, N. Tsuya, S. Ohnuma and T. Masumoto, IEEE Trans. Magn. MAG-13, 1553 (1977).

52. J.K. Krause, T.C. Long, D.G. Onn and F.E. Luborsky, J. Appl. Phys. 50, 7665 (1979).

53. B. Golding, B.G. Bagley, F.S.L. Hsu and H.S. Chen, Phys.Rev.Lett. 29, 68(1972).

54. M. Matsuura, U. Mizutani and Y.Yazawa,J.Phys.F. Metal Phys. 11, 1393 (1981).

55. H.S. Chen and D. Turnbull, Appl.Phys.Lett. 10, 284(1967).

56. F. Yonezawa, Proc. Fourth Int.Conf. on Liquid and Amorphous Metals, Grenoble, 1980 [J.De. Phys. C8, 459(1980)].

57. L.M. Roth and V.A. Singh, Phys.Rev. B25, 2522(1982).

58. E. Esposito, H. Ehrenreich and C.D. Gelatt.Jr., Phys.Rev. B18, 3913(1978).

59. P. Cote and L.V. Meisel in Topics in Appl.Phys., vol.46, edited by Güntherodt and Beck (Springer-Verlag, Berlin, Heidelberg, New York, 1981).

60. O. Dreirach, R. Evans, H.J. Güntherodt and H.V. Kunzi, J. Phys.F. Metal Phys. 2, 709(1972).

61. K. Hirata, Y. Waseda, A. Jain and R.Srivastava,J.Phys.F. Metal Phys 7, 419(1977).

62. H.N.Dunleavy and W. Jones, J.Phys.F. Metal Phys. 8, 1477(1978).

63. R. Kubo, J.Phys.Soc.Jpn. 12, 570(1957).

64. A. Chen, G. Weisz and A. Sher, Phys.Rev. B5, 2897(1972).

65. F. Brouers and M. Brauwers, J.Phys. 36, L17(1975).

66. R. Harris, M. Shalmon and M. Zuckerman, Phys.Rev. B18, 5906(1978).

67. J. Richter and W. Sniller, Phys.Stat.Solidi(b) 92, 511(1979).

68. G. Bergmann and P. Marquardt, Phys.Rev. B17, 1355(1978).

69. R. Richter, M. Wolf and F. Goedsche, Phys.Stat.Solidi(b), 95, 473(1979).

70. E. Babic, M. Ocko, Z. Marohnic, A.S. Schaafsma and I. Vincze, J. De. Phys., 41 (C8), 473(1980).

71. E. Babic, Z. Marhonic, M. Ocko, A. Hamzic, K. Saub and B. Pivac, J.Mag.Mag. Mater. 15-18, 934(1980).

72. A. Mogro-Campero, J.L. Walter and T.E. Coan, Phys.Rev. B24, 3579(1981).

73. M. Naka, R. Kern and U. Gonser, J.Appl.Phys. 52, 1448(1981).

74. J. Yamasaki, H. Fukunaga and K. Narita, J.Appl.Phys. 52, 2202(1981).

75. K. Fukamichi, R.J. Gambino and T.R. Mc Guire, 4th Int. Conf. Rapidly Quenched Metals,(Sendai), 835(1982).

76. Y. Obi, H. Fujimori and H. Morita, in the 1669th report of the Research Inst. for Iron, Steel and other Metals, 1976 (Sci. Rep. Tohoku.Univ. A26, 214 (1976)).

77. R. Kern and U. Gonser, J. Mag.Mag. Mater. 13, 74(1979).

78. Z. Marohnic, E. Babic and D. Pavuna, Phys.Lett. 63A, 348(1977).

79. G. Bhonke, N. Croitoriu, M. Rosenberg and M. Sostarich, IEEE Trans. Magn. MAG-14, 955(1978).

80. G. Bhonke and M. Rosenberg, Journal De Phys. C8, 481 (1980).

81. K. Fukamichi, R.J. Gambino and T.R. McGuire, J.App. Phys. 53, 8254(1982).

82. A.K. Nigam and A.K. Majumdar, Physica 95B, 385(1978).

83. R.C. O'Handley, Phys.Rev.B18, 2577(1978).

84. R. Malmhall, G. Backstrom, S.M. Bhagat and K.V. Rao, J.Non.Cryst. Solids 28, 159(1978).

85. K.V. Rao, R. Malmhall, S.M. Bhagat, G. Backstrom and H.S. Chen, IEEE Trans. Magn.MAG-16, 896(1980) (Proc. of Intermag-1980 held at Boston).

86. R. Malmhäll, K.V. Rao, G. Bäckström and S.M. Bhagat, Physica B86-88 B,796(1977).

87. R. Malmhäll, G. Bäckström and S.M. Bhagat, K.V. Rao, Bull.Am.Phys.Soc. 22, 265(1977).

88. T.R. McGuire, R.J. Gambino and R.C. O'Handley, in Hall Effect and its Applications, edited by C.L. Chien and C.R. Westgate (Plenum Press, New York, 1980).

89. E.P. Wohlfrath, Trans. on Magn. MAG-14, 933(1978).

90. A.J. Freeman and M. Shimizu, in the Invar Problem (North-Holland, Amsterdam, 1979).

91. S.N. Kaul, Phys.Rev. B27, 6923(1983).

92. H. Masumoto, Sci.Rep. Tohoku. Imp.Univ. 20, 10(1931).

93. N. Banerjee, Ratnamala Roy, A.K. Majumdar and R. Hasegawa, Phys.Rev. B24, 6801 (1981).

94. J.M. Ziman, Advan. Phys. 16, 551(1967).

95. R. Evans, D.A. Greenwood and P. Lloyd, Phys.Lett. A35, 57(1971).

96. R. Evans, B.L. Gyorffy, N. Szabo and J.M. Ziman, in the Properties of Liquid Metals (Proc.Int.Conf.Liquid Metals, 2nd) edited by S. Takeuchi (Taylor and Francis Ltd., London, 1973).

97. G. Busch and H.J. Guntherodt, in Solid State Phys. vol.29, edited by Ehrenreich, Seitz and Turnbull (Academic Press, New York, 1974).

98. S.R. Nagel, Phys.Rev. B16, 1694(1977).

99. P. Duwez, Ann.Rev.Mater.Sci, 6 (1976).

100. R.W. Cochrane, R. Harris, J.O. Stromolson and M.J. Zuckermann, Phys.Rev.Lett. 35, 676(1975).

101. T.E. Faber and J.M. Ziman, Philos.Mag. 11, 153(1965).

102. J.P. Jan, in Solid State Phys. vol.5, edited by Seitz and Turnbull (Academic Press, New York, 1957).

103. J. Smit, Physica 17, 612 (1951).

104. C.L. Chien and R. Hasegawa, in Amorphous Magnetism II, edited by Levy and Hasegawa (Plenum Press, New York, 1977).

105. L. Berger, in Hall Effect and its Applications, edited by C.L. Chien and C.R. Westgate (Plenum Press, New York, 1980).

106. A.K. Majumdar and L. Berger, Phys.Rev. $\underline{B7}$, 4203 (1973).

107. L. Berger, AIP Conf.Proc. $\underline{29}$, 165(1975).

108. A.K. Majumdar and A.K. Nigam, J.Appl.Phys. $\underline{51}$, 4218 (1980).

109. R. Hasegawa and Ranjan Ray, J.Appl.Phys.$\underline{49}$, 4174(1978).

110. U. Gönser, M. Ghafari, H.G. Wagner and R. Kern, J. Mag. Mag. Mater. $\underline{23}$, 279(1981).

111. R. Hasegawa, R.C. O'Handley and L.I. Mendelsohn, AIP. Conf.Proc. $\underline{34}$, 298(1976); C.L. Chien and R. Hasegawa, Phys.Rev. $\underline{B16}$, 3024(1977).

112. K. Suzuki, F. Itoh, M. Misawa, M. Matsuura, T. Fukunaga and K. Ikeno, Suppl. Sci. Rep.Res.Inst. Tohoku Univ., Sec. $\underline{A28}$, 12(1980); T. Fukunaga, M. Misawa, K. Fukamichi, T. Masumoto and K. Suzuki, in Rapidly Qunehced Metals III, vol.2, edited by B. Cantor (Metals. Soc, London, 1978).

113. A. Mogro-Campero and J.L. Walter, Phys.Rev. $\underline{B20}$, 5030 (1979).

114. A. Mogro-Campero, Phys.Lett. $\underline{76A}$, 315(1980).

115. M. Matsuura and U. Mizutani, J.Mag.Mag.Mater. $\underline{31-34}$, 1481(1983).

116. D.G. Onn, W.D. Johnson, P.F. Gleeson, T.A. Donnelly, T. Egami and H.H. Libermann, J.Phys.$\underline{C10}$, L639(1977).

117. K. Fukamichi, T. Masumoto, M. Kikuchi, IEEE Trans. Magn. MAG-15, 1404(1979).

118. M. Matsui and K. Adachi, J. Mag.Mag.Mater.$\underline{10}$, 152(1979).

119. R. Caudron, J.J. Meunier and P. Costa, Solid State Commun. $\underline{14}$, 975(1974).

120. Ratnamala Roy and A.K. Majumdar, to be published.

121. S.M. Bhagat, S. Haraldson and O. Beckman, J.Phys. Chem. Solids 38, 593(1977).

122. R.C. O'Handley, M.C. Narasimhan and M.O. Sullivan, J. Appl. Phys. 50, 1633(1979).

123. Y. Waseda and H.S. Chen, Phys.Stat.Solidi(a) 49, 387(1978).

124. T. Kemeny, I. Vincze, B. Fogarassy and Sigurds Arajs, Phys.Rev. B20, 476(1979).

125. R.C. O'Handley and D.S. Boudreaux, Phys.Stat.Solidi(a) 45, 607(1978).

126. T. Soumura, J.Phys.Soc.Jpn. 42, 826(1977).

127. K. Fukamichi, M. Kikuchi, S. Arakawa, T. Masumoto, T. Jagielinski, K.I. Arai and N. Tsuya, Solid State Commun. 27, 405(1978).

128. R.C. O'Handley, in Hall Effect and its Applications, edited by Chien and Westgate (Plenum Press, New York, 1980).

129. K. Fukamichi, M. Kikuchi, S. Arakawa and T. Masumoto, Solid State Commun. 23, 955 (1977).

130. Allied Chemical Co., Data Sheet, Metglas alloy 2605 SC.

131. C.L. Chien, D. Musser, E.M. Gyorgy, R.C. Sherwood, H.S. Chen, F.E. Luborsky and J.L. Walter, Phys.Rev. B20, 283(1979).

132. F.E. Luborsky, J.J. Becker, J.L. Walter and H.H. Lieberman, IEEE Trans. Magn. MAG-15, 1146(1979).

133. F.E. Luborsky, J.J. Becker, J.L. Walter and D.L. Martin, IEEE Trans. Magn. MAG-16, 521 (1980).

134. J. Danon, in Chemical Applications of Mossbauer Spectroscopy, edited by V.I. Goldanskii and R.H. Herber (Academic Press, New York, London, 1968).

135. X-ray Powder Data File, sets 1-5, 6-10, Inorganic(1960), R. Fruchart and A.Michel,Mem. Soc. Chem, 422 (1959), J.L. Walter, S.F. Bartram and R.R. Russel, Met.Trans.A9, 303(1978), Handbook of Metallic Systems, vol.1, edited by A.E. Vol. ; KWIC Guide to Powder Diffraction(1966).

PHY- 1984 - D- ROY - TRA